Russian Original Vol. 40, No. 6, June, 1976

December, 1976

SATEAZ 40(6) 539-604 (1976)

SOVIET ATOMIC ENERGY

АТОМНАЯ ЭНЕРГИЯ
(ATOMNAYA ÉNERGIYA)

TRANSLATED FROM RUSSIAN

c/b CONSULTANTS BUREAU, NEW YORK

SOVIET ATOMIC ENERGY

Soviet Atomic Energy is a cover-to-cover translation of *Atomnaya Énergiya*, a publication of the Academy of Sciences of the USSR.

An agreement with the Copyright Agency of the USSR (VAAP) makes available both advance copies of the Russian journal and original glossy photographs and artwork. This serves to decrease the necessary time lag between publication of the original and publication of the translation and helps to improve the quality of the latter. The translation began with the first issue of the Russian journal.

Consultants Bureau journals appear about six months after the publication of the original Russian issue. For bibliographic accuracy, the English issue published by Consultants Bureau carries the same number and date as the original Russian from which it was translated. For example, a Russian issue published in December will appear in a Consultants Bureau English translation about the following June, but the translation issue will carry the December date. When ordering any volume or particular issue of a Consultants Bureau journal, please specify the date and, where applicable, the volume and issue numbers of the original Russian. The material you will receive will be a translation of that Russian volume or issue.

Subscription
$107.50 per volume (6 Issues)
2 volumes per year
Prices somewhat higher outside the United States.

Single Issue: $50
Single Article: $7.50

CONSULTANTS BUREAU, NEW YORK AND LONDON

c/b
227 West 17th Street
New York, New York 10011

Published monthly. Second-class postage paid at Jamaica, New York 11431.

Soviet Atomic Energy is abstracted or indexed in *Applied Mechanics Reviews, Chemical Abstracts, Engineering Index, INSPEC—Physics Abstracts and Electrical and Electronics Abstracts, Current Contents,* and *Nuclear Science Abstracts.*

SOVIET ATOMIC ENERGY

A translation of *Atomnaya Énergiya*

December, 1976

Volume 40, Number 6 June, 1976

CONTENTS

CONTENTS

(continued)

The Russian press date (podpisano k pechati) of this issue was 5/21/1976. Publication therefore did not occur prior to this date, but must be assumed to have taken place reasonably soon thereafter.

ARTICLES

THE KIEV 240-cm ISOCHRONOUS CYCLOTRON

A. F. Linev

UDC 621.584.633.5

The development of the isochronous cyclotron project was started at the D. V. Efremov Scientific-Research Institute of Electrophysical Equipment (NIIÉFA) at the beginning of the 1960's. Approximately at the same time, the basic concepts of isochronous cyclotrons were formulated: The theoretical principles of the dynamics of acceleration processes and the system for withdrawal and monochromatization of external beams were worked out, and possible causes for the loss of beam intensity, resonance phenomena and orbital selection were investigated.

The planning assignment provided for the construction of a versatile accelerator installation, satisfying most completely the problems of the present-day nuclear physics of average energies. It was proposed that the facility constructed should accelerate a large collection of particles with a wide range of maximum energy, high monochromaticity and quality of the beam. Later, directly in the course of planning, a neutron spectrometer system was introduced additionally, which considerably complicated the design of the accelerator vacuum chamber.

The important and most critical part of the project is the choice of form of the magnetic field and its method of formation to ensure stability of the acceleration process. Initially, a three-sector design with a controlled spirality was chosen. In order to regulate the spirality angle, the sectors consisted of two independent parts, and the trough winding was connected in order to correct the magnitude of the flutter both for low and high energy of the accelerated particles. However, as additional modeling of the magnetic field showed, the trough winding and the nonuniformity of the sectors did not provide satisfactory quality of the magnetic field. The new magnetic design does not require the trough windings to be connected during acceleration of protons up to an energy of 80 MeV, and the shape of the sectors has been simplified considerably for the purpose of improving the manufacturing technology (Fig. 1).

In order to increase the quality of the beam, an acceleration system with constant orbit geometry was introduced, which required a current stability in the primary winding of $2 \cdot 10^{-5}$ and 10^{-4} in the correcting windings. Stabilization and control circuits by currents in micromodule elements and thyristors have been developed and manufactured, which have proved to be so compact that they have been arranged in a single standard rack of the Vishnya type.

The collection of plants and the various facilities permits one of three principal operating regimes of the accelerator to be achieved: spectrometric, neutron-pulse, and heavy-ion acceleration regime after the electrostatic recharging accelerator [1]. Each of these cycles requires the installation in the vacuum chamber

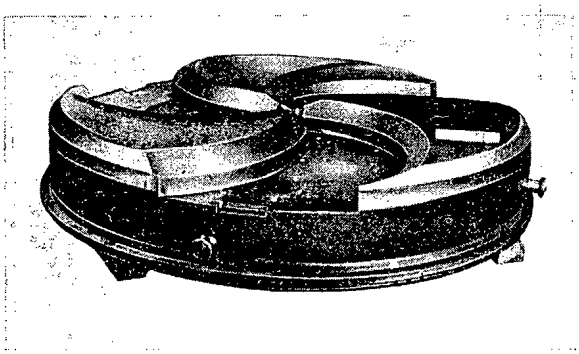

Fig. 1. Polar head with sector cover plates.

Translated from Atomnaya Énergiya, Vol. 40, No. 6, pp. 451-456, June, 1976. Original article submitted January 29, 1976.

TABLE 1. Principal Characteristics of Accelerator Operating Cycles and Measurement-Computational Systems

Energy of accelerated ions, MeV:	
protons	10–80
deuterons	20–70
helium-3	20–180
heavy ions	140
Max. current, mA:	
protons, deuterons, helium	50
heavy ions (by particles)	10
Beam emittance, mm · mrad:	
horizontal	20
vertical	20
Min. size of beam cross section, mm	8
Energy spread:	
at the accelerator outlet	$2 \cdot 10^{-3}$
after the monochromator	$1 \cdot 10^{-4}$
Monochromator:	
angular spread, deg	270
energy resolution	$1 \cdot 10^{-4}$
Neutron spectrometer cycle:	
max. pulse duration, nsec	2.0
freq. repetition range, kHz	1–100
length of flight base, m	180
pulsed neutron flux, sec^{-1}	$3 \cdot 10^{18}$
av. neutron flux, sec^{-1}	10^{14}
Time structure of beam:	
duration of cluster pulse, nsec	2–10
freq. of repetition of bunch, MHz	7–22
handling freq., Hz	25–300
handling pulse duration, msec	0.5–32
Beam extraction system:	
Electrostatic deflector:	
angular spread, deg	30
potential, kV	90
Current channel:	
angular spread, deg	38
gradient, G/cm	200
Magnetic shield:	
length, cm	25
gradient, G/cm	350
Exptl. compartments:	
working area, m^2	1200
No. of compartments	6
No. of beams	16
length of communication lines from measurement center, m	50–200

TABLE 1 (continued)

Measurement-computational center:	
working area of computational center, m^2	400
working area of meas. center, m^2	2×100
No. of Vishnya-type racks	22
No. of standard units	500
No. of computers:	
M-600 ("Parameter")	1
AI-4096	3
M-4030	1
BÉSM-4	1
M-400	2

TABLE 2. Principal Parameters of Accelerator and Engineering Systems

Magnet	
Max. induction, G	17.0
Diam. of pole pieces, cm	240
Final acceleration radius, cm	103
No. of sectors	3
Gap between poles, cm:	
at humps	23.7
in troughs	53.7
Spirality near final radius, deg	45
Max. depth of variation, %	
with trough winding	0.45
without trough winding	0.39
No. of pairs of concentric windings	15
No. of pairs of harmonic windings	3×3
Max. input power, MW:	
primary winding	0.9
correcting windings	0.8
High freq. system	
No. of dees	1
Aperture of dee, cm	5
Generator power, kW	450
Range of retuning, MHz	7.5–22
Freq. stability	$2 \cdot 10^{-8}$
Max. voltage on dee, kV	125
Stability of voltage on dee	10^{-3}
Assumed time of retuning of operating cycles:	
change of energy, type of particles, h	3.0
transfer of beam to another position, h	1.0
Correcting magnet:	
length, cm	65.0
aperture, cm^2	5×23
gradient, G/cm	300
Beam transport system	
SP-018 rotary magnets:	
max. induction, kG	11.0
gap between poles, cm;	12.0
angle of rotation, deg	45
No. of magnets	14
SP-106 commutating magnets:	11.0

TABLE 2 (continued)

max. induction, kG	12.0
gap between poles, cm	8
No. of magnets	
Quadrupolar magnetic lenses 15K-50A-1:	
max. gradient, G/cm	500
aperture, cm	15.0
length, cm	50.0
No. of lenses	34
Quadrupolar magnetic lenses 20K-50A-1:	
max. gradient, G/cm	700
aperture, cm	20
length, cm	50.0
No. of lenses	11
Sectional magnetic lenses 12-40Sh40:	
max. field, G	830
aperture, cm^2	10×35.4
length, cm	40.0
No. of lenses	4
Structure and engineering plant of accelerator	
Working area, m^2	12,000
Working volume, m^3	126,000
Area of main hall, m^2	1000
Wall thickness of biological shield, cm	450
Installed power, MW	20
Consumable power, MW	12.8
Capacity of ventilation center, M^3/h	230,000
Multiplicity of air exchange, min^{-1}	8
Water consumption per day, m^3	3900
Circulating water:	
external circuit, m^3/h	1200
internal circuit (distillate), m^3/h	235

of the accelerator of a specific plant. A change of the operating cycle is associated with a considerable time expenditure, especially as the disassembled plant becomes quite highly radioactive.

Complication of the problems solved by means of the accelerator has taken place gradually, according to the origination of new ideas, but the design of the vacuum chamber has remained as before and therefore it has been found impossible to rearrange the equipment for all cycles of operation under these conditions. In the future, if the versatility of the accelerator is to be justified, obviously a special chamber should be designed in which the collection of equipment can be varied without disassembly. The principal parameters of the accelerator are given in Tables 1 and 2.

In the spectrometric cycle, guaranteeing the production of a high-quality extracted beam, acceleration is accomplished with a constant orbit geometry [2]. When changing the energy and, correspondingly, the magnetic field, the amplitude of the accelerating voltage is changed, so that the number of revolutions for achieving the final energy remains unchanged. Seperation of the orbits and improvement of the quality of the extracted beam are achieved because of internal selection and increase of stability of the current in the windings which shape the magnetic field. A proton and deuteron energy of 80 MeV and 50 MeV, respectively, are achieved without the use of the trough winding, which considerably improves the structure of the magnetic field and ensures the production of betatron oscillations with minimum amplitudes.

The beam is extracted from the cyclotron by means of a short 30° deflector, the current channel, the magnetic shield and the correcting magnet [3]. A special system compensates the effect of the current channel and the magnetic shield on the cyclotron magnetic field.

The position of the deflector, the magnetic channel and the magnetic shield is remotely adjusted for optimization of the coupling with the trajectories of the particles extracted from the accelerator. When changing the energy of the particles, because of the constant geometry of the orbits, it is not necessary to change the position of the extraction elements. Only some correction of their position for optimization of the extrac-

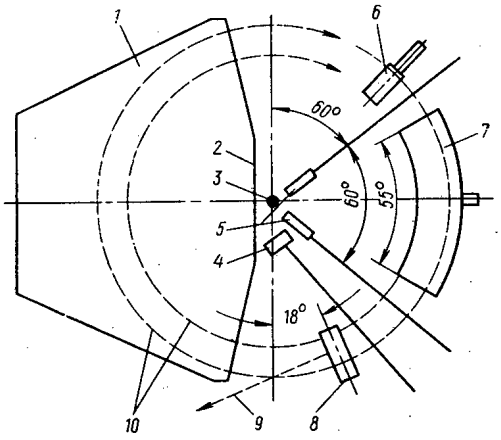

Fig. 2

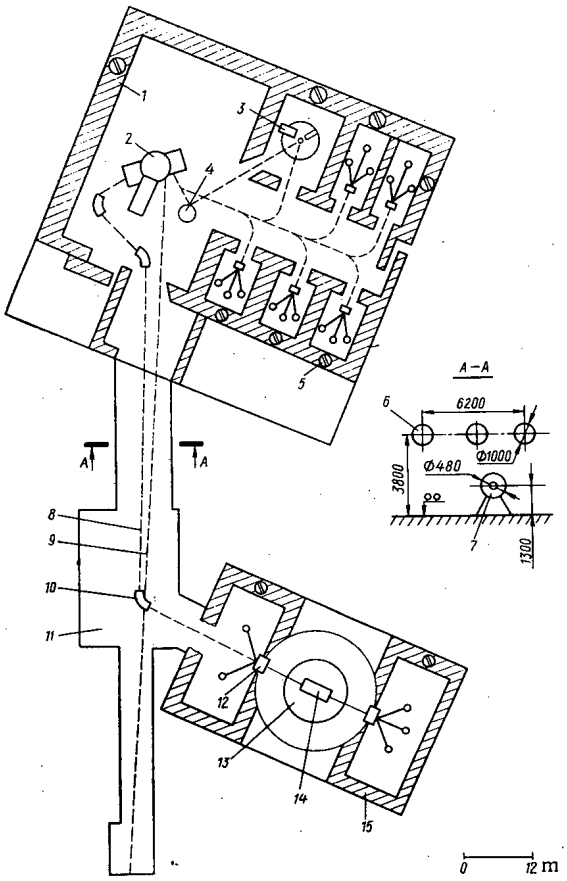

Fig. 3

Fig. 2. Neutron pulse shaping system: 1) dee; 2) puller; 3) ion source; 4) internal deflector; 5) diaphragm; 6) stop frame; 7) external deflector; 8) target; 9) neutron beam; 10) orbits.

Fig. 3. Beam separation system: 1) cyclotron building; 2) cyclotron; 3) spectrometer; 4) monochromator; 5) deflecting door; 6) neutron guide; 7) heavy-ion transmission line lens; 8) direction of heavy-ion beam; 9) direction of neutron beam; 10) deflection magnet; 11) path length of neutron spectrometer; 12) commutative magnet; 13) electrostatic recharging accelerator; 14) analyzer; 15) recharging accelerator building.

tion conditions is necessary.

The initial section of the ion conductor of the beam separation system has an aperture of 20 cm, and after the analyzer on the rectilinear section it is reduced to 15 cm. The separation system of the corridor-type standardizes the beam parameters at the various experimental positions. This makes it possible to dispense with specialization of the compartments for specific experiments.

The separation system directs the beam in advance, analyzed with a resolution of 10^{-4}, to any of 16 targets. In addition, the deflection of the beam from the corridor into the measurement compartments compensates its nonmonochromaticity. Dispersionless deflection of the beam is effected by a system consisting of two magnets (45°) and lenses.

Instruments and scanning devices for monitoring the beam parameters, and also collimators which shape its requisite quality and reduce the radiation background in the measurement compartments, are arranged in the transmission line. A system is used for regulating the scattering angles of the particles within the limits of 50° without changing their direction [4]. Secondary particles, including also particles polarized by the scatter, can be directed into any measurement compartment of the beam separation system. The analyzing magnet reduces the energy spread to $1.0 \cdot 10^{-4}$. At the inlet and outlet of the analyzer, hexagonal lenses are installed for compensating aberration of the second order. A paired analyzer for secondary particles is located in one of the measurement compartments, consisting of a precision spectrometer and a wide-range spectrograph with a resolution of 10^{-3}.

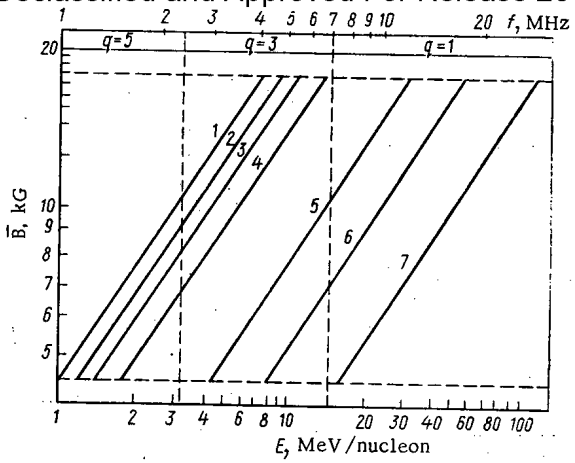

Fig. 4

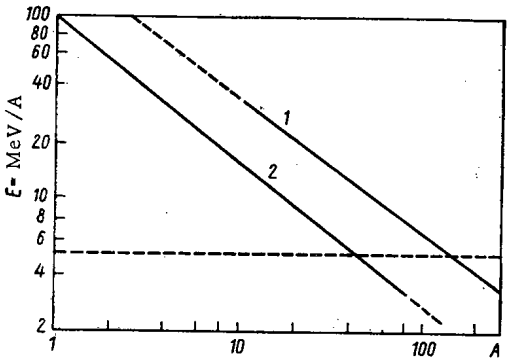

Fig. 5

Fig. 4. Energy of ions in the cyclotron: 1) $^{40}Ar^{8+}$; 2) $^{20}Ne^{5+}$; 3) $^{14}N^{4+}$; 4) $^{12}C^{4+}$; 5) $^{4}He^{2+}$, $^{2}H^{1+}$; 6) $^{3}He^{2+}$; 7) $^{1}H^{1+}$.

Fig. 5. Energy of accelerated heavy ions in the cyclotron (1) and in the TATsIT system (2): - - -) Coulomb barrier at a uranium target.

In the neutron-pulsed cycle of operation, protons are accelerated to an energy of 100 MeV. In order to ensure the necessary focussing at this energy, the trough coils are switched in to increase the amplitude of the fundamental harmonic of the magnetic field up to the required magnitude.

The internal deflector shapes the pulse and consists of 25 - 100 microbunches. Subsequently, these bunches are diverted in the axial direction by the external deflector, which occupies the region along the radius from 86 to 100 cm, and are incident on a thick target, cooled by water, where a pulsed neutron flux is generated with an intensity of $3 \cdot 10^{18}$ sec^{-1} (Fig. 2). The pulse duration is 2 nsec at a pulse frequency of 1 - 100 kHz.

The beam of neutrons is directed into three neutron guides, pumped down to a pressure of 10^{-3}mm Hg in order to reduce losses during passage of the neutrons. The neutron guides are arranged in a special gallery with three measurement pavilions, which serve simultaneously the compartment for conducting heavy ions from the electrostatic recharging accelerator to the cyclotron (Fig. 3). The central neutron guide has a length of 180 m.

The heavy-ion acceleration cycle, with a maximum central field of B = 16.7 kG and a final radius of 103 cm, enables particle energies of $E = 140\ Z^2/A$ to be obtained, where Z and A are the charge and mass, respectively. The radiofrequency system is tuned over the range of wavelengths from 13 to 43 m, which provides acceleration for ions with a specific charge in the range Z/A = 0.2 to 1.0. Thus, by using multiple harmonics q = 1, 3, and 5 of the accelerating field, the facility provides acceleration up to an energy in excess of the Coulomb barrier at a uranium target for all heavy ions up to ^{40}Ar. Heavier particles will have a lower energy (Fig. 4).

In connection with the proposed design of the electrostatic recharging accelerator at an energy of 20 MeV, the possibility was studied also of using the isochronous cyclotron for preacceleration of superheavy ions after stripping – the TATsIT system [5]. In this system, the ions are accelerated first of all up to an energy of about 1 MeV/nucleon in the recharging accelerator, and then they are injected into the cyclotron using stripping and they are additionally accelerated (Fig. 5) Curve 1 in Fig. 5 is the energy of heavy ions, accelerated in the cyclotron with an intensity of $3 \cdot 10^{14}$ sec^{-1}, an energy resolution of $2 \cdot 10^{-3}$ and an emittance of 20 mm · mrad; curve 2 is in the TATsIT system at an intensity of 10^{12} sec^{-1} and with the same energy resolution and emittance.

Calculations were carried out of the limiting permissible energy for particles of different mass with different preliminary acceleration conditions (position of source, conductor potential, intermediate stripping, etc.). The intensity losses due to scattering by residual gas, the nonconformity of the time structures and the phase volumes of the beam were also evaluated. The results of the calculations showed the feasibility of accelerating all particles, including ions of ^{200}Hg up to an energy in excess of the Coulomb barrier in a uranium target, with a beam intensity of $\sim 10^{12}$ sec^{-1}. The heavy ions, at the outlet from this system, after passing through the monochromator will possess spectrometric characteristics for carrying out qualitative experiments.

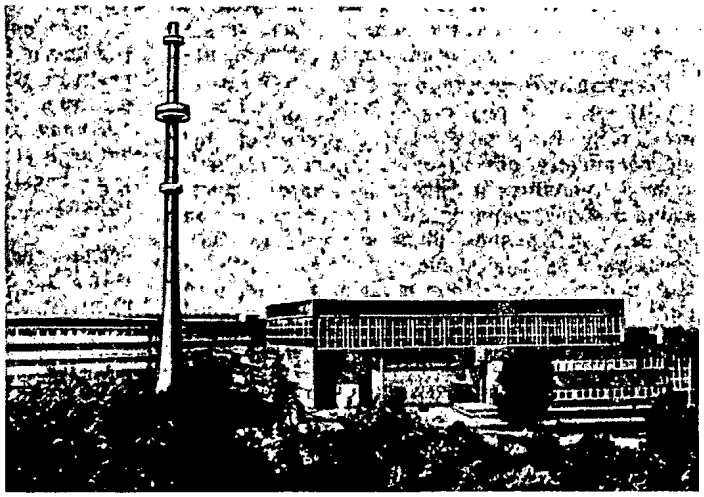

Fig. 6. Accelerator building with laboratory structure.

In order to obtain ions of light particles, accelerated in the spectrometric and neutron-pulsed cycles, an axial source will be used with a controllable position relative to the center of the accelrator. In the case of acceleration of heavy ions, a radial source of the Penning type will be used, similar to that installed in the 300-cm cyclotron in Dubna.

At the present time, construction and commissioning of the cyclotron building with auxiliary units and facilities has been completed (Fig. 6); plant in addition to the monochromator, which would be ready at the end of 1976, has been installed and aligned. Tests of the vacuum and high-frequency systems, the cooling system, and the power supplies have been carried out. The investigation of the magnetic field of the accelerator has been completed. Assembly and alignment of the sectors have been effected with an error of up to 0.2 mm. The bending of the I beam of the electromagnet with a maximum field does not exceed 0.4 mm, and when the load is removed, the initial magnitude of the gap is restored. The magnetic field has been measured with a semi-automatic equipment with an error of better than 1 G and a speed of response of 1.5 sec per point. In all, about 150 charts of the field and up to 6700 points on each have been measured. The results were processed on a BÉSM-4 computer by a special program. The deviation of the corrected magnetic field from isochronous in the working acceleration region does not exceed 10 G.

The Kiev isochronous cyclotron was started up on March 19, 1976. An internal beam of neutrons on the final radius of acceleration was obtained with an energy of 50 MeV and an intensity of 10 μA. The beam intensity was practically unchanged with change of radius. Protons were accelerated in the pulsed cycle with a pulse frequency of 50 Hz, a pulse duration of 4 msec and an amplitude of the accelerating voltage of 70 kV.

The path length of the neutron spectrometer and the electrostatic recharging accelerator are being designed. A polarized particle source with an axial injection system is being developed. The feasibility of automatic control of the isochronous cyclotron using a computer is being studied also.

Extraction of the beam and its transport to the measurement compartments is expected at the end of 1976. The acceleration of heavy ions and the startup of the neutron-pulsed cycle will be effected somewhat later, after acquiring operating experience with light charged particles.

LITERATURE CITED

1. V. Kolotyi et al., in: Proceedings of the 6th International Cyclotron Conference, Vancouver (1972), p. 87.
2. A. F. Linev et al., in: Proceedings of the 4th All-Union Conference on Accelerators, Moscow, Session 5, Report 5 (1974).
3. V. Belyakov, R. Litunovskii, and O. Minyaev, in: Proceedings of the 7th International Cyclotron Conference, Zurich, Session D (1975).
4. Yu. G. Basargin, N. I. Zaika, and A. M. Yasnogorodskii, Izv. Akad. Nauk SSSR, 32, No. 2, 384 (1968).
5. A. F. Linev, Preprint KIYaI-73-9Ya [in Russian], Kiev (1973).

INVESTIGATION OF THE RANDOM COMPONENT OF THE HEAT-RELEASE DISTRIBUTION IN A NUCLEAR REACTOR

V. A. Karpov, V. G. Nazaryan, and V. V. Postnikov

UDC 621.039.512.45

Increase of accuracy and identification of the sources of error in neutron-physical calculations of the heat-release distribution (HRD) in nuclear reactors is of considerable interest for the planning and operation of high-energy reactor facilities.

The discrepancy between the calculated and actual values of HRD [W(r) and $\tilde{W}(r)$] may by due to the methodical inadequacy of the numerical model and the actual unit, and the difference of the actual structural and physical characteristics of the reactor elements from the characteristics used in the neutron-physical calculations, which may be caused by inaccuracy in achieving the specified dimensions and nuclear concentrations in the reactor elements, and also by errors in measurements and control of the various operating parameters: the positions of the control and safety rods, the power level, the fuel temperature and the coolant temperature, etc.

The discrepancy $\mathring{W}(r) = \tilde{W}(r) - W(r)$, due to the combined effect of these factors will be considered in the future as the random component of HRD (RCHRD) in contrast to the determined component W(r).

The results of a neutron-physical calculation of HRD at present are most frequently used in the station computers for monitoring the energy release field together with the readings of the intrareactor sensors, disposed discretely in the active zone [1, 2].

In solving the problems arising during planning and operation of a reactor, first and foremost problems of the discrete monitoring and control of HRD, it is essential to know the space–time characteristics of RCHRD – the harmonic composition and correlation moments [1].

These characteristics may prove useful for the analysis of the causes of HRD misalignments, observed sometimes during nominally symmetrical loading of the active zone of the reactor, and when estimating the necessity for complication of the numerical model of the reactor for the purpose of increasing the accuracy of the calculations, etc.

Previously, the space characteristics of the RCHRD usually were determined [1] by comparison of the calculated and measured values of HRD on the reactor, which made difficult the solution of certain problems in the reactor planning stages. In this case, the RCHRD included components due both to errors of the initial calculated characteristics and to the inadequacy of the numerical model of the unit.

This method of determining the RCHRD characteristics required a large volume of laborious experimental investigation.

In this present paper, a method is considered for determining the RCHRD space characteristics, based on a statistical experiment. The results are given, obtained for the RBMK uranium–graphite reactor. In order to study the RCHRD, the PINK program was used, which was developed for the BÉSM-6 computer, in which a two-dimensional few-group diffusion approximation was used. The program calculates HRD in the reactor, on the basis of an iteration solution of a system of finite-difference equations for a square reference grid [3]. The applied algorithm permits the neutron flux and heat release in every fuel channel (FC) to be calculated, taking into account the individual neutron-physical properties of each cell of the reactor.

Experiments on the uranium–graphite reactors of the Beloyarsk nuclear power station have enabled a

Translated from Atomnaya Énergiya, Vol. 40, No. 6, pp. 456-460, June 1976. Original article submitted June 23, 1975.

TABLE 1. Results of Calculations of the RCHRD Characteristics and the Random Component of the Multiplication Factor of the RBMK Reactor

Taking account of the characteristics, subjected to "drawing"	RCHRD mean-square deviation, %	Max. amplitude of HRD variation, %	Variations for a single "drawing"	
			reactivy, % $\Delta K/K$	coeff. of variation of HRD, $K_r - K'_r$
Spread of uranium dioxide charge in FC's	1	3	0.0035	0.005
Spread in fuel enrichment of FC's	6	16	0.0170	0.060
Simultaneous and independent spread in the uranium dioxide charge and the fuel enrichment of FC's	6	16	0.0170	0.060
Simultaneous and independent spread in the uranium dioxide charge in FC's, in the fuel enrichment, and in the absorbing properties of the control rods and auxiliary absorbers	7	19	0.0300	0.080

method for computing the control rods located in intermediate positions to be developed, according to which each partially inserted rod is replaced in the calculations by a completely inserted rod, equal in efficiency.

The PINK program has been used widely in the planning stages during the forming of the initial charge, and also during operation of the RBMK reactor of the V. I. Lenin nuclear power station at Leningrad [4].

In the determination and analysis of the RCHRD, first of all a calculation was carried out of HRD by the PINK program for some actual reactor charge [5]. Then, for one or independently for several parameters of each cell of the active zone, the random deviations from the law of probability density were calculated by the Monte Carlo method, corresponding to a field of tolerances of the parameter and assumed to be uniform according to the data of the design specifications. Subsequently, calculation of the HRD was carried out by the PINK program for a reactor state which differs from the original state by the random deviations of the parameters. Comparison of the first (initial) value of HRD $[W(\mathbf{r})]$ and the second (perturbed) value of HRD $[\tilde{W}(\mathbf{r})]$ enables the RCHRD $[\mathring{W}(\mathbf{r})]$ to be obtained, which is the homogeneous centered random distribution. On the basis of the RCHRD obtained, the space correlation moments $K_{\mathring{W}}(\tau)$ were calculated, which are dependent on the distance between two points of the active zone.

An analysis of the experimentally obtained values of RCHRD for the uranium–graphite reactors of the Beloyarsk nuclear power station, carried out previously, showed that the RCHRD within the limits of practical requirements [1] possess the property of ergodicity, and therefore its correlation function can be calculated on the basis of a single application.

Analysis of the calculated RCHRD characteristics showed that the principal contribution to it for the RBMK reactor is made by spreads in the enrichment, in the ^{235}U charge of the fuel channels, in the absorbing properties of the control rods and auxiliary absorbers (AA). Therefore, in future calculations random deviations only of these parameters were introduced. As deviations in enrichment and the fuel channel charge have almost no effect on the moderation cross section and the diffusion coefficient, these deviations were taken into account only by means of changes of the macroscopic neutron fission and absorption cross setions.

The results of the RCHRD calculations and of the random component of the multiplication factor of the RBMK reactor are shown in Table 1 for different versions of "drawing" of the characteristics of the active-zone charge elements of the reactor.

The mean-square deviations of the RCHRD ($\sigma_{\mathring{W}}$), shown in Table 1, are due only to the nonidenticity of the neutron-physical characterstics assumed in the calculations and their actual values and therefore are almost independent of the choice of methods for the neutron-physical calculation. The value of $\sigma_{\mathring{W}} = 7\%$ agrees within the limits of statistical accuracy with the similar quantity (5-6%) obtained experimentally during the physical and power startup of the RBMK reactor.

Figure 1 shows the RCHRD for two mutually perpendicular directions through the center of the RBMK core, obtained in the calculation of the charge for the physical startup. Figure 2 shows schematically the

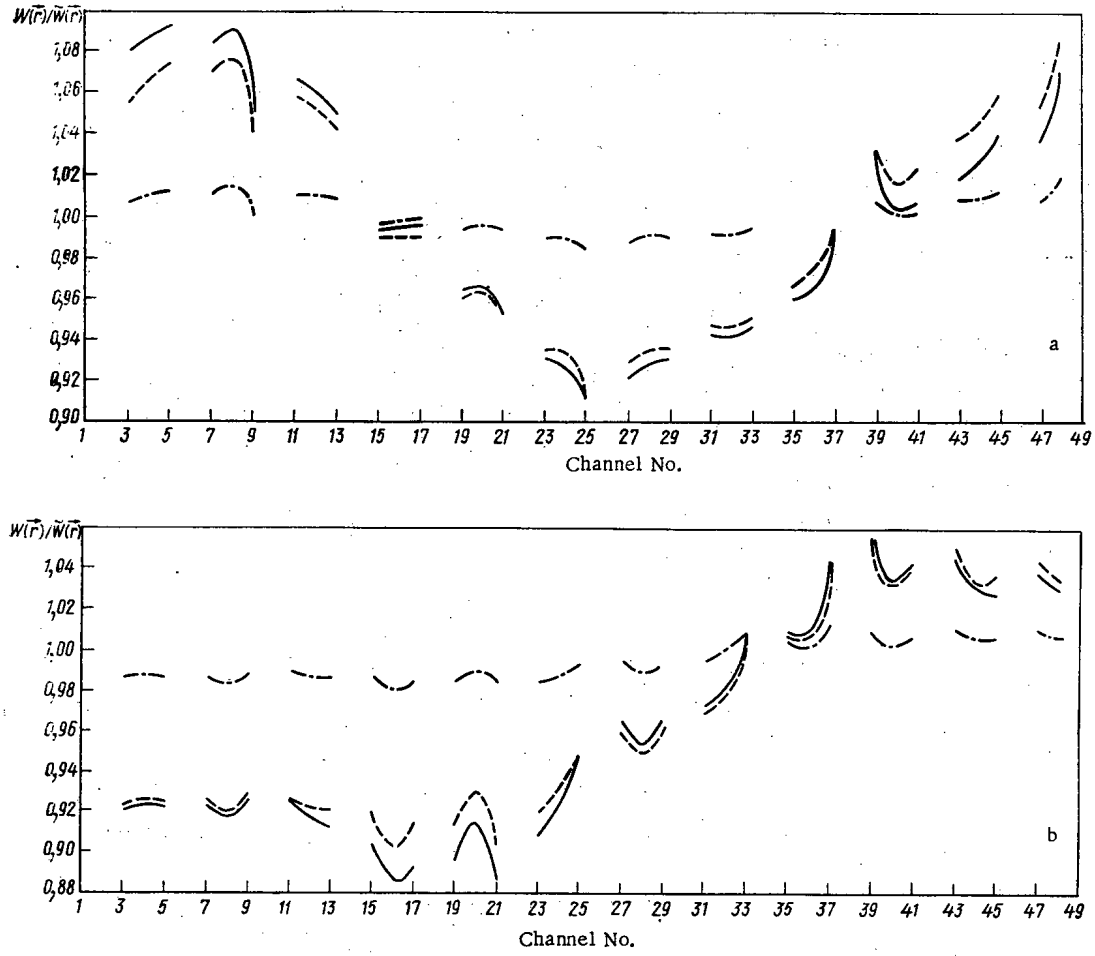

Fig. 1. Field distribution of the ratio $W(\mathbf{r})/\tilde{W}(\mathbf{r})$ for the central array of channels of the RBMK core in the (a) latitudinal and (b) longitudinal directions for different spreads in the charge component properties: -.-, ---, and ——) taking account of variations in the amount of UO_2 in the fuel rods, in the ^{235}U fuel enrichment, and in the properties of the fuel rods, the auxiliary absorbers and the control rods, respectively.

regions of positive and negative values of the RCHRD in the reactor core. Analysis of the results of the calculations for the RBMK reactor showed that the main contribution to the amplitude of the RCHRD are the lowest radial-azimuthal harmonics. In other words, the random spreads in the channel characteristcs give rise to the appearance of smoothly varying HRD misalignments. In this case, the sign of $\mathring{W}(\mathbf{r})$ in each fuel channel of the active zone is varying in a random manner from calculation to calculation.

The RCHRD correlation functions, used in the mathematical processing of discrete control for the RBMK reactor, on a computer, and obtained by this method, are plotted in Fig. 3. For comparison, the correlation function found experimentally by means of a detailed scanning of the active zone is plotted also. It follows from Fig. 3 that the agreement of the results is completely satisfactory.

Also of interest is the investigation of the relation between the mean-square deviation of the nominal values of the fuel channel macroscopic cross sections for the RBMK reactor and the mean-square deviations of the RCHRD. Table 2 shows the values of σ for different mean-square variations of the fission and neutron-absorption cross sections for the fuel channels. Analysis of the data from Tables 1 and 2 permits the conclusion to be drawn that a close to linear dependence is observed of the mean-square deviation of HRD over the reactor on the mean-square deviations of the cross-sections $\nu_f \Sigma_f$ and Σ_a. The effect of the deviations in the fission and absorption cross sections on the RCHRD is approximately equal.

The results presented obviously permit the nature to be established of the significant unidentified misalignments of HRD in the case of a symmetrical initial charge for a series of reactors, in particular the reactors of the Beloyarsk nuclear power station. These effects were explained previously as the consequence

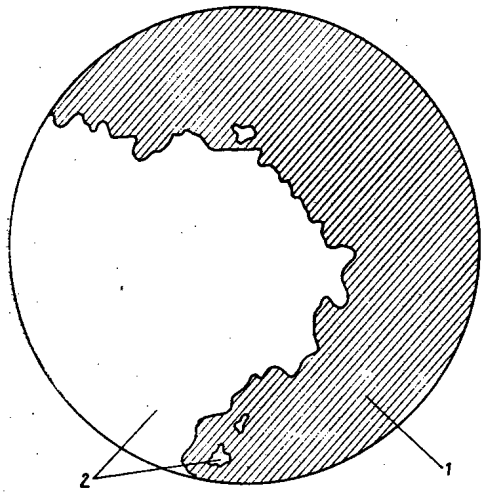

Fig. 2. Deformation of the heat release field as a consequence of the spread in properties of the fuel rods, the auxiliary absorbers and control rods, within the limits of the physical bounds of the RBMK reactor: 1) increase and 2) reduction of power.

TABLE 2. Dependence of Mean-Square Deviations of HRD on Deviations of the Fission and Absorption Cross Sections of the Fuel Channels for the RBMK Reactor

Devia. of fission and absorption cross section of FC's from nominal, %	Mean-square devia. of HRD over reactor, %	Corresponding variations	
		breeding properties of reactor, % $\Delta K/K$	coeff. of variation of HRD, $K_r - K_r'$
0,25	2,70; 2,52	—0,0055; 0,008	0,011; 0,034
0,50	3,64; 4,44	—0,0023; 0,018	0,047; 0,063
1,00	6,74; 8,24	0,0003; 0,041	0,129; 0,144
2,00	12,66; 15,26	0,0188; 0,101	0,302; 0,307
3,00	17,82; 21,55	0,0552; 0,180	0,552; 0,474

Note. The first figure refers to the fission cross section and the second figure refers to the absorption cross section.

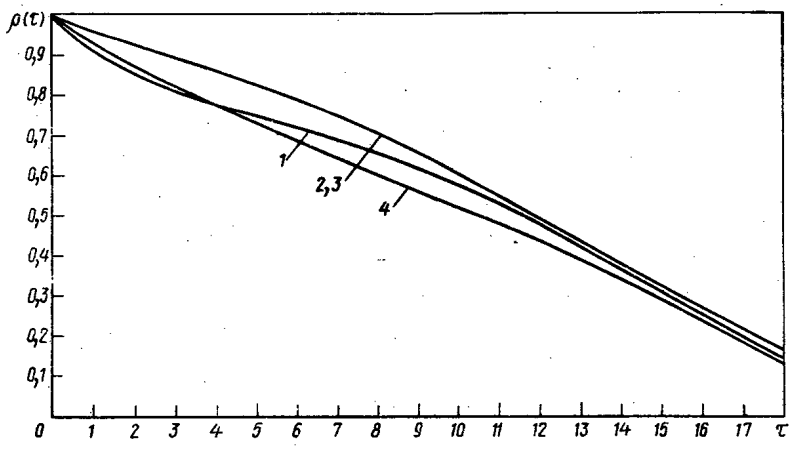

Fig. 3. Normalized $\rho(\tau)$ correlation functions, obtained for different variations in the fuel charge (1), in the fuel charge and enrichment (2), and the absorbing properties of the auxiliary absorbers (3); also the normalized correlation function obtained experimentally (4) [τ is the unit pitch of the lattice].

of filling up with water or contamination of the graphite stack, uncontrolled repositioning of rods, etc. The data from the recent work show that the cause of the HRD misalignments might be entirely due to the variations in the enrichment and charge of the fuel channels, the variations in dimensions of the control rods, etc.

The method devised for calculating RCHRD and its characteristics, permits, at the planning stage, an estimate of the accuracy of the calculated HRD, and also the provision of the necessary starting data for the development of a system for the discrete monitoring of HRD with previously defined characteristics.

LITERATURE CITED

1. I. Ya. Emel'yanov et al., At. Énerg., 34, No. 2, 75 (1973).
2. I. Ya. Emel'yanov et al., At. Énerg., 29, No. 4, 298 (1970).
3. V. A. Karpov, in: Collection of Reports on the Programs and Methods of Calculating Nuclear Reactors [in Russian], Izd. CMEA, Dimitrovgrad (1975), p. 89.
4. I. Ya. Emel'yanov et al., in: Experience in the Operation of Nuclear Power Stations and Paths for the Further Development of Nuclear Power Generation [in Russion], Vol. 1, Izd. FÉI, Obninsk (1974), p. 81.
5. I. Ya. Emel'yanov et al., Report on the Conference of Mutual Economic Aid Countries on Methods of Monitoring and Controlling Nuclear Reactors and Nuclear Power Stations [in Russian], Warsaw (1973).

SPECTRA OF FAST NEUTRONS FROM A PULSED REACTOR

G. G. Doroshenko, S. N. Kraitor, T. V. Kuznetsova, K. K. Kushnereva, E. S. Leonov, and G. A. Frolova

UDC 621.039.526

The possibility of deriving the spectra of fast neutrons from the readings of threshold detectors by minimizing the directional spread was considered in [1, 2]. It was shown in an experiment on paper that the method is characterized by higher accuracy and renders more information than, say, the method of orthonormal expansion. But as far as we know, to date no neutron-spectrometrical measurements have been made in this manner. Such measurements have been made in our work, in which the spectra of fast neutrons of a pulsed HPRR-type reactor [3] were measured.

The core of the HPRR reactor consists of a cylinder with a diameter of 20 cm and a height of 23 cm, which is made of an alloy of molybdenum (10%) and uranium enriched to 93% with the ^{235}U isotope. The reactor can be used in stationary or pulsed operation with about 10^{17} fissions per pulse.

A set of threshold detectors consisting of $^{237}Np(n,f)$, $^{238}U(n, f)$, $^{32}S(n, p)$, $^{27}Al(n, p)$, $^{27}Al(n, \alpha)$, and supplemented by $^{235}U(n,f)$ in a filter of 1 g/cm^2 ^{10}B were used for the measurements. Both the calibration and the determination of the detector readings were analogs to [4]. The detectors were irradiated in the experimental hall of the reactor. The reactor core was at a height of 2 m in the center of a hall having the dimensions 11 × 10 × 10 m. The detectors were placed on that height at a distance of 3.3 m from the center of the core. The measurements were made either without shielding or with shields consisting of 13-cm iron or 12-cm Plexiglas inserted between the detectors and the core at a distance of 3 m from it.

The differential neutron spectrum $\varphi(E)$ was derived from the readings N_i of a set of m detectors by solving a system of integral equations

$$N_i = \int \varphi(E)\,\sigma_i(E)\,dE, \qquad (1)$$

where $\sigma_i(E)$ denotes the cross section of the corresponding reaction; i = 1, 2, 3 . . . m (m = 6). The informa-

Translated from Atomnaya Énergiya, Vol. 40, No. 6, pp. 460-464, June, 1976. Original article submitted July 27, 1975.

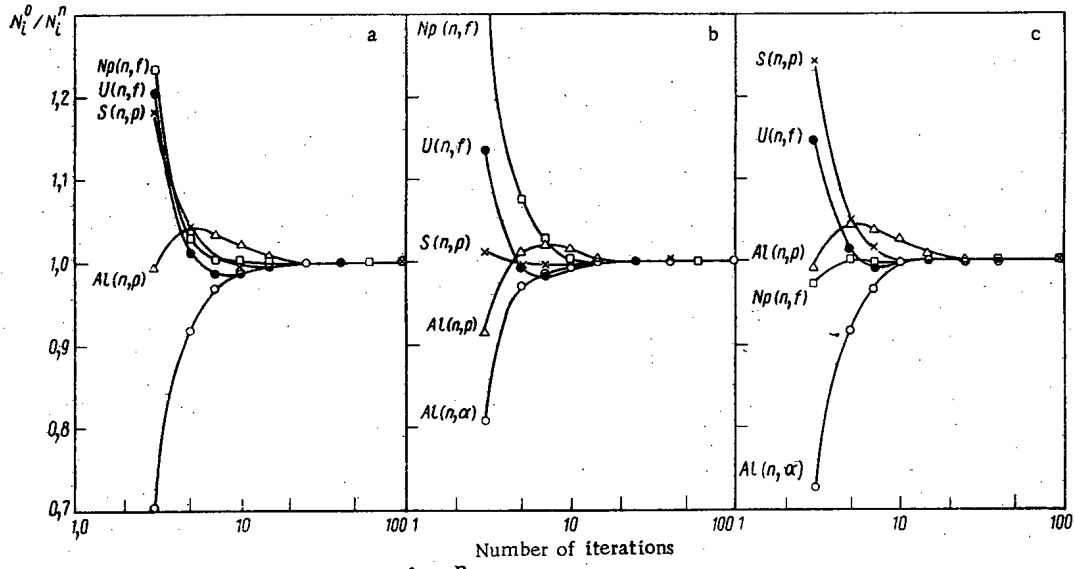

Fig. 1. Dependence of the ratio N_i^0/N_i^n of detector readings upon the number of iterations when the neutron spectra were derived: a) without shielding; b) with 13-cm iron shielding; and c) with 12-cm Plexiglas shielding.

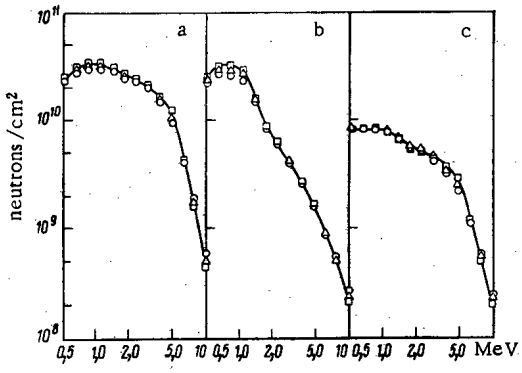

Fig. 2. Spectra of the fast neutrons of a pulsed HPRR-type reactor: a) without shielding; b) with 13-cm iron shielding; and c) with 12-cm Plexiglas shielding. Spectra derived after: ○) 3, △) 5, and □) 25 iterations.

tion measure

$$J[N, \hat{\sigma}\varphi] = \sum_{i=1}^{m} N_i \ln \frac{N_i}{\int \varphi(E)\,\sigma_i(E)\,dE} \qquad (2)$$

was used as a measure for the difference between the left and right sides of the above equations; the information measure denotes the directional spread in aleatoric function space. In order to determine the minimum of functional (2), an iteration process was developed. The algorithm of the iteration process was assumed in the form of [2]:

$$\varphi_{n+1}(E) = \frac{\varphi_n(E)}{\sum_{j=1}^{m} \frac{\sigma_i(E)}{N_j^0}} \sum_{i=1}^{m} \frac{\sigma_i(E)}{N_i^0} \frac{N_i^0}{N_i^n}, \qquad (3)$$

($\varphi_n(E)$ and $\varphi_{n+1}(E)$ denote the neutron spectra of the n and n+1 iteration, respectively; N_i^0 denotes the measured

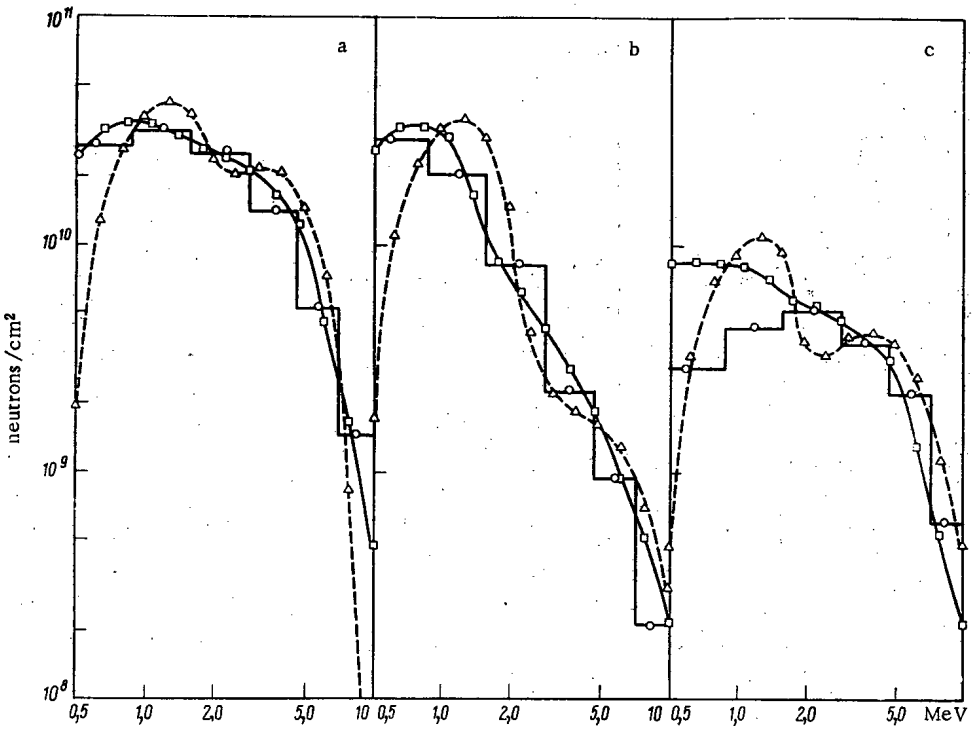

Fig. 3. Spectra of the fast neutrons of a pulsed HPRR-type reactor: a) without shielding; b) with 13-cm iron shielding; and c) with 12-cm Plexiglas shielding: □ and Δ) minimizing the directional spread and orthonormal expansion, respectively; ○) calculations for the HPRR reactor.

detector readings; and N_i^n denotes the detector readings which were calculated from the spectrum derived after n iterations). Calculations were made on a computer with a program written in ALGOL. The time required for performing 100 iterations on a Minsk-22 computer amounted to about 2 min. $\varphi_0(E) = 1$ was assumed as the zeroth approximation.

Figure 1 shows the ratio of the detector readings N_i^0 to N_i^n. As early as after 10-25 iterations, the detector readings calculated from the restored spectrum correspond to the experimental values with an error of less than fractions of a per cent and are practically constant thereafter. Figure 2 proves that the form of the spectra hardly changes. It follows from the spectra which are shown in Fig. 2 for various numbers of iterations that the iteration process converges rapidly toward a stable solution and that no oscillations occur.

According to [5], this form of convergence indicates that the errors which are made in the determination of the detector readings and of the energy characteristics used are insignificant.

Figure 3 shows the results of measurements for 25 iterations (the results are similar in the case of 100 iterations) and the calculated data for the HPRR reactor used with the above shieldings [6]. The structure of the measured spectra results from the superposition of the spectrum of the fission neutrons with a total energy of about 2 MeV and the spectrum of the inelastically scattered neutrons with the maximum at several hundred keV. The contribution of the latter neutrons increases behind the iron shielding and dominates. The relative contribution of the neutrons in that region increases also behind a water-containing shielding. But in that case the increase is caused by the moderation of the incident neutrons in the shield and by the relative increase in the contribution of neutrons reflected from the walls of the building.

It follows from a comparison of the calculated and experimental results that they are in good agreement in the entire energy range from 0.5 to 10 MeV when no sheilding or when iron shielding is employed. The spectra were measured with adequate accuracy even when only the set of 5 detectors was used. The agreement is observed only above about 2 MeV in the case of Plexiglass shielding, because the neutrons which are scattered in the building and have a softer spectrum influence the results. These neutrons were disregarded in the calculations, because the HPRR reactor is practically in an open place.

Figure 3 includes the fast-neutron spectra which were derived from the detector readings by the orthonormal expansion of [7]. According to that method, the differential neutron spectrum is represented as a

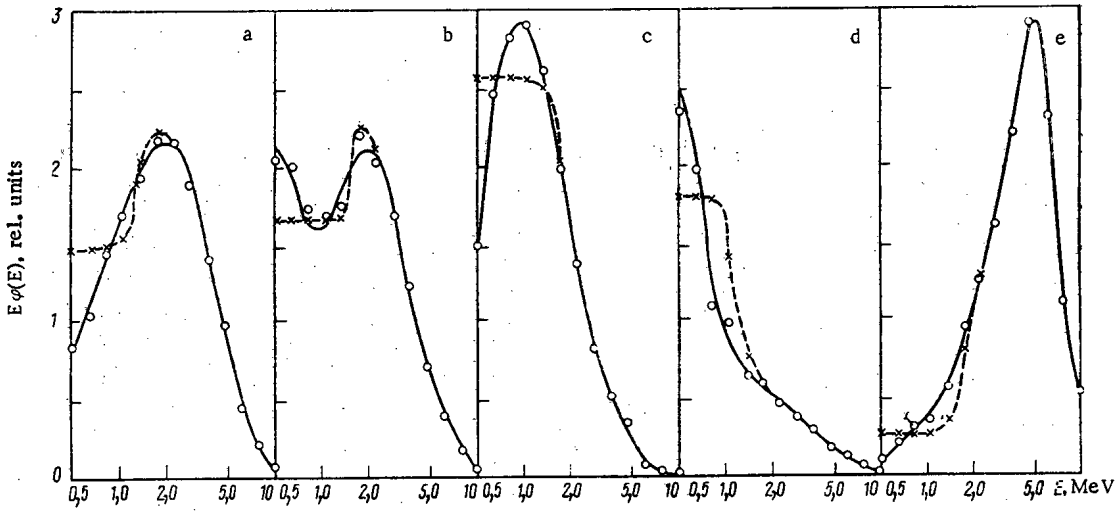

Fig. 4. Spectra of fast fission-induced neutrons: a) without shielding, c) with lead shielding, e) with polyethylene shielding; b) heavy-water reactor, and d) BR-1 reactor. The spectra were derived with the full set of detectors (○) or without the ^{235}U + 1-g/cm^2-^{10}B detector (x); ——) given spectra.

linear combination of the efficiencies of the detectors used, i.e.,

$$\varphi(E) = \sum_{k=1}^{m} \alpha_k \sigma_k(E), \tag{4}$$

where the coefficients α_k are obtained from the condition that the difference between the unknown spectrum $\varphi(E)$ and its approximation to all the functions $\sigma_i(E)$ must be orthogonal:

$$\int \left[\varphi(E) - \sum_{k=1}^{m} \alpha_k \sigma_k(E)\right] \sigma_i(E)\, dE = 0.$$

We therefore obtain with Eq. (1)

$$\varphi(E) = \sum_{i=1}^{m} N_i \sum_{k=1}^{m} \rho_{ki}^{-1} \sigma_k(E), \tag{5}$$

where $\rho_{ki} = \int \sigma_k(E)\sigma_i(E)dE$ denotes matrix elements which depend only upon the efficiency of the neutron detectors.

The neutron spectra obtained in this fashion have the form of waves. In all cases maxima were noted in the spectra at ~ 1.2 MeV; the maxima do not depend upon the form of the spectrum, i.e., they are an effect originating from the instruments. The neutron spectrum below 1 MeV is not reproducible by the method of orthonormal expansion. The results confirm the relative merits of the two methods, which were assessed in [8] on the basis of calculations. The results are important as far as applications are concerned, because the results show that the method of minimizing the directional spread for deriving neutron spectra has advantages.

The advantages are essentially explained by the substantial differences between algorithms (3) and (5). Algorithm (5) represents the spectrum as a linear combination of the efficiencies of detectors; the consequence is the wave-like structure which originates from the efficiencies rather than from the energy distribution of the neutrons. In algorithm (3), the dependence of the derived neutron spectrum upon the efficiency is less pronounced and the wave-like structure of the spectrum is practically not noticeable. This algorithm precludes the appearance of negative values of the spectrum, which are observed in certain cases when algorithm (5) is used.

Since equation system (1) is poorly defined and since its solution in the form of Eq. (5) implies the determination of the inverse matrix (ρ_{ki}^{-1}), the resulting solution depends very strongly upon the errors of the detector efficiencies and upon experimental reading errors. The error in the determination of the neutron

spectrum can many times exceed the above errors. When the method of minimizing the directional spread is employed, the inverse matrices need not be determined so that the influence of the errors in the initial data is extremely small.

In addition to the threshold detectors, we used in the present measurements also a detector which contained ^{235}U and was surrounded by a boron filter with a thickness 1 g/cm^2 ^{10}B. This detector records neutrons with an energy in excess of ~ 400 eV and has an efficiency which varies very little with energy. In order to determine whether the detector should be employed for measurements of fast neutrons, an initial experiment was made "on paper" to derive spectra which sharply differ in their forms at energies of 0.5-10 MeV: spectra of fission neutrons without shielding and with shielding by lead or polyethylene, the neutrons stemming from a heavy-water reactor or the BR-1 reactor [2]. The spectra were derived by minimizing the directional spread with algorithm (3) and by using the calculated readings of scaled threshold detectors inclusive (or exclusive) the detector with ^{235}U + 1 g/cm^2 ^{10}B. The results (Fig. 4) show that the ^{235}U + 1-g/cm^2-^{10}B detector substantially increases the accuracy at energies below 1.5 MeV and facilitates the reliable determination of the spectra with 0.5 MeV.

Obviously, the same effect can be obtained when one uses in place of the ^{235}U + 1-g/cm^2-^{10}B detector some other detector which responds to neutrons with energies below 0.5 MeV, e.g., a detector based on ^{63}Cu (n, γ), ^{6}Li(n, α), etc. Though the spectrometric information which is obtained in that case is without interest in the entire response range of the supplemental detector, the incorporation of it allows a better utilization of the spectrometric possibilities of the neptunium detector near its energy threshold.

The authors thank I. B. Keirim-Markus for interest in the present work and useful discussions.

LITERATURE CITED

1. M. Z. Tarasko, E. A. Kramer-Ageev, and E. B. Tikhonov, in: Problems of Dosimetry and Radiation Shielding [in Russian], No. 11, Atomizdat, Moscow (1970), p. 125.
2. G. G. Doroshenko et al., At. Énerg., 35, No. 5, 343 (1973).
3. I. B. Keirim-Markus, V. A. Knyazev, and S. N. Kraitor, in: Metrology of Neutron Radiation at Reactors and Accelerators [in Russian], Vol. 2, Izd. VNIIFTRI (All-Union Scientific-Research Institute of Physicotechnical and Radiotechnical Measurements), Moscow (1974), p. 121.
4. K. K. Koshaeva, S. N. Kraitor, and L. B. Pikel'ner, At. Énerg., 32, No. 1, 68 (1972).
5. G. G. Doroshenko, S. N. Kraitor, and E. S. Leonov, in: Metrology of Neutron Radiation at Reactors and Accelerators [in Russian], Vol. 2, Izd. VNIIFTRI (All-Union Scientific-Research Institute of Physicotechnical Measurements), Moscow (1974), p. 36.
6. J. Poston, J. Knight, and G. Whitesides, Health Physics, 26, 217 (1973).
7. I. B. Keirim-Markus and V. I. Popov, in: Problems of Dosimetry and Radiation Shielding [in Russian], No. 10, Atomizdat, Moscow (1969), p. 14.
8. G. G. Doroshenko et al., in: Metrology of Neutron Radiation at Reactors and Accelerators [in Russian], Vol. 2, Izd. VNIIFTRI (All-Union Scientific-Research Insitute of Physicotechnical and Radiotechnical Measurements), Moscow (1974), p. 45.

NUMERICAL INVESTIGATION OF THE OPTIMUM CONDITIONS FOR THE POWER REDUCTION OF A REACTOR

V. M. Desyatov, V. I. Pavlov and V. D. Simonov

UDC 621.039.516

The problem of the optimum cycle with respect to time for the power reduction of a reactor is considered in [1, 2]. The optimum power reduction trajectory is shown in Fig. 1, where x^1 and x^2 are the concentrations of iodine and xenon, respectively, normalized to the fission cross section, and ξ is the curve of the reactor states, stable with respect to iodine and xenon. In the general case, when limited to the maximum concentration of xenon ($x^2 = x^2_{max}$), the trajectory has a section of minimum power (ab), a section where the power is varying (bc), a i a section of maximum power (cd_1). The section cd_1 is completed by the curve ξ, tangential to $x^2 = x^2_{max}$, and represents the change of the iodine and xenon concentrations during instantaneous reduction of the reactor power to the state defined by the point d on the curve ξ.

The special features of the individual sections of the optimum trajectory and the optimum time of reduction of power T_0 depend on such reactor characteristics as the operative reserve of reactivity $\Delta\rho$, the maximum $x^{(3)}_{max}$ and minimum x^3_{min} permissible neutron fluxes, and also the values of the neutron fluxes corresponding to the initial $x^{(3)}_0$ and final $x^{(3)}_f$ reactor power level and the rate of change of power α.

In this present paper a numerical investigation is given into the development of these relations which affect significanly the feasibility of the practical achievement of the optimum reactor power reduction cycle. The calculations were carried out by a specially devised program, which allows T_0, the time of operation of the reactor with minimum (t_{ab}), variable (t_{bc}), and maximum (t_{cd1}) power, to be found in terms of the known values of $\Delta\rho$, $x^{(3)}_0$, $x^{(3)}_f$, $x^{(3)}_{min}$, and $x^{(3)}_{max}$. A reactor is considered, with physical characteristics which are typical for the water-cooled/water-moderated power reactor (VVÉR).

Figure 2 represents the dependence of the time of movement on the sections of the optimum trajectory, on the operative reserve of reactivity, obtained on the assumption of a stepwise power change at the points a, b, c, and d_1. When $\Delta\rho < 1.5\%$, the main contribution to the total time of power reduction is the time of operation with variable power t_{bc}. This time decreases rapidly with increase of $\Delta\rho$ and when $\Delta\rho = 1.9\%$, it becomes equal to zero, so that over the range of values $1.9\% \leq \Delta\rho \leq 2.35\%$, the optimum transition is achieved by a two-stage cycle: operation at the minimum and maximum permissible power. When $\Delta\rho \geq 2.35$, $T_0 = 0$, i.e., it becomes equal to a "direct" transition at a power equal to $0.2\ x^{(3)}_0$, without a forced standstill in the "iodine well."

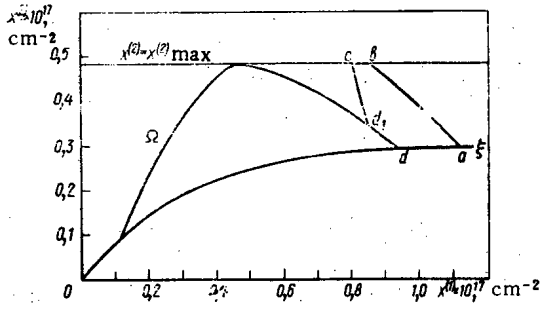

Fig. 1. Optimum power reduction trajectory ($x^{(3)}_{max} = x^{(3)}_0$; $x^{(3)}_f = 0.1\ x^{(3)}_0$; $x^3_{min} = 0$).

Translated from Atomnaya Énergiya, No. 6, pp. 464-467, June, 1976. Original article submitted July 23, 1975.

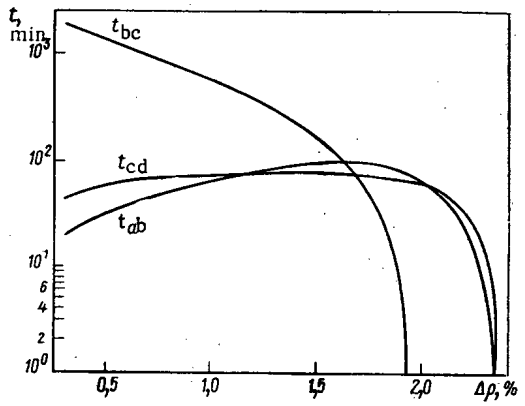

Fig. 2

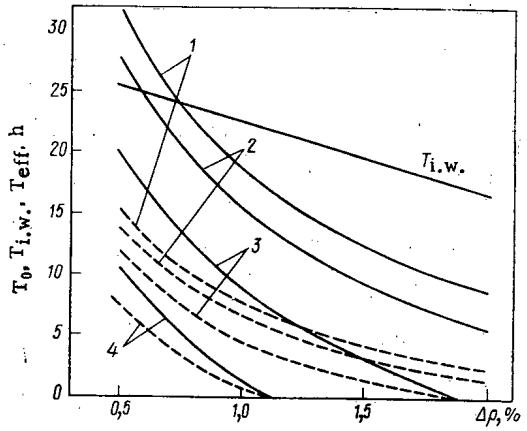

Fig. 3

Fig. 2. Dependence of operating time of the VVÉR-440 reactor at various sections of the optimum trajectory t on the operative reserve of reactivity $\Delta\rho$ [$x^{(3)}_{max} = x^{(3)}_0$; $x^{(3)}_f = 0.2x^{(3)}_0$; $x^{(3)}_{min} = 0$].

Fig. 3. Dependence of T_0, $T_{i.w.}$, and T_{eff} on the operative reserve of reactivity ($x^{(3)}_{max} = x^{(3)}_0$; $x^{(3)}_{min} = 0$): 1) $x^{(3)}_f = 0$; 2) $x^{(3)}_f = 0.1x^{(3)}_0$; 3) $x^{(3)}_f = 0.3\ x^{(3)}_0$; 4) $x^{(3)}_f = 0.5x^{(3)}_0$; ——) T_0; - - - -) T_{eff}.

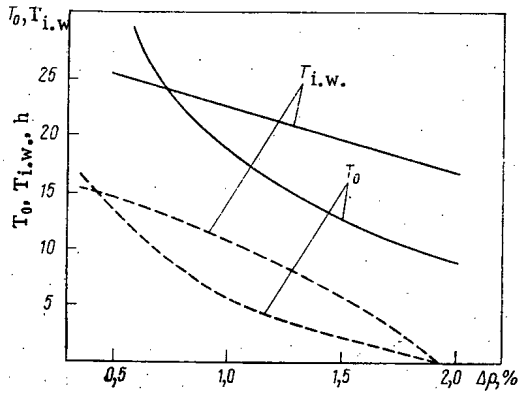

Fig. 4

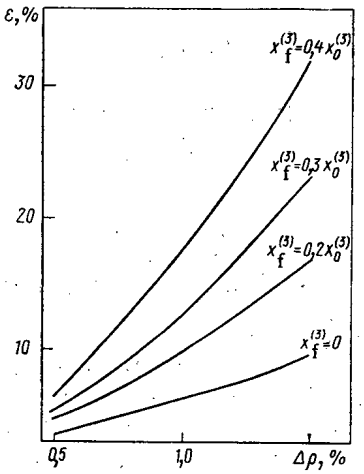

Fig. 5

Fig. 4. Effect of the reactivity power effect on the magnitude of the optimum time of power reduction [$x^{(3)}_{max} = x^{(3)}_0$; $x^{(3)}_{min} = 0$ and $x^{(3)}_f = 0$]: —— and - - -) without and with account of the power effect, respectively.

Fig. 5. Relative increase of optimum time of power reduction ε, for a cycle with a limitation on the rate of change of power as a function of $\Delta\rho$ ($x^{(3)}_{max} = x^{(3)}_0$; $x^{(3)}_{min} = 0$; $\alpha = 10\%$ min).

The optimum reduction cycle of a power reactor has more significance from the point of practical achievement the lesser T_0 is and the less the generation of energy which accompanies it. For this, it is obvious to compare the optimum time with the time of stay of the reactor in the "iodine well" $T_{i.w.}$, and to estimate the power output in effective hours T_{eff}. For each value of $x^{(3)}_f$ values of $\Delta\rho$ can be assigned for which the power reduction cycle from the level $x^{(3)}_0$ to the level $x^{(3)}_f$ is achieved during the time $T_0 < T_{i.w.}$. It can be seen in Fig. 3, where the dependence to T_0, $T_{i.w.}$, and T_{eff} on the operative reserve of reactivity for a reactor of the VVÉR-440 type are plotted, that, for example, for $x^{(3)}_f = 0$, this region is determined by the inequality $\Delta\rho > 0.7\%$, and for $x^{(3)}_f = 0.1x^{(3)}_0$, $\Delta\rho > 0.6\%$. Taking into account the negative power effect of reactivity, which is characteristic for VVÉR reactors, the boundary of this region is displaced to the side of a lower value of $\Delta\rho$ (Fig. 4).

TABLE 1. Optimum Time of Power Reduction for Different Values of the Parameters which Define the State of the VVÉR-440 Reactor in the Transition Process, h

$x^{(3)}_{max}/x^{(3)}_0$	$x^{(3)}_f/x^{(3)}_0$	$x^{(3)}_{min}/x^{(3)}_0$*			$x^{(3)}_{min}/x^{(3)}_0$†		
		0	0,2	0,4	0	0,2	0,4
1,0	0	31,48	31,55	31,66	18,81	18,96	19.25
	0,2	23,74	23,81	23,92	11,68	11,82	12,11
	0,4	15,32	15,39	15,50	4,74	4,88	5.17
0,8	0	31,59	31,66	31,77	18,95	19,09	19,38
	0,2	23,88	23,95	24,06	11,86	12,00	12.29
	0,4	15,53	15,60	15,71	5.02	5,16	5.45
0,6	0	31,78	31,84	31,96	19,17	19,31	19.60
	0,2	24,15	24,22	24,33	12,19	12,34	12,62
	0,4	16,09	16,15	16,27	5,74	5,89	6,18

* $\Delta\rho = 0{,}5\%$.
† $\Delta\rho = 1{,}0\%$.

The relations in Figs. 3 and 4 have been obtained on the assumption that the rate of change of power is not restricted and at the points *a*, b, c, and d_1 the power is changing stepwise.

The problem concerning the optimum power reduction cycle of a reactor was considered in [3] in the case of a finite rate of change. This restriction is justified and is conditional on the capabilities of the control system and the safety requirements.

The calculations show that a noticeable increase of the optimum time in comparison with the case of infinite rate of change of power is observed, in the case of the actual rate of change of power of power reactors ($\alpha = 1\%/\text{min}$). The results of these calculations are shown in Fig. 5 in the form of the dependence of the relative increase of T_0 when $\alpha = 1\%/\text{min}$ on the operative reserve of reactivity and the power at which the reactor changes over.

As a result, an increase of T_0 leads to the appearance of sections of the trajectory which "smooth" the power flash-up. Therefore, by reducing the size of the flash-up "step," the solutions of both problems can be brought together. Moreover, a cycle with small fluctuations of the total power is simpler to use and is more reliable with respect to safety conditions. The dependence of T_0 on $x^{(3)}_{min}$ and $x^{(3)}_{max}$ is shown in Table 1. It can be seen that over a wide range of values of $x^{(3)}_{min}$ and $x^{(3)}_{max}$ the optimum time varies only weakly. Obviously, for every value of $x^{(3)}_f$, values of $x^{(3)}_{min}$ and $x^{(3)}_{max}$ can be calculated, for which the cycle, with an insignificant increase of T_0, will be suitable for practical achievement.

LITEREATURE CITED

1. A. P. Rudik, Nuclear Reactors and Pontryagin's Maximum Principle [in Russian], Atomizdat, Moscow (1971).
2. A. P. Rudik, Xenon Transition Processes in Nuclear Reactors [in Russian], Atomizdat, Moscow (1974).
3. T. S. Zaritskaya and A. P. Rudik, At. Énerg., 36, No. 2, 140 (1974).

DEVELOPMENT OF AN APPARATUS FOR CLARIFYING SOLUTIONS PRIOR TO THE EXTRACTION REPROCESSING OF VVÉR FUEL ELEMENTS

A. M. Rozen, K. A. Dolgova,
A. M. Nudel', I. M. Balakin,
I. M. Mal'tsev, V. I. Koblov,
A. N. Levishchev, and B. R. Borisov

UDC 621.039.59.001.57

When reprocessing fuel elements from VVÉR (water-cooled/water-moderated power reactors) [1] by extraction technology [2], the problem arises of the clarification of the solutions [2-4], as suspensions can clog the control-and-measuring instrument and the analyzer, and also can stabilize emulsions, which leads to the formation of interphase films and disruption of the normal flow of the process in the extractors [5]. Therefore, it was decided to use filtration or centrifugation [3, 4].

Preliminary investigations showed that when dissolving VVÉR fuel elements, highly dispersed, difficultly separable suspensions arise, the clarification of which is a problem [4]: with settling (even during 24 h, only 50-60% of the solid phase can be separated), the rate of filtration through a paper filter "blue ribbon" with a drop in pressure of 0.5 kg/cm^2 is negligibly small (curve 1, Fig. 1); with centrifugation, a fugate containing < 5 mg/liter of solid suspension is obtained only with a separation factor of 20 thousand; in this case, the decantate, filtrate, and fugate, just like the crude solution, on contact with 25% tributylphosphate (TBP) formed interphase films. Because of the defined properties of suspensions, for complete separation of the suspension and in order to prevent the formation of films, it is necessary to prepare solutions – use flocculants and

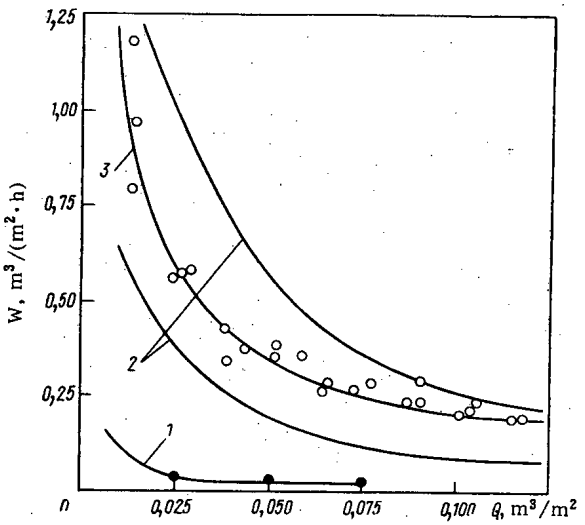

Fig. 1. Dependence of the rate of filtration on the volume of filtrate obtained: 1) actual (unprocessed) solution of VVÉR fuel elements; 2) actual solution treated with gelatin; 3) simulated VVÉR fuel elements, treated with gelatin. Pressure drop 0.5 kg/cm^2.

Translated from Atomnaya Énergiya, Vol. 40, No. 6, pp. 467-471, June, 1976. Original article submitted July 9, 1975.

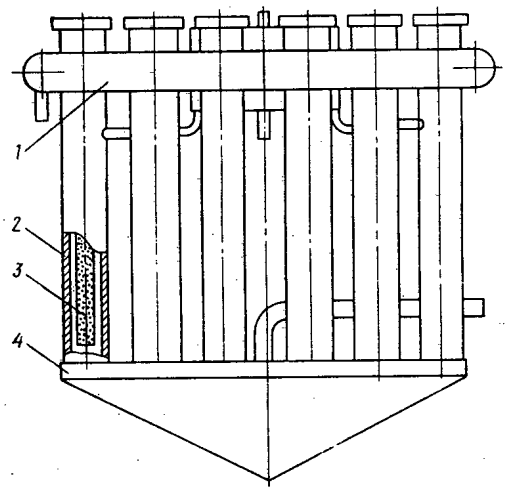

Fig. 2. Diagram of experimental-industrial filter: 1) filtrate assemblage receiver; 2) casing; 3) filtration element; 4) conical slotted bottom.

subsidiary filtration methods.

In [3, 4], the results are discussed of investigations into the choice of conditions for clarifying solutions on cartridge filters; these investigations were carried out on laboratory apparatus, using solutions of unirradiated fuel elements; the results have been verified on irradiated solutions.

The present paper is devoted to the development of an industrial clarifying apparatus – a filter and a centrifuge. In order to test it, it was necessary to develop special simulant-solutions.

Simulant-Solution for Testing Semiindustrial and Experimental-Industrial Apparatus. In order to test industrial filters, a large quantity of solution is required and the use of solutions of actual fuel elements would be far too expensive. It was necessary to devise simulant-solutions.

Solutions of VVÉR fuel elements contain uranium (300-330 g/liter), 2-3 M HNO_3, have a specific gravity of 1.4-1.5, and a viscosity of 2.2-2.6 cp. The content of suspended matter amounts to up to 1 g/liter, the bulk of which is finely dispersed graphite; also present are silicic acid and other impurities (including uranium up to 5%), 80% of the particles have a size of $<5\ \mu$ and the average density is $\sim 2.1\ g/cm^3$.

In the simulant-solution, uranyl nitrate was replaced by aluminum nitrate, and the graphite was simulated by carbon black. The following finely dispersed suspension was used as the simulant-solution for the unirradiated VVÉR fuel elements: The liquid phase was a solution of aluminum nitrate (240 g/liter), containing 2.5 M HNO_3 and 50 mg/liter (with respect to SiO_2) of polymerized silicic acid, viscosity 2.6 cp, density 1.25 g/cm^3; the solid phase was a previously prepared mixture of lamp black and PM-70A soot with a dispersivity of 0.2 to 90 μ, including 45-50% of particles with a diameter of 5 μ or less; the density of the soot particles was 2.0 g/cm^3.

The completeness of the simulant was determined by the convergence of the results with respect to filterability of the simulant and actual solutions, untreated and treated with gelatin (curve 3, Fig. 1), determined on a laboratory funnel with a "blue ribbon" paper filter and with a pressure drop of 0.5 kg/cm^2; the simulant-solution, just like the actual solution, formed interphase films on contact with 25% TBP.

Filtration

Apparatus. And investigation of the filtration process [3, 4] showed a number of advantages of cartridge filters. Similar apparatus can be relatively easily remotely reactivated, individual elements can be replaced in them, a safe geometry can be ensured, etc. Because of this, an experimental-industrial annular cartridge filter was developed, with a surface area of 1.8 m^2 (see Fig. 2). Wire cartridges were used (with a wire diameter of 0.3-0.8 mm and a gap between turns of 20-100 μ), metal–ceramic cartridges of stainless steel (pore diameter 40-60 μ) and titanium (pores 7 μ). The experimental-industrial filter (see Fig. 2) consists of 14 casings with a nuclearly safe diameter of 120 mm, joined at the lower section by a conical bottom, and at the upper section by the collectors of a filter assembly, and a compressed air supply and blow-off for "shock" regeneration. In each casing, along the center, a filtration cartridge with a length of 1000 mm and a diameter of 40 mm

was installed. The design of the head of each casing ensures a guaranteed separation of the initial solution zone from the filtrate zone, remote inspection, replacement and detachment of any filteration unit, and also fastening of the filtration elements to the body of the filter.

Test of Experimental-Industrial Filter. Filtration was undertaken at a pressure of 3-4 kg/cm^2. The filtering capability of the barrier was established by the reverse flow of filtrate, by means of "shock" regeneration with a pressure drop of 3-4 kg/cm^2 and, in the case of metal–ceramic barriers, by boiling in a solution of 5 M NaOH and 4 M HNO_3. The experimental equipment was provided with reservoirs for the preparation and treatment of the original suspension, batching of a suspension of perlite, assembly of the filtrate and coagulation of the sediment. The transfer of all suspensions and their mixing was carried out with compressed air. The facility was provided with control-and-measuring instruments for adjusting the pressure and for measuring the flow rate. The filter design permitted the filtering elements to be replaced and the thickness of the sediment layer to be measured. Chemical regeneration of the elements was effected outside of the filter, in special tanks, which ensured that the regenerated solutions were heated up to the specified temperature.

Preparation of the simulant-solutions for filtration, in accordance with the recommendations of [3, 4], consisted in treatment with flocculant-gelatin (100 mg/liter at 50°C over 30 min) and the introduction into the solution of an auxiliary filtering substance – perlite (2 g/liter).

Tests on an experimental-industrial annular filter confirmed the data obtained on laboratory apparatus [3, 4]: A high quality filtrate was obtained (with a suspended matter content of < 5 mg/liter), and an average filtration rate of 0.7 m^3/(m^2·h). As in the laboratory experiments, the specific resistance of the sediment r was constant (the dependence of t/q on the specific volume of filtrate q was linear, which confirms the constancy of the quantity r [6]); clogging of the pores was not observed.

In this filter, together with the filtration operations, a washing-off and pulp discharge cycle was devised. Before washing the sediment (filter cake) free from the important components it is necessary to dry it on compressed paper cartridges, and in order to ensure complete removal of the filter cake, to pulp it while feeding wash-water into the body of the filter.

It was found that the advantage of metalloceramic elements (especially finely porous titanium elements) is the small volume of the initial fraction of filtrate in which the passage of suspended matter was observed. It was found that periodically carried out "shock" and chemical regeneration permits the filteration capability of the barrier to be almost completely restored.

Life tests of the experimental-industrial filter, carried out during filtration of a solution with a makeup of 2 g/liter perlite and a pressure drop of 3 kg/cm^2 with "shock" regeneration of the cartridges after every filtration cycle and pulp discharge according to the above cycle, confirmed its efficiency. A total of 30 filtration cycles were carried out. On opening the filter after the life tests, the integrity of the cartridges was not damaged and no deposits had formed in the body of the filter.

Centrifugation

Preliminary investigations, carried out with suspensions of unirradiated VVÉR fuel elements on a special sector centrifuge and on laboratory test TsLN-2 and TsLS-31 centrifuges, showed that the required clarification (< 5 g/m^3 solid suspended matter in the fugate) is not achieved with separation factors of Fr < 20,000. The reason for this is the bouyancy of the fine particles of suspended matter, despite the relatively large difference of density of the solid ρ_s = 2.1 g/cm^2 and liquid ρ_l = 1.4 kg/cm^2 phases, which is caused obviously by the poor wettability of the particles (mainly graphite particles [3, 4], possessing hydrophobic properties). As a result of this, it was found that the quantity of particles settled in the centrifuges after a time t is not described by the well-known [7] linear or exponential expressions used in numerical centrifuge calculations, and based on the experimental determination of the separability of suspensions.

The particles could be separated only by using flocculants and surface-active substances such as gelatin, detergents (e.g., polyoxyethylene esters of isooctylphenol), and others, with Fr ≥ 8000.

The investigations showed the necessity for defining the separability of suspensions by the magnitude of the hydraulic coarseness ν_0 of the particles, the separation of which provides the required clarification. Moreover, it is necessary to know the magnitude of the minimum separation factor Fr_{min}, below which no separation of the suspensions takes place (in this case, Fr_{min} = 8000). It is obvious that in the centrifuge being designed, Fr must be not less than Fr_{min}, determined on laboratory centrifuges; ν_0 for laboratory centrifuges has been calculated from the equation

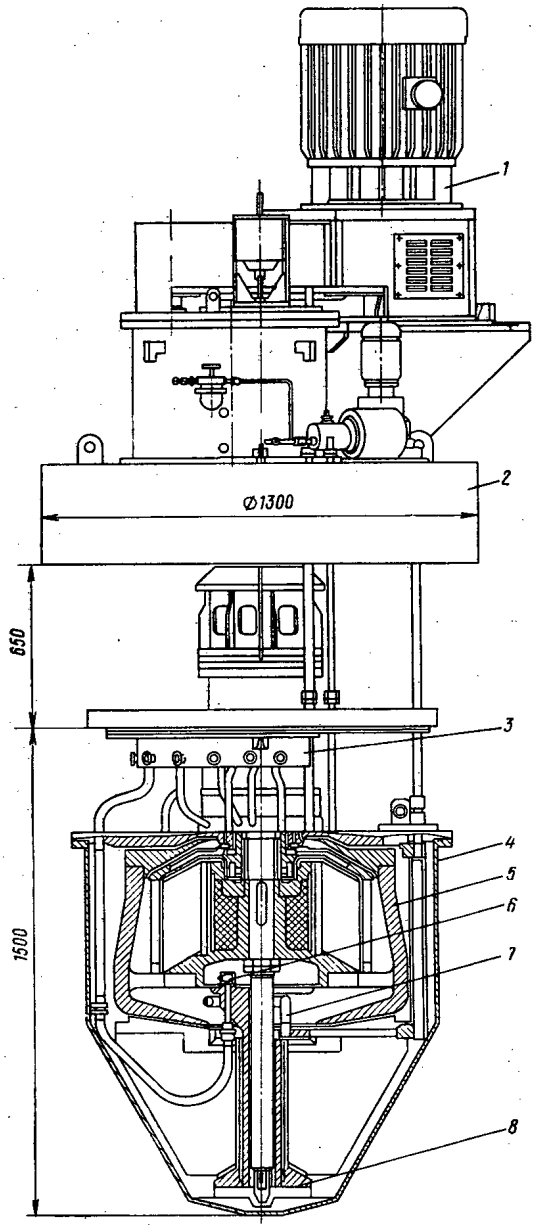

Fig. 3. General view of the OVS-540-80K supercentrifuge.

$$v_0 = \frac{g \ln \frac{R}{r_0}}{\omega^2 t}, \qquad (1)$$

where r_0 and R are the distances and radii from the axis of rotation to the free surface of the liquid and to the level of decantation of the clarified solution; ω is the angular velocity; t is the time; and g is the acceleration due to gravity.

The separability of the suspensions after their treatment with different flocculants, estimated by formula (1), varied over the range $(0.56\text{–}0.71) \cdot 10^{-6}$ cm/sec.

In order to choose the most effective flocculant, it is not sufficient to follow the greatest value of v_0, as loose, coarse floccules in the rotors of industrial centrifuges may be split up by the intensively moving streams of liquid, whereby some flocculants may form a foam, from which fine particles of suspended matter may be carried into the fugate. Therefore, the investigations were continued on the S-44 laboratory supercentrifuge, through the rotor of which the liquid passes turbulently.

During work on this machine, v_0 was determined by the formula

$$v_0 = \frac{gQ \ln \frac{R}{r_0}}{\pi\omega^2 l (R^2 - r^2)}, \quad (2)$$

where l is the length of the rotor; Q is the output of the centrifuge; r_0 and R are the radius of the free surface of the liquid in the rotor and in the inner part of the rotor, respectively.

The best flocculants were acknowledged to be not only those, which after treatment of the suspensions, provided the greatest value of $v_0 = 0.71 \cdot 10^{-6}$ cm/sec, calculated by formula (2); we also took into account the simplicity of the treatment cycle of the suspensions with the flocculants, the dosage, and the cost of the latter.

The results of the investigations permitted (for a known value of $v_0 = 0.71 \cdot 10^{-6}$ cm/sec) the basic parameters of the OVS-540-80K experimental separating supercentrifuge (Fig. 3) to be calculated, using the expression.

$$Q/v_0 = \Sigma,$$

where Σ is the productivity index of the machine.

The OVS-540-80K centrifuge is a settling, vertical centrifuge with a stack of separating plates, a rotor diameter of 540 mm and a useful reactor volume of 80 liter; the rotor is made from titanium and the remaining components, adjoining the working medium, are made from stainless steel. The machine (see Fig. 3) is made with the capability of remote servicing and disassembly; for this purpose, the drive 1 is fixed behind the biological shield 2, and all the conduits 3 which connect it with intermediate tanks and adjacent equipment, are coupled by means of the mechanism for remotely joining the conduits. In the centrifuge reactor 4 is located the rotor 5 with the plates, from which the clarified phase (fugate) is withdrawn during operation under pressure, by means of the fixed suction tube 6. The sediment, after accummulating in the rotor, is discharged by the pulping rotary tube 7 and is washed, for which the wash liquid is flushed into the reactor and is pumped over into the rotor by the high-capacity pump-turbine 8, whence the washed sediment is dumped in the form of a pump once again into the reactor by the tube. Finally, the washed and pulped sediment is removed from the centrifuge under the pressure of the turbine. The sediment can be discharged also without the tube by means of special scrapers.

The principal technical data of the machine are: $Fr_{max} = 11{,}000$; Q = 1 m^3/h; sump volume of rotor ~20 liters; number of plates 200. Cycle of operation: centrifuging up to filling of the rotor with sediment ~ 10 h and washing and discharge of the sediment ~ 3 h.

Thus, a cartridge filter and a centrifuge have been developed, with an output of 1 m^3/h, which provide a high degree of clarification of the VVÉR fuel element solutions (through-slippage of suspended matter < 5 mg/liter).

LITERATURE CITED

1. A. S. Zaimovskii, V. V. Kalashnikov, and I. S. Golovnin, Fuel Elements of Nuclear Reactors [in Russian], Atomizdat, Moscow (1966), p. 358.
2. V. B. Shevchenko et al., 4th Geneva Conference, Report No. 435 (1971).
3. A. M. Rozen, I. M. Mal'tsev, and D. V. Simakov, At. Énerg., 36, No. 6, 502 (1974).
4. A. M. Rozen et al., Proceedings of the 3rd CEMA Symposium on Investigations in the Field of Irradiated Nuclear Fuel Reprocessing [in Russian], Marianske Lazne, Czechoslovakian SSR, April 22-26 (1974).
5. M. F. Pushlenkov, At. Énerg., 33, No. 2, 625 (1972).
6. V. A. Zhuzhikov, Filtration [in Russian], Khimiya, Moscow (1968).
7. V. I. Sokolov and D. S. Torosyan, Izv. Vyssh. Uchebn. Zaved., Pishchevaya Tekhnologiya, No. 1 (1967).
8. M. G. Leibovskii, Filters under Pressure [in Russian], Izd. TsINTIkhimneftemash, Moscow (1969).

THEORY OF A MASS-DIFFUSION SEPARATIVE UNIT

V. A. Chuzhinov, V. A. Kaminskii,
B. I. Nikolaev, O. G. Sarishvili,
G. A. Sulaberidze, and A. A. Tubin

UDC 639.039.341.7

The mass-diffusion method of separation attracts the attention of specialists because of its universality in the separation of gaseous isotopic mixtures and because of the simplicity of instrumental design. Cascades of mass-diffusion units have been used for a long time in the production of isotopes of light and medium mass (^{13}C, ^{22}Ne, ^{36}Ar, ^{84}Kr, etc.) [1]. However, existing theory for a mass-diffusion separative unit does not yet permit one to solve the optimization problem for it.

The authors of [1, 2] used an approximation which considered a nearly ideal operating mode for mass-diffusion units in constructing a theory. Such an approximation enables one to make estimates of the overall separative effect in a unit but does not allow one to investigate the mutual effect on the separation process of the distributions of the vapor and gas flows on which the separative characteristics of mass-diffusion units depend significantly.

Based on a mathematical model which takes into account the actual processes taking place in the apparatus, this paper investigates the characteristics of a mass-diffusion unit and presents practical recommendations on the selection of optimal operating parameters for the unit.

The basic scheme of separative units based on the method of diffusion counter to a flow of vapor is shown in Fig. 1. The mass-diffusion unit consists of four basic elements: the evaporator 1, the diaphragm 3, and the two condensation surfaces 2 and 4. The thickness of the diaphragm is l; the coefficient of transparency is λ, which is defined as the ratio between the surface area open to flow and the total surface area of the diaphragm; the perimeter is P, and the height of the working portion is H.

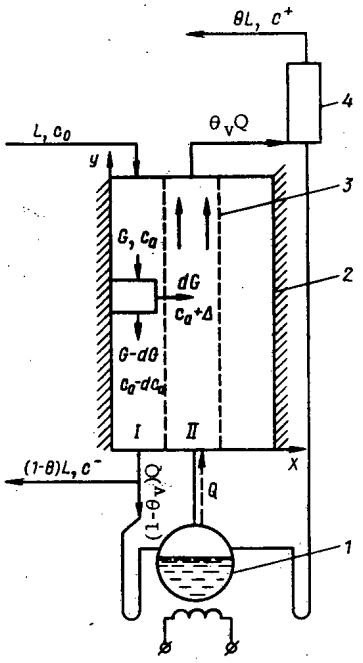

Fig. 1. Basic scheme of mass-diffusion unit.

Translated from Atomnaya Énergiya, Vol. 40, No. 6, pp. 471-475, June, 1976. Original article submitted July 27, 1975.

A flow L of the mixture being separated having a concentration c_0 of the light component is fed into the upper portion of the space between the diaphragm and the internal condenser 2. A portion $L' = \Theta L$ of the gas diffuses against the vapor flow through the porous diaphragm, being enriched in the process to a concentration c^+ of the light component because of the difference in the diffusion coefficients of the components of the mixture, and is extracted by the vapor from the upper end of the space II. The remaining portion of the gas, $L''=(1-\Theta)L$, emerges from the lower end of the space I depleted in the light component to a concentration c^-.

A vapor flow Q is fed into the lower portion of the space II. A portion $(1-\Theta_V)Q$ of the vapor flow passes through the openings of the diaphragm into the space I and is condensed on the surface of the internal condenser. The remaining portion of the vapor, $\Theta_V Q$, emerges from the upper portion of the space II together with the diffused gas and goes to the external condenser 4. We call the quantity $0 \leq \Theta_V \leq 1$ the vapor distribution factor.

In this process, the diaphragm serves to produce hydrodynamic flows in the required direction and is a partition with openings having a diameter exceeding the mean free path of the molecules.

The presence of a diaphragm in the diffusion space reduces the area through which diffusion occurs. It is easy to see that the reduction of this area is equivalent to an increase in the diffusion path in comparison with the geometric thickness of the diaphragm. This is taken into account by the introduction of the effective diaphragm thickness $l_e = l/\lambda$ [3].

In the theoretical analysis of the operation of mass-diffusion units, we limit ourselves to a two-dimensional, steady-state separation of a binary mixture neglecting thermal and pressure diffusion effects, which are unimportant in this process.

For an isotopic mixture, the relative difference of the diffusion coefficients of the components in the vapor,

$$\varepsilon_y = (D_{10} - D_{20})/D_{10} \tag{1}$$

is much less than one, which makes it possible in first approximation to write the diffusion equations for the two isotopes and the vapor in the form [1]

$$\tau - u\gamma = -nD_{10}\nabla\gamma; \tag{2}$$

$$\tau_1 - \tau c = -nD\gamma\,[\nabla c + \varepsilon c\,(1-c)\,\nabla \ln \gamma], \tag{3}$$

where $D = D_{10}D_{12}/[D_{10}\gamma + D_{12}(1-\gamma)]$ is the effective diffusion coefficient. These equations together with the equations of continuity for τ and τ_1 and the hydrodynamic equations form a complete system which is sufficient for a description of the process.

The solution of the problem of convective diffusion of a three-component mixture (vapor and the two components of the gas being separated) within the working volume of a unit is made difficult both by the complexity of simultaneous solution of the diffusion and hydrodynamic equations and by the complexity of the formulation of boundary conditions. Therefore a simplified model of a separative unit is considered. In that case, the following assumptions are made: Separation in the transverse direction is accomplished in an effective diffusion path length l_e; the concentrations γ and c in the spaces I and II are independent of the coordinate x; the longitudinal components u_y, τ_y, and τ_{1y} of the flux densities over the length l_e are small and can be neglected; since the hydraulic resistance of the diaphragm is considerably greater than the resistance of the internal spaces, one can assume that the flux density u of the vapor–gas mixture in the transverse direction is constant over the height of the unit.

Allowing for the assumptions made, integration of the x projection of Eq. (2) [1],

$$\tau_x - u\gamma = -nD_{10}\,(d\gamma/dx) \tag{4}$$

under the boundary conditions $\gamma(0) = \gamma_a$ and $\gamma(l_e) = \gamma_b$ yields expressions for the distribution of gas concentration in the vapor–gas mixture over the length of the diffusion path,

$$\gamma(x) = \frac{q(\gamma_a - \gamma_b)\exp(-ux/nD_{10}) - (\gamma_a - q\gamma_b)}{q-1} \tag{5}$$

and for the gas flux density through the diaphragm,

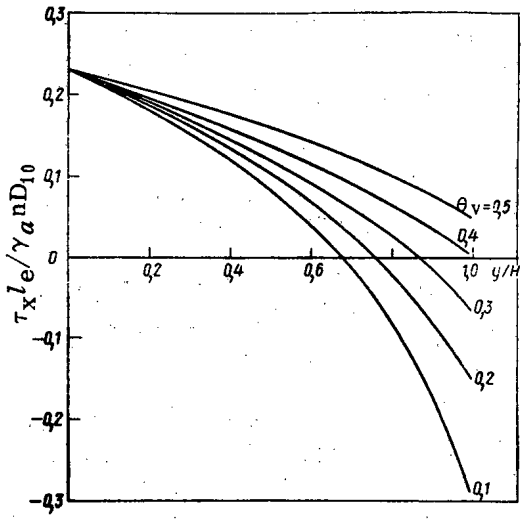

Fig. 2. Distribution of dimensionless gas flux density $\tau_x l_e/\gamma_a nD_{10}$ over height of unit for various values of Θ_V and ln q = 2.

$$\tau_x = u\,\frac{\gamma_a - q\gamma_b}{q-1} = \frac{nD_{10}}{l_e}\,\frac{\gamma_a - q\gamma_b}{q-1}\,\ln q, \tag{6}$$

where $\ln q = ul_e/nD_{10}$ is the Peclet diffusion number.

We determine the average gas concentration in the outer and inner spaces of the unit. Since the concentration in the outer space is mainly determined by condensation conditions, its value can be considered constant over the height of the unit. By integration of the x projection of Eq. (2) under the assumption gas flow can be neglected in comparison with vapor flow, one an easily find the distribution of gas concentration in the space I,

$$\gamma_I(x) = \gamma_0 \exp(-ux/nD_{10}), \tag{7}$$

where γ_0 is the gas concentration at the condenser wall.

Averaging the quantity γ_I (x) over the width a of the outer space yields

$$\gamma_a = \gamma_0 \frac{l_e}{a}\,\frac{1-\exp(-ux/nD_{10})}{\ln q}. \tag{8}$$

Since the flow of vapor is much greater than the flow of the light fraction ($\Theta_V Q \gg L'$), the flow of the vapor–gas mixture along the diaphragm in the space II can be expressed by the relation

$$U(y) = Q - u_P y, \tag{9}$$

and, consequently, the expression for the gas flow in this plane is written as

$$G'(y) = (Q - u_P y)\,\gamma_b(y). \tag{10}$$

The longitudinal variation of gas flow in the space II with Eq. (6) taken into consideration can be represented in the form

$$\frac{d}{dy}[(Q - u_P y)\,\gamma_b(y)] = u_P\,\frac{\gamma_a - q\gamma_b}{q-1}. \tag{11}$$

Integration of this equation under the boundary condition γ_b (y = 0) = 0 yields

$$\gamma_b(y) = \gamma_a\left[1 - \left(1 - \frac{u_P}{Q}\,y\right)^{1/(q-1)}\right]. \tag{12}$$

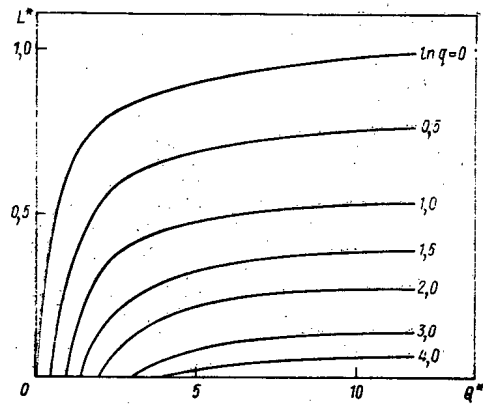

Fig. 3. Dependence of light-fraction flow on total vapor flow for various values of Peclet number.

Considering that gas flow through the partition is much less than vapor flow, one can write

$$uPy = (1-\theta_v)\,Q\frac{y}{H}. \tag{13}$$

The expression for γ_b is then tranformed to

$$\gamma_b(y) = \gamma_a\left\{1-\left[1-(1-\theta_v)\frac{y}{H}\right]^{1/(q-1)}\right\}. \tag{14}$$

Figure 2 shows the dependence on the longitudinal coordinate of the gas flux density through the partition in the dimensionless form $\tau_x l_e/\gamma_a nD_{10}$ for $\Theta = 0.5$. The quantity $\tau_x l_e/\gamma_a nD_{10}$ is a function of Peclet number and Θ_v only and does not depend on the geometry of the unit or on the properties of the gas being separated.

The behavior of $\tau_x l_e/\gamma_a nD_{10}$ shows that the gas flux density decreases with height and possibly changes sign for a given relation between Θ_v and ln q. This is explained by the fact that reverse convective transport $u\gamma$ begins to predominate over diffusion gas transport through the diaphragm as the gas concentration rises in the inner space. Having set $\tau_x = 0$ in Eq. (6), it is easy to obtain the inversion point for the flux density with a given operating mode of the unit (given Θ_v and ln q):

$$y^* = \frac{1-(q-1/q)^{q-1}}{1-\theta_v}H. \tag{15}$$

A change in the sign of $\tau_x(y)$ means that a portion of gas which has diffused into the inner space of the unit is retransported into the condenser space, i.e., the unit operates with an internal gas circulation. Assuming that the coordinate of the inversion point is H, we obtain from Eq. (15) the condition under which internal circulation is as yet absent in the unit:

$$\theta_v^* = (q-1/q)^{q-1}. \tag{16}$$

For values $\Theta_v < \Theta_v^*$, the unit operates with internal circulation.

To determine the flow L' of the light fraction emerging from the unit, we consider the gas balance in an arbitrary cross section of the unit. Neglecting transport of matter by longitudinal diffusion, we have

$$dG = -P\,\tau_x\,dy, \tag{17}$$

where G(y) is the flow in some cross section y of the outer space of the unit.

Considering Eqs. (8) and (15), and integrating Eq. (17) along the channel,

$$\int_{(1-\theta)L}^{G} dG = -\int_0^y P\,\tau_x\,dy, \tag{18}$$

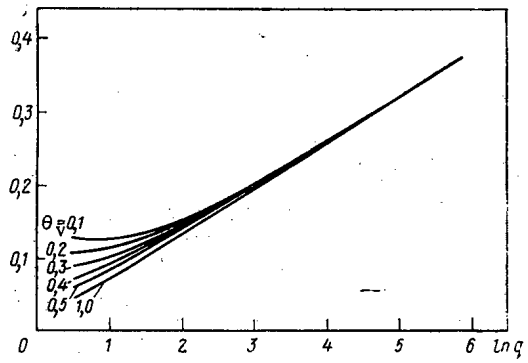

Fig. 4. Dependence of enrichment factor ε on ln q for various values of the vapor distribution factor and Θ = 1/2.

we obtain the distribution of gas flow in the outer space:

$$G=(1-\theta)L-\mathrm{P}H\frac{nD_{10}}{l_e}\gamma_a\ln q\times\left\{\frac{y}{H}-\frac{1}{1-\theta_V}\{1-[1-(1-\theta_V)\,y]^{q/(q-1)}\}\right\}. \tag{19}$$

Considering that G(H) = L, we obtain from Eq. (19) the magnitude of the flow of the light fraction,

$$L'=\theta L=\mathrm{P}H\frac{nD_{10}}{l_e}\gamma_a\theta_V\frac{1-\theta_V^{1/(q-1)}}{1-\theta_V}\ln q \tag{20}$$

and of the flow into the unit,

$$L=\frac{1}{\theta}\mathrm{P}H\frac{nD_{10}}{l_e}\gamma_a\theta_V\frac{1-\theta_V^{1/(q-1)}}{1-\theta_V}\ln q. \tag{21}$$

Equation (21) shows that the feed flow L depends on the gas-flow partition factor Θ, i.e., on the scheme for combining units into a cascade. One should make note of the particular feature of a cascade of mass-diffusion units operating in a given mode (for given Θ_V and ln q) which is manifested by the fact that the flow L' of the light fraction does not depend on Θ.

Using the condition (13), Eq. (20) can be presented in the form of a criterial equation,

$$L^*=Q^*\left(1-\frac{\ln q}{Q^*}\right)\left[1-\left(1-\frac{\ln q}{Q^*}\right)^{1/(q-1)}\right], \tag{22}$$

which is suitable for explaining the physics of the process and for establishing a relation between total vapor flow, Peclet diffusion number, and the flow of light fraction produced by the unit. In Eq. (22), $L^*=L'l_e/\mathrm{PH}\cdot\gamma_a n\bar{D}_{10}$ and $Q^*=Ql_e/\mathrm{PHn}D_{10}$ are dimensionless quantities respectively characterizing the flow of the light fraction and the total vapor flow fed into the unit. Figure 3 gives the dependence of L* on Q* calculated from Eq. (22) for various Peclet numbers. Setting y = H in Eq. (13), it is easy to obtain a relation between ln q and the total vapor flow:

$$\ln q=(1-\theta_V)\,Q^*. \tag{23}$$

It is clear from Fig. 3 that the flow of the light fraction depends on the total vapor flow and on the vapor distribution factor. When $Q_V = 0$, which corresponds to passage of all the vapor through the partition, L* = 0. Therefore, each curve begins at the point Q* = ln q when L* = 0. It is then also clear that the flow of the light fraction increases as Θ_V increases.

We turn to a calculation of the separation produced by a mass-diffusion unit. Equation (6) indicates that τ_x is independent of the x coordinate and therefore, for the assumed model of a mass-diffusion unit, one can consider that transverse transport of the light component is only realized because of its concentration gradient along the diffusion path l_e. Then one can obtain from Eq. (3) the differential equation

$$\frac{d(c'-c)}{dx}-\frac{\tau_x}{nD\gamma}(c'-c)-\varepsilon_0 c(1-c)\frac{d\ln\gamma}{dx}=0 \tag{24}$$

for transverse transport of the light component, assuming $\tau_{1x}=\tau c'$ where c' is its concentration at the beginning of the diffusion path.

In separation of isotopes, their concentration changes little in the transverse direction of the unit, which makes it possible to consider the quantity c(1−c) a constant in Eq. (24). Using this assumption, integration of Eq. (24) over the diffusion path length under the boundary conditions c(0) = c' and $c(l_e)$ = c" leads to an expression for the concentration differential of the light component produced in the partition:

$$\Delta=c''-c'=\varepsilon_0 c(1-c)\frac{q}{\mu\gamma_a}\frac{\gamma_a-\gamma_b}{\gamma_a-q\gamma_b}\times[\exp(\mu\tau_x l_e/nD_{10})-1], \tag{25}$$

where $\mu = 1 - (D_{10}/D_{12})$.

Let the gas flow be G in some cross section y of the outer space and let the concentration of the light component be c_a. In an interval dy, the flow through a channel boundary is dG at a concentration $c_a + \Delta$, with the increment of concentration being given by Eq. (25). Denoting the small change of concentration along dy by dc_a, we obtain from the balance of flows in the selected elementary segment

$$dG\Delta=G\,dc_a \tag{26}$$

neglecting smallness of second order and transport of matter by longitudinal diffusion. Using Eqs. (17) and (25), introducing the notation

$$\alpha=\frac{q}{\mu\gamma_a}\frac{\gamma_a-\gamma_b}{\gamma_a-q\gamma_a}[\exp(\mu\tau_x l_e/nD_{10})-1] \tag{27}$$

and separating the variables, we rewrite Eq. (25) in the form

$$\frac{dc_a}{c_a(1-c_a)}=-\varepsilon_0\frac{\alpha P\tau_x}{G}\,dy. \tag{28}$$

Integration of Eq. (28) along the unit,

$$\int_{c^-}^{c_0}\frac{dc_a}{c_a(1-c_a)}=-\varepsilon_0 P\int_0^H\frac{\alpha\tau_x}{G}\,dy \tag{29}$$

yields a relation for the enrichment factor of the heavy fraction:

$$\varepsilon^-=\ln\frac{c_0/(1-c_0)}{c^-/(1-c^-)}=-\varepsilon_0 P\int_0^H\frac{\alpha\tau_x}{G}\,dy, \tag{30}$$

where τ_x and G are defined by the appropriate equations.

Using the well-known relation between the enrichment factors for the light and heavy fractions (ε^+ and ε^-) and the total enrichment factor ε [4],

$$\frac{\theta}{1-\theta}\varepsilon^+=\varepsilon^-=\theta\varepsilon, \tag{31}$$

we obtain for the quantity ε the expression

$$\varepsilon=-\frac{1}{\theta}\varepsilon_0 P\int_0^H\frac{\alpha\tau_x}{G}\,dy. \tag{32}$$

The integral on the right side of Eq. (32) can only be evaluated numerically in the general case. In the

particular case of very high vapor flow rates, where the value of the vapor distribution factor Θ_v is close to one, the value of gas concentration in the inner space of the unit can be assumed to be zero. Then the solution of the equation system (2)-(3) is considerably simplified and yields for the enrichment factor and flow of the light fraction expressions which agree with those given in [1, 2]:

$$\varepsilon = \varepsilon_0 \frac{q \ln q}{q-1} \frac{1}{\theta} \ln \frac{1}{1-\theta}; \tag{33}$$

$$L' = P H \frac{nD_{10}}{l_e} \gamma_a \frac{\ln q}{q-1}. \tag{34}$$

Figure 4 shows typical relationships between the enrichment factor and the diffusion Peclet number calculated from Eq. (32) for various values of the vapor distribution factor and $\Theta = 1/2$. The curve for $\Theta_v = 1$ corresponds to the limiting case $\gamma_b = 0$. The fact that the curves $\varepsilon = \varepsilon(\Theta_v, \ln q)$ practically coincide when $\ln q \gg 2$ indicates the insignificant effect of the gas in the space II on the diffusion of the components of the mixture being separated. Therefore the approximate theory, which is based on the assumption of an absence of gas in the inner space, can be used successfully to evaluate the enrichment factor. Equation (33) is particularly convenient in that the dependence of ε on the gas flow partition factor Θ is explicitly expressed in it.

However, the approximation $\gamma_b = 0$ is unsuitable for calculation of the flow of the light fraction. The fact is that there is a reverse convective transport of gas in actual separative units which depends on the magnitude of γ_b, and neglect of gas concentration in the inner space is equivalent to neglect of this reverse transport. Such a situation leads to an overestimate in the calculated values of the emerging flow L' in comparison with the values achieved in practice.

The authors are grateful to I. G. Gverdtsiteli for discussions of the results, valuable advice, and continuing consideration of the work.

LITERATURE CITED

1. I. G. Gverdisiteli and V. K. Tskhakaya, in: Isotope Production [in Russian], Izd. Akad. Nauk SSSR, Moscow (1958), p. 113.
2. I. G. Gverdtsiteli et al., in: Proceedings 2nd Geneva Conference [in Russian], Reports of Soviet Scientists, Vol. 6, Atomizdat, Moscow (1959), p. 69.
3. R. Ivans et al., J. Chem. Phys., 35, 2076 (1961).
4. N. A. Kolokol'tsov, At. Énerg., 27, No. 1, 9 (1969).

INDUCED ACTIVITY OF BUILDING AND STRUCTURAL MATERIALS IN THE 680-MeV SYNCHROCYCLOTRON HALL

V. F. Kas'yanov, M. M. Komochkov, Yu. G. Teterev, and V. V. Mal'kov

UDC 539.16.04:621.384.67

In this paper, we have investigated the principal mechanisms of activation of building and structural materials in the scattered field of neutrons, which would permit the induced activity to be forecast at any point of the accelerator hall. The problem is solved by determining the radioisotopic composition in irradiated samples of materials and by measuring the radiation dose intensity from the induced activity. The activity of the isotopes and the dose intensity from the induced activity were compared with the flux densities of neutrons of different energy groups, measured by threshold detectors. The neutron flux density (neutrons/$cm^2 \cdot sec$) at different parts of the synchrocyclotron hall amounts to $10^5 - 10^6$, $10^5 - 10^6$ for thermal and intermediate neutrons, $10^3 - 10^6$ for fast neutrons with E = 2 - 20 MeV and $10^2 - 10^6$ for relativistic neutrons when E > 20 MeV.

Samples of iron, normal concrete, copper, and aluminum at different points of the accelerator hall served as building and structural materials. The activity of the isotopes in the samples was measured with NaI(Tl) and Ge(Li) spectrometers.

Table 1 shows the specific activity of the isotopes in structural materials, which make the main contribution to the radiation hazard and the spread of its values. The samples of iron and concrete are taken at different parts of the accelerator hall. The presence in iron of ^{60}Co is explained by impurities of cobalt (~ 10^{-4} g/g) and the isotope ^{56}Mn with its origin is due mainly to impurities of $3 \cdot 10^{-3}$ g/g of manganese.

Similar irradiation conditions permitted different materials to be compared with respect to their radiation hazard from induced activity. The total of the specific activities of the products formed were compared by their totoal γ constants for each material. For Fe, Cu, Al, and concrete, the ratios of these values at infinite irradiation are as follows: 10:20:10:1, respectively, over 1 h, and 1:0.6:0.4:0.1 over 90 days after completion of irradiation.

A relation was established between the dose intensity generated by the γ radiation from the induced activity, and the flux density of neutrons with energies of 2 < E < 20 MeV, which applies within the limits of $(0.4\text{–}1.5) \cdot 10^4$ mrem/h $\cdot$ n/$cm^2 \cdot$ sec.

Measurements showed that the dose intensity of the γ radiation from the induced activity of the dee is predominant only in the vicinity of the accelerator; at other locations, the dose intensity is determined by the radiation of all the structures in the hall.

(No. 848/8375. Paper submitted June 23, 1975. Complete text 0.6 author's folio, 2 Figs., 6 Tables, 12 Refs.)

TABLE 1. Specific Activity of Isotopes, disintegrations/(sec · g)

Material	^{64}Cu	^{60}Co	^{58}Co	^{59}Fe	^{56}Mn	^{54}Mn	^{24}Na	^{22}Na
Copper	$2 \cdot 10^4$	45	100	—	—	20	—	—
Iron	—	2—15	—	4—50	100—1300	1—400	—	—
Aluminum	—	—	—	—	1000	10	400	50
Ordinary concrete	—	—	—	—	3—30	0,1—2	4—40	0,2—10

Translated from Atomnaya Énergiya, Vol. 40, No. 6, p. 478, June, 1976.

CALCULATIONS OF SOME CHARACTERISTICS OF THE γ-RADIATION FIELD INDUCED IN AIR BY FAST NEUTRONS

A. V. Zhemerev, Yu. A. Medvedev, and B. M. Stepanov

UDC 539.124.17

The article describes a method of calculating the intensity and the absorbed energy of γ radiation and the electron flux generated by γ radiation which is induced in air by a pulsed isotropic point source of fast neutrons ($E \leqslant 14$ MeV).

The Monte Carlo method was used to calculate the intesity of the γ radiation induced in air by fast neutrons. When the history of a neutron is modeled, neutron capture is brought into account by statistical weights. The yield of the γ radiation induced by neutrons depends upon the probability of a γ quantum leaving after a neutron collision; the probability is equal to the ratio of the sum of the cross sections of the processes accompanied by the emission of γ quanta to the total cross section. The energy of the induced γ quantum is statistically determined from all possible energies of γ quanta. Algorithmic expressions for the space-and time-dependent intensity of the γ radiation generated by a γ quantum induced by a collision of neutrons are stated. When the neutron reaches an energy $E \leq 0.45$ MeV, the neutron history is no longer modeled and the intensity of the γ radiation is calculated with the results given in the article by A. V. Zhemerev et al. [At. Énerg., 38, No. 3, 174 (1975)].

The method was used to calculate the intensity of the γ radiation induced by fast neutrons at high energies (neutron energies in excess of 4 MeV); monochromatic neutron sources with the initial energies 6, 8, 10, 12, and 14 MeV were considered. A program for the calculation was written in FORTRAN for the BÉSM-6 computer. The results of the calcuation for a neutron source with the initial energy 10 MeV are stated. The qualitative characteristics of the γ-radiation intensity induced by neutron sources with other initial energies are the same. A maximum is observed in the spatial dependence of the γ-radiation intensity; the distance between the maximum and the source increases in the course of time, because the number of neutrons at a large distance from the source increases.

The article includes algorithmic expressions for calculating with the Monte Carlo method the absorbed energy of γ radiation and the radial component of the electron flux caused by the γ radiation which was induced in air by fast neutrons.

(No. 852/8377. Article received June 23, 1975; annotation received December 22, 1975. Complete text 0.4 author's folio, 1 Fig., 1 Table, and 6 Refs.)

ELECTROCHEMICAL BEHAVIOR OF METALS IN THE RADIATION FIELD OF A NUCLEAR REACTOR

G. Z. Gochaliev and S. I. Borisova

UDC 539.12.08

The investigations were concerned with the electrochemical behavior of platinum and gold in an H_2SO_4 solution and of silver of various degrees of oxidation in an alkaline solution; the solutions were exposed to the radiation field of the water-cooled target reactor. The tests were made in reactor channels which are either inside the core or beyond it; the power ranged from 0.05 to 3.0 MW.

The electrochemical behavior of these metals in the radiation field of the reactor depends mainly upon the radiolysis products of the solutions. At high intensities of $1.2\text{-}2.10^4$ rad/sec of a mixed radiation, the platinum potential, which is close to the hydrogen potential, is hardly affected by disturbances of stoichiometry, which result from the air's oxygen dissolved in the solution or from gaseous hydrogen leaving the system.

The stability of the hydrogen potential at platinum is explained by the selectivity of the electrode on the one hand and by the high rates at which radiolysis products are formed, on the other. The possibility of the

solution being oversaturated with hydrogen at high dose rates cannot be ruled out.

The potential of gold is first shifted to positive values under the influence of the reactor radiation and stabilizes at ~ 0.80 V. However, prolonged irradiation shifts the potential to the negative side of the stationary value; the extent of the shift increases with increasing power of the reactor.

The stationary potential of silver stabilizes at ~ 0.90 V in alkaline solutions. Platinum electrodes and oxidic silver electrodes reach the same potential value upon prolonged irradiation in the same alkaline solution.

The instability of the potential of the oxidic silver electrode is explained by the interaction of the radiolysis products (particularly hydrogen peroxide formed upon irradiation) with the oxidic phase of the silver. The validity of this explanation was confirmed by control tests without irradiation.

The slope of the cathodic polarization curves of silver is ~ 10 mV on a semilog scale. This small slope was explained by a reduction of the radiolysis products at silver; the reduction of the superificial oxides formed by the chemical interaction of the radiolysis products with the metal is the electrochemical stage. The chemical stage with the oxidation of the surface implies that products identical with unstable radiolysis products are simultaneously formed. In alkaline solutions the processes are described by the following scheme

$$Me + O_2' + H_2O \rightarrow Me{-}O + OH + OH'$$
$$Me{-}O + 2e + H_2O \rightarrow Me + 2OH'$$
$$OH + H_2O_2 + OH' \rightarrow O_2' + 2H_2O$$

The corresponding scheme for acid solutions is stated.

(No. 849/8460. Paper submitted August 6, 1975. Complete text 0.65 author's folio, 5 Figs. and 25 Refs.)

PRODUCTION AND STUDY OF CORROSION RESISTANCE IN ZIRCONIUM DIBORIDE AND ITS SOLID SOLUTIONS WITH TITANIUM DIBORIDE

V. V. Svistunov, A. R. Beketov, V. G. Vlasov, and N. V. Obabkov

UDC 546.831.271:620.193.2

The practical application of zirconium boride is of special interest because of its high chemical durability. In order to improve some of the physical and chemical properties of ZrB_2, admixtures of TiB_2 are added to form solid solutions.

In these studies samples were used that were obtained by a combination method including high temperature self-ordering fusion and activated sintering. The samples had a residual porosity of 2.4 vol.% and were in the shape of plates of size 2 × 6 × 6 mm. They were used for oxidation in a $3 \cdot 10^{-4}$ liter/min flow of pure oxygen.

During oxidation of ZrB_2 samples it was found that over the temperature interval 300–700°C the rate of oxidation increases somewhat while remaining insignificant, then decreases (800°C) and increases sharply at temperatures above 800°C. All the curves fit a paralinear oxidation law.

The dependence of the oxidation rate on the oxygen pressure is complicated. In the low pressure range up to 50 torr the oxidation rate increases with a pressure rise. This is due to the high volatility of boron oxides. A further increase in the pressure to 75 torr suppresses the volatility of the oxides, the amount of B_2O_3 in the protective film increases, and the oxidation rate decreases and later increases again.

The kinetics of the oxidation process is complex and to a great extent depends on the amount of boron oxides in the protective layer. During oxidation of mixed borides the oxide layer is enriched in titanium which causes formation of $ZrTiO_4$ in all samples, which sharply impairs the protective properties of the surface scale [1].

The apparent activation energy for oxidation of ZrB_2 is 20 kcal/mole. Small admixtures of TiB_2 (about

8 mol. %) reduce this to 14 kcal/mole, but depending on the increased amount of TiB_2 in the solid solution the activation energy increases and for 30 mol. % TiB_2, it is 30 kcal/mole.

The paralinear oxidation law, experiments with an inert tracer, and the appearance of the oxidized samples [2] lead us to assume that oxidation of ZrB_2 in solid solutions takes place in a diffusive regime with predominant diffusion of oxygen to the reaction interface at the boride–oxide film.

LITERATURE CITED

1. I. N. Frantesevich, R. F. Voitovich, and V. A. Lavrenko, High-Temperature Oxidation of Metals and Alloys [in Russian], Gostekhizdat UkrSSR, Kiev (1963).
2. J. Benard, Oxidation of Metals [Russian translation], Metallurgiya, Moscow (1968).

(No. 850/8465. Paper submitted August 12, 1975. Complete text 0.5 author's folio, 3 Figs., 2 Tables, 19 Refs.)

THERMALIZATION OF NEUTRONS IN SOLIDS

V. A. Baikulov

UDC 621.039.512.45

The variational method for calculating the distribution of slow neutrons in infinite homogeneous media with uniformly distributed sources of fast neutrons described and tested in [1] for a gaseous moderator model is extended to a solid medium.

No limitations of any kind are placed on the behavior of the neutron absorption cross section in the thermalization region. The incoherent Gaussian approximation is used for the differential scattering cross section.

A method for computing the dispersion is described which is based on use of experimental values of the generalized frequency distribution for liquids and the characteristic normal oscillation mode functions for crystals. A method is developed for calculating the matrix elements characterizing the scattering of neutrons by solid systems.

The energy distribution of slow neutrons in water is computed at temperatures of 295 and 423°K with ^{10}B, ^{113}Cd, and ^{149}Sm as absorbers. The effect of various regions of the generalized frequency distribution for water on the slow neutron spectrum is studied. A comparison is made with known models and experimental data. It is shown that a model using the low frequency distribution given in [2] in combination with the high frequency distribution of Nelkin (two vibrational levels with energies of 0.205 and 0.481 eV with the "weights" of the two levels in the ratio 1:2) with the ratio of the contributions from these distributions being 1:2.38 agrees better with the experimental data of [3] than Nelkin's model (see Fig. 1).

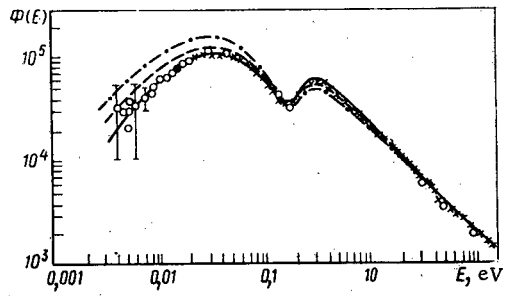

Fig. 1. Energy distribution of the slow neutrons, Φ(E), in water at a temperature of 295°K with the absorption cross section of cadmium equal to 15.4 barns per atom of hydrogen at energy E = kT: ———) model in this work; - - - -) Nelkin's model; - · - · -) gaseous model; ○) and ×) experiment.

LITERATURE CITED

1. V. A. Baikulov, At. Énergy., 31, No. 5, 507 (1971).
2. P. Egelstaff, B. Haywood, and J. Thorson, in: Inelastic Scattering of Neutrons in Solids and Liquids, Vol. 1, IAEA, Vienna (1963), p. 343.
3. J. Beyster, Nucl. Sci. and Engng, 9, No. 2, (1961).

(No. 851/8483. Paper submitted Novermber 16. 1975. Complete text 0.6 author's folio, 7 Figs., 1 Table, 10 Refs.)

LETTERS

USING DIAMOND DETECTORS AS IMMERSED α COUNTERS

S. F. Kozlov, E. A. Konorova,
M. I. Krapivin, V. A. Nadein,
and V. G. Yudina

UDC 621.376

The parameters of diamond detectors for ionizing radiations were studied in [1-3]. The fact that the diamond detectors are not affected by chemically agressive media is one of the main advantages of these detectors. It is interesting to explore the possibilities of using diamond detectors for measuring the α activity without need for preparing thin, dry samples when the detector is in direct contact with the solution.

It is known from the previously published papers that when the sensitive surface of semiconductor detectors, e.g., silicon detectors [4], is in contact with a liquid, there occur several phenomena which imply that the characteristics of immersed detectors differ substantially from the characteristics of detectors with gold coating.

We consider in the present work the characteristics of a diamond detector recording the α radiation from solutions; the sensitive surface of the detector was in contact with the electrolyte. For the measurements on the solution, the detector was hermetically glued to a lateral ground-in joint of a glass column (Fig. 1). The α activity was measured in bimolar nitric acid solutions of ^{239}Pu in concentrations between 10 and 100 $\mu g/cm^3$. An "Amur" pulse amplifier, a 512-channel LP-4050 pulse analyzer, and a PP9-1 scaler were used to record the α particles and to measure the amplitude spectra of the pulses. A detector in the form of a $\sim$ 100-μ-thick diamond plate was used for our measurements. One of the detector faces had a chemically stable contact which had been obtained by ionic alloying of the diamond with boron; the opposite face of the detector carried a contact of deposited gold.

Two series of measurements were made. In the first series, the detector was glued to the column so that the diamond surface alloyed with the boron was in direct contact with the solution on which the measurements were to be made. A bias voltage of +330 V was applied to the gold contact; the second contact was grounded through the electrolyte with the aid of a stainless steel electrode. Figure 2a shows the amplitude spectrum obtained in this case. In the second series, the gold contact was removed from the detector and the diamond plate was glued to the ground-in column section with the diamond face from which the gold coating had been removed. Thus, the α active solution was in direct contact with a surface of pure diamond. A bias voltage of +450 V was applied to the boron contact; an external electrode was used for grounding via the electrolyte (Fig. 2b). When the pure surface of the diamond crystal was in direct contact with the electrolyte (gold contact removed), the maximum amplitude of the pulse spectrum was 4.5 times smaller than the maximum amplitude of the spectrum obtained in measurements made with the detector provided with two contacts. This result can obviously be explained by phenomena which occur at the contacts, i.e., at the diamond–electrolyte interface.

The time-dependent counting characteristics of the diamond detector were checked with the surface of the pure diamond in contact with the α active solution. Plutonium nitrate solutions with concentrations of 10.3, 20.7, 52.4, and 102.3 $\mu g/cm^3$ were used for the measurements. The number of pulses counted per unit time depended linearly upon the plutonium concentration of the solutions. No changes of the counting characteristics of the diamond detector were observed during ten days when the diamond detector was continually in contact with the plutonium nitrate solution.

The experiments have shown that, in principle, diamond detectors can be used as immersed α counters

Translated from Atomnaya Énergiya, Vol. 40, No. 6, pp. 482-483, June, 1976. Original article submitted December 30, 1974.

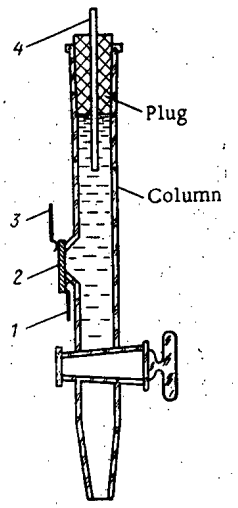

Fig. 1

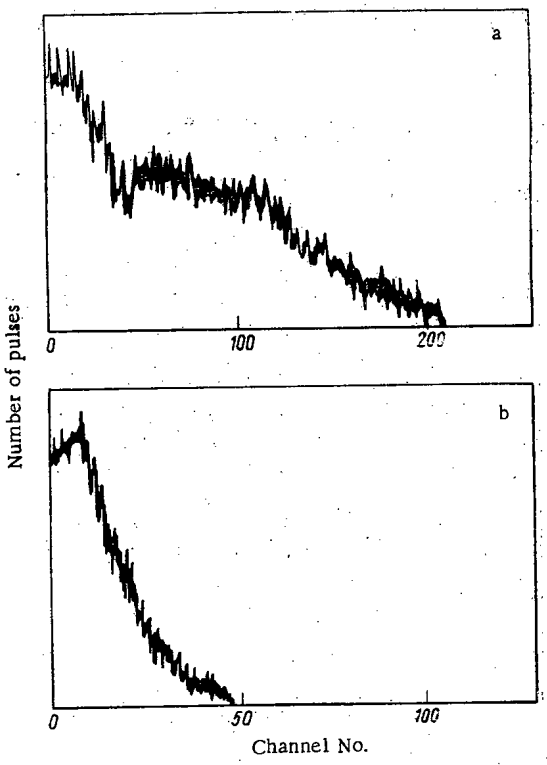

Fig. 2

Fig. 1. Glass column with a diamond detector glued to it: 1) contact with the surface obtained by ionic alloying of the diamond with boron; 2) diamond plate; 3) contact with the surface, sputtered gold; 4) stainless steel electrode.

Fig. 2. Amplitude spectra of the pulses obtained by recording the α radiation of a solution: a) when the electrolyte touched the boron contact; and b) when the electrolyte was in direct contact with the diamond surface.

either when diamond is alloyed with boron or when pure diamond is in direct contact with the solution. However, immersed diamond detectors with a chemically stable contact obtained by ionic alloying (doping) or carbidizing have the best counting characteristics.

LITERATURE CITED

1. E. A. Konorova, S. F. Kozlov, and V. S. Vavilov, Fiz. Tverd. Tela, 8, 3 (1966).
2. E. A. Konorova and S. F. Kozlov, Usp. Fiz. Nauk, 98, No. 4, 735 (1969).
3. E. A. Konorova and S. F. Kozlov, Fiz. i Tekh. Poluprov., 4, No. 10, 1865 (1970).
4. L. Cathey and W. Jenkins, Trans. Nucl. Sci., 9, No. 3, 193 (1962).

SENSITIVITY OF EMISSION DETECTORS TO γ RAYS

G. V. Kulakov and B. V. Mukhachev

UDC 539.1.08

An emission detector is a system of electrodes of different materials spatially separated in vacuum. The current in the detector is caused by counter flow of electrons knocked out of the electrodes by γ quantas.

The object of the present work is to construct analytical models and to investigate experimentally the sensitivity of emission detectors with quartz tube between the electrodes in the fields of stationary high intensity (up to 10^6 R/sec) γ radiation. The main advantages of such detectors are the operation without external supply sources, high thermal and radiation stability, small dimensions, and the absence of an upper limit of the intensity of the exposure dose [1, 2].

The construction of a vacuum emission detector is shown in Fig. 1. Tantalum with 0.3 mm thickness, zirconium or stainless steel with 0.7 mm thickness was used as the emitter. The outer diameter of the emitters was 5.4 mm. A quartz tube of 3.2-mm diameter and 0.5-mm-thick wall was used as the insulator. The remaining parts were made of stainless steel. The diameter of the collector was 1.8 mm. The length of the sensitive part was 150 mm. A heat and radiation proof KTMS(S) cable with magnesium oxide insulation and stainless steel casing was used for signal transmission. The detector was assembled in $5 \cdot 10^{-5}$ mm Hg vacuum.

When the detector is irradiated, electric current is produced not only in the sensitive part but also in its connecting part and in the cable. In order to take into consideration the contribution of these currents to the detector sensitivity measurements were carried out with a compensated detector having similar construction but without the sensitive part.

It is shown in [3, 4] that the basic characteristics of emission detectors are well described by an analyt-

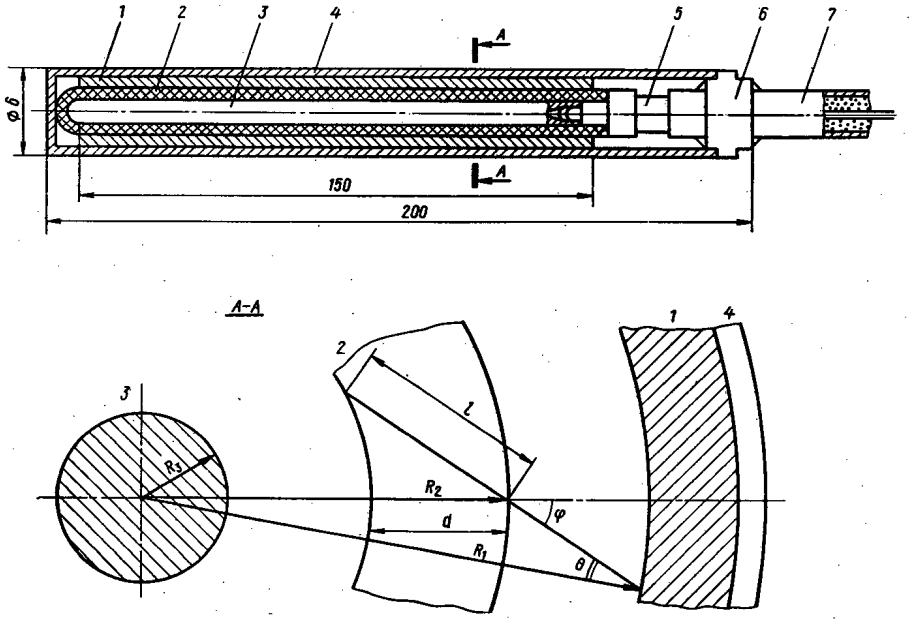

Fig. 1. Vacuum emission detector: 1) emitter; 2) insulator (quartz tube); 3) collimator; 4) vacuum casing; 5) metal–ceramic joint; 6) sleeve; 7) cable.

Translated from Atomnaya Énergiya, Vol. 40, No.6, pp. 483–485, June, 1976. Original article submitted January 10, 1975; revision submitted October 20, 1975.

TABLE 1. Sensitivity of Emission Detectors, pA(R/sec)

Emitted material	Energy; MeV	Computation		Experiment
		without tube	with tube	with tube
^{73}Ta	1,25	2,34	2,60	2,32±0,18
	0,661	5,70	2,82	—
	0,412	5,60	1,82	—
^{40}Zr	1,25	0,62	0,73	0,60±0,04
	0,661	1,01	0,50	—
	0,412	4,32	1,81	—
^{26}Fe	1,25	0,14	0,82	0,22±0,03
	0,661	0,13	0,92	—
	0,412	0,07	1,82	—

ical model that provides for the separation of the spectrum of the emitted electrons into fast (E > 50 eV) and slow (E < 50 eV) groups. When the difference in the atomic numbers of the electrode materials is quite large, the contribution of the slow electrons is small (15-20%) and can be disregarded [4].

In view of the lack of data on the secondary emission characteristics of quartz glass in the present work we do not consider the contribution of the slow electrons in constructing the analytical model; also it is assumed that the sensitivity does not depend on the angle of incidence of γ quanta at the electrodes [5] and that the probability of electron yield in the "forward" direction is equal to one half the probability of yield in 4π steradian.

Under these assumptions the analytical models of the sensitivity due to fast electrons have the following form:

for the detector with quartz tube

$$S_{cal} = -(eN2\pi h/2)\{F_1R_1T_{1;2}A_{2;3} + F_2R_2A_{2;3} - F_3R_3A_{3;2}[1-A_{2;3}(1-A_{3;2})]\}; \quad (1)$$

for the detector without quartz tube

$$S_{cal} = -(eN2\pi h/2)\{F_1R_1A_{1;3} - F_2R_3A_{3;1} \times [1-A_{1;3}(1-A_{3;1})]\}, \quad (2)$$

where S_{cal} is the calculated sensitivity of the detector, A/(R/sec); e is the electron charge ($1.6 \cdot 10^{-19}$ C/electron); h is the length of the electrode, cm; N is the flux of γ quanta with energy E_γ, MeV, causing unit exposure dose, quant/(R·cm^2); F_c is the yield probability of fast electron from the i-th material per γ quantum in 4π steradian, electron/quantum; R_c is the radius of the i-th material, cm; $T_{1,2}$ is the probability of an electron from the emitter falling into the space between the quartz tube and the collector; A_{ij} is the probability of absorption of electrons from the i-th material in the j-th material.

The probability of yield of fast electrons F_i from the materials of the emitters, collectors, and quartz glass for different energies of γ quanta is computed from the data of [4, 6]. The probability $T_{1,2}$ is obtained under the assumption that all the electrons fly off in the plane perpendicular to the axis of the detector (see Fig. 1):

$$T_{1;2} = \left(\int_0^{\theta_{max}} d\theta \int_{E_{min}}^{E_{max}} dE\Psi(\theta, Z_1) \times m(E, Z_1)\, P_{1;2}\right) \Big/ \int_0^{2\pi} d\theta \int_{E_{min}}^{E_{max}} dE\Psi(\theta, Z_1)\, m(E, Z_1). \quad (3)$$

Here $P_{1,2}$ is the probability of an electron with energy E passing the quartz tube when it is incident on it at an angle φ [7]; the angular distribution of the fast electrons is taken in the form $\Psi(\Theta, Z_1) = \cos^2\Theta$ for $Z_1 < 50$ and $\Psi(\Theta, Z_1) = \cos^2\Theta + 0.717\cos\Theta$ for $Z_1 \geq 50$; $m(E, Z_1)$ is the energy distribution of the electrons [8] (the energy distribution of lead was used for tantalum, while the energy distribution of copper was used for zirconium and stainless steel); $\Theta = \arcsin(R_2\sin\varphi/R_1)$ is the angle of escape of the electrons from the emitter [electrons with escape angle $\Theta \leq \Theta_{max} = \text{arc sin}(R_2/R_1)$ fall on the quartz tube].

The probability of absorption of fast electrons A_{ij} is obtained from similar considerations:

$$A_{ij}=\frac{\int_0^{\theta_{max}} d\theta \int_{E_{min}}^{E_{max}} dE\Psi(\theta, Z_i)\, m(E, Z_i)\,[1-g(\varphi_{ij}, E, Z_j)]}{\int_0^{2\pi} d\theta \int_{E_{min}}^{E_{max}} dE\Psi(\theta, Z_i)\, m(E, Z_i)} \quad (4)$$

where g is the differential (over angle and energy) inelastic reflection coefficient of fast electrons [4].

The results of computations of the sensitivity of emission detectors with and without quartz tube according to models (1) and (2) are given in Table 1. The experimental sensitivity of the emission detectors was determined on high-power ^{60}Co γ installations [7] according to the formula

$$S_{exp}=-(Y-Y_c)/\bar{P}, \quad (5)$$

where Y and Y_C are the currents for the detector and the compensated detector, respectively, A; $\bar{P}$ is the value of the exposure dose intensity averaged over the length of the sensitive part of the detector, and is equal to 1210 and 1640 R/sec for K-120000 and K-200000 installations, respectively.

The detector currents were recorded by a DFG2-20 electrometer; the exposure dose intensity was measured by a DRG2-03 dose meter with carry-out ionization chamber. The experimental error in the determination of the sensitivity for detectors with tantalum, zirconium, and stainless steel emitters is ± 8, ± 9, and $\pm 10\%$, respectively.

As evident from Table 1, for detectors with tantalum and zirconium emitters the agreement between the computation and the experiment is entirely satisfactory for the energy of γ quanta equal to 1.25 MeV. This confirms the validity of our assumption that the sensitivity of this type of detector is determined mainly by the fast electrons. For detectors with stainless steel emitter the divergence between the computed and experimental values of the sensitivity is appreciable, as was to be expected. The emitter and collector of this detector have the same atomic number; therefore the contribution of the slow electrons must be taken into consideration in computing the sensitivity. The sensitivity of the detector with tantalum emitter and a quartz tube between the electrodes has the smallest dependence of the energy of γ quanta. The deviation of its sensitivity from the mean value does not exceed $\pm 25\%$. The sensitivity of the detectors without the quartz tube has a considerably stronger dependence on the energy of γ quanta.

LITERATURE CITED

1. B. V. Mukhachev et al., in: Nuclear Instrumentation [in Russian], Vol. XVII, Atomizdat, Moscow (1972), p. 63.
2. B. V. Mukhachev et al., in: Proc. IAEA Symp. Dosimetry in Agriculture, Industry, Biology, and Medicine, May 1972, Vienna (1972), p. 515.
3. V. I. Ivanov et al., ibid., p. 663.
4. G. V. Kulakov, Author's Abstract of Candidate's Dissertation, MIFI, Moscow (1973).
5. G. V. Kulakov et al., Measurement Technology, Metrology, No. 5, 69 (1974).
6. V. V. Smirnov et al., in: Applied Nuclear Spectroscopy, Vol. 3, Atomizdat, Moscow (1972), p. 161.
7. B. Mar, Boein Rep. D2-90414 (1963).
8. N. Oda and H. Sudzuki, J. Phys. Soc. Japan, 15, 2365 (1960).
9. A. Kh. Breger et al., Fundamentals of Radiational–Chemical Instrumentation, Atomizdat, Moscow (1967).

MIGRATION OF RADIOGENIC LEAD IN THE HYDROTHERMAL METAMORPHISM OF URANIUM MINERALS

V. M Ershov

UDC 550.424:553.492

In the majority of uranium minerals and minerals that contain uranium, lead is present in two forms, with diffusion coefficients 10^{-6} and 10^{-20} $cm^2 \cdot sec^{-1}$. Such mineral aggregates may easily lose about half of the radiogenic lead that they contain without visible change [1-4]. The investigation of the migration of radiogenic lead is of practical interest in order to determine whether an aureole is formed around the zone of uranium mineralization.

Hydrothermal metamorphism of uranium minerals of the Precambrian deposits led to the isolation of part of the radiogenic lead in a separate mineral phase [4-6]. In the studied deposits, mineralization has an age of around 1800 million years. A later metamorphism occurring, as A. I. Tugarinov has established, in the Paleozoic period caused the formation of galenite with radiogenic lead, while the aggregates of pitchblende and uraninite in the main retained their initial forms. Hence, we may speak of the preferential migration of radiogenic lead.

For the investigated mineralization, the calculated value of the ratio of radiogenic lead to uranium is $0.306 \simeq 0.31$. The fraction of radiogenic lead in the mineralized zones is 0.94-0.96, and therefore the correction for impurities of nonradiogenic lead can be neglected.

Since it is impossible to determine the lead/uranium ratio for the whole volume of the mineralization zone, the results of determining the lead/uranium ratio in five industrial samples may be used (Table 1). The deviation of the mean value of this ratio from the calculated value does not exceed the analytical error.

From the same zone, a further 51 similar samples were taken. The mean value of the lead/uranium ratio was found to be 0.307. Hence it can be concluded that practically all of the radiogenic lead is found within the limits of the mineralization zone, and that its mean migration length in the metamorphism is significantly less than the dimensions of this zone. A similar picture is observed for the Witwatersrand deposits [1].

In [6], Tarkhanov and Zhukova presented data on the lead content in ores of the Precambrian uranium deposits, on the basis of which they concluded that radiogenic lead had migrated beyond the limits of the ore body and formed a surrounding aureole of scattering. If these data relate to 66 random samples, the value of the mean migration length of radiogenic lead may be compared with the dimensions of the ore body. Without taking into account the acceptable error, the mean value of the ratio of the actual lead content and that calculated from the uranium concentration is 0.99. Taking into account only arithmetic errors in calculating the lead content, this ratio is 1.03. Hence, in this case too, all of the radiogenic lead is found within the limits of

TABLE 1. Lead/Uranium Ratio in Industrial Samples

Type of mineralization	Pb/U
Silicate	0,308
Ferrocarbonate	0,298 0,274 0,306
Carbonate	0,296
Mean . . .	0,297±0,013

Translated from Atomnaya Énergiya, Vol. 40, No. 6, pp. 485-486, June, 1976. Original article submitted January 30, 1975; revision submitted December 19, 1975.

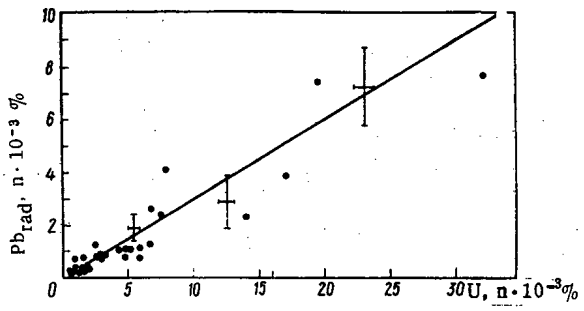

Fig. 1. Dependence of concentration of radiogenic lead in the enclosing rock on the uranium concentration.

TABLE 2. Mean Values of Lead/ Uranium Ratio

Sample mass, kg	Type of mineralization	
	ferrocarbonate type	silicate type
0,001—0,01	0,40±0,27	—
0,1—1,0	0,338±0,080	0,346±0,208
1,0—2,0	0,315±0,082	0,654±0,363
2,0—5,0	0,320±0,014	0,33
5,0—10,0	—	0,340±0,040

the ore body, and the mean migration length is less than the dimensions of the ore body.

This conclusion is confirmed by the absence of excess radiogenic lead in the region surrounding the ore, since the lead content corresponds to the uranium concentration (Pb = 0.001 + 0.3U, %). In regions of low uranium concentration (< 0.003%), this dependence becomes less clear due to variation in the impurity lead content, and the ratio between uranium and lead may become rather arbitrary, which, however, does not indicate excess or deficiency of radiogenic lead. In samples with low uranium content, there is no excess of radiogenic lead [the slope of the regression equation corresponds to the age of the mineralization zone (Fig. 1)].

Thus, for metamorphized deposits and ore zones in general, we may conclude that the migration length of radiogenic lead on metamorphism is much less than the dimensions of the ore body.

In a homogeneous medium for nonuniform distribution of uranium, the ratio of radiogenic lead to uranium depends on the relative magnitude of the linear dimensions of the sample lump as compared with the mean migration length of radiogenic lead. If the sample dimensions are equal to double the migration length of lead, or more, then the lead/uranium ratio in the sample should correspond to the absolute age. Here, the dependence of the mean migration length of lead l on the dimensions of the sample lump of mass Q may be written in the form

$$l = \sqrt[3]{3Q/4\pi\rho},$$

where ρ is the specific gravity, while the sample dimensions are approximated by the dimensions of a sphere of corresponding mass.

Table 2 shows mean values of the lead/uranium ratio calculated from the results of analyzing 5–7 samples in each weight class. According to these data, the mean migration length of lead for mineralization of ferrocarbonate type, determined as indicated, is 5.4–7.5 cm, while for mineralization of silicate type it is ~ 9.3 cm.

The mean value of the lead/uranium ratio for 47 core samples, of length 0.5 mm along the core axis, taken systematically over all parts of the mineralization zone, was 0.31 ± 0.01, which corresponds accurately with the calculated value and agrees with the value of the mean migration length of radiogenic lead.

The value of the mean migration length of radiogenic lead is of great use in geochronological investigations, since it permits an objective choice of samples in which the uranium–lead system may be regarded as "closed." Hydrothermal metamorphism evidently does not always lead to scattering of radiogenic lead over the area surrounding the ore.

LITERATURE CITED

1. A. I. Tugarinov, E. V. Bibikova, and S. I. Zykov, At. Énerg., 16, No. 4, 332 (1964).
2. S. B. Brandt and S. N. Voronovskii, Izv. Akad. Nauk SSSR, Ser. Geol., No. 7, 83 (1963).
3. V. A. Kirkinskii and E. S. Makarov, in: Problems of Geology [in Russian], Nauka, Moscow (1965), p. 463.
4. V. M. Ershov, Geokhimiya, No. 10, 1565 (1974).
5. U. Libenberg, in: Geology of Atomic Raw Materials [in Russian], Atomizdat, Moscow (1959), p. 377.
6. A. V. Tarkhanova and V. I. Zhukova, At. Énerg., 34, No. 6, 455 (1973).

QUANTITATIVE ANALYSIS OF VARIOUS FACTORS AFFECTING THE INTENSITY OF THE X-RAY SIGNAL BACKSCATTERED FROM A SEMIINFINITE REFLECTOR

F. L. Gerchikov

UDC 539.171:539.12

In the past, a considerable number of works have appeared, both inside and outside the USSR, investigating the integral characteristics of backscattered γ radiation. However, these calculations relate to monoenergetic radiation with $E_\gamma > 0.1$-0.3 MeV [1]. Increasingly, in recent years, systems for the automatic control and regulation of various objects and industrial processes have made use of devices in which the information source is retarded, pulsed x radiation with $\bar{E}_\gamma < 150$ keV [2, 3]. Such a device includes a pulse or continuous emitter generating x radiation and a receiver consisting of a detector of direct or backscattered x radiation, together with a data-processing block that feeds signals to the automatic control system for the object.

Consider a pulsed x-ray source emitting radiation of energy E_0 (MeV/pulse) in the direction of a semiinfinite reflector lying a distance H away in an atmosphere of air. Within the range of working angles, characterized by the collimation angle $2\Psi_0$, the radiation is isotropic; the linear dimensions of the emitter and detector are much less than H; and the emitter–detector line (the base d) is parallel to the plane reflector surface (Fig. 1).

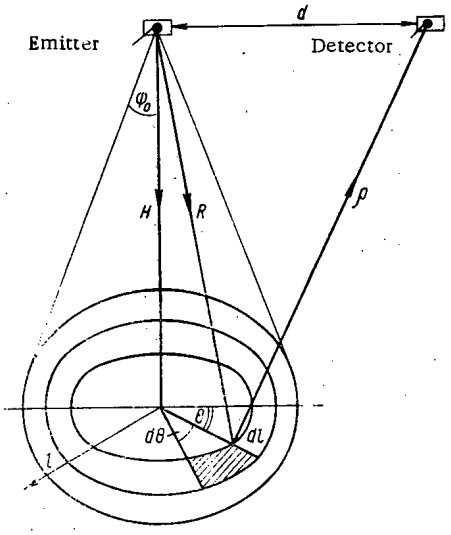

Fig. 1. Geometry of the apparatus.

Translated from Atomnaya Énergiya, Vol. 40, No. 6, pp. 487-490, June, 1976. Original article submitted May 12, 1975.

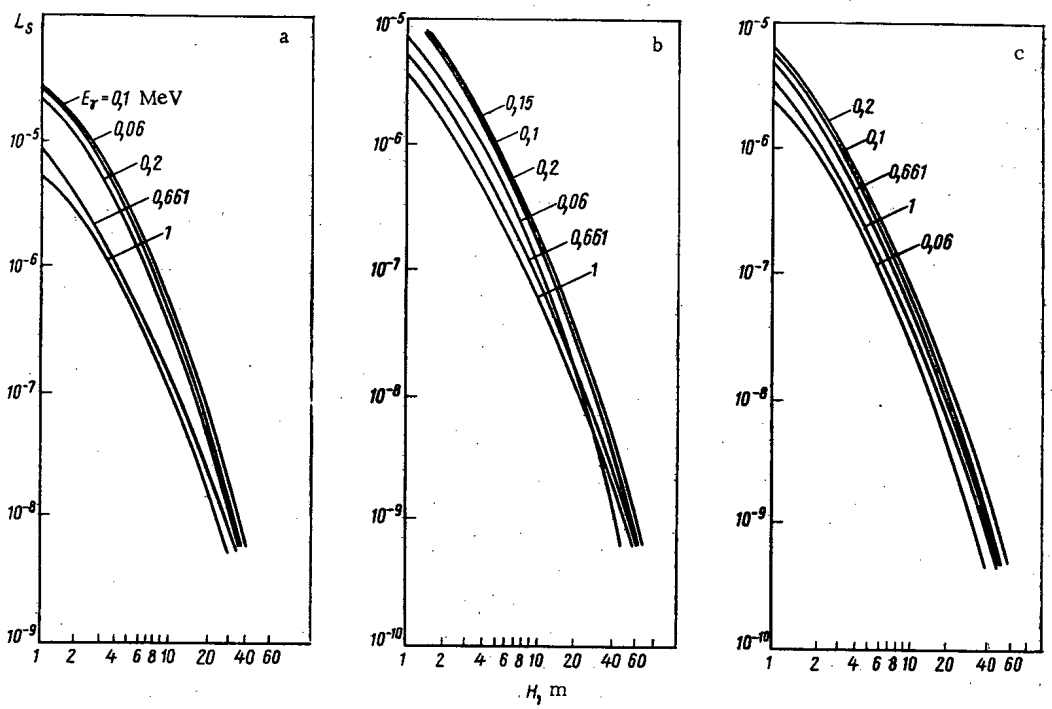

Fig. 2. Change in the signal reflected from water (a), concrete (b), and iron (c) as a function of $\overline{E}_\gamma$.

The x-ray energy incident on an elementary area of the reflector surface $dS = l\,dl\,d\Theta$ is

$$dE_{\text{inc}} = E_0 R^{-2} \exp(-\mu_1 R)\, dS,$$

where $R^2 = H^2 + l^2$; μ_1 is the absorption coefficient of x radiation in air on the emitter–reflector path. The energy of the signal reflected from an elementary area of the reflector is

$$dE_{\text{ref}} = \frac{dE_{\text{inc}}}{2\pi\rho^2} A_E \exp(-\mu_2 \rho),$$

where $\rho = H^2 + d^2 + l^2 - 2dl\cos\Theta$; μ_2 is the absorption coefficient of x radiation on the reflector–detector path; A_E is the energy albedo of the reflector.

Integrating over the whole surface of the semiinfinite reflector, we obtain at the detector inlet

$$E_{\text{rec}} = E_0 A_E \int_{l=0}^{l_0} \int_{\theta=0}^{\pi} \frac{\exp(-\mu_1 \sqrt{H^2+l^2}) \exp(-\mu_2 \sqrt{H^2+l^2-2dl\cos\theta})}{(H^2+l^2)(H^2+l^2+d^2-2dl\cos\theta)} \tag{1}$$

Let

$$A_E \int_{l=0}^{l_0} \int_{\theta=0}^{\pi} \frac{\exp(-\mu_1 \sqrt{H^2+l^2}) \exp(-\mu_2 \sqrt{H^2+l^2-2\,dl\cos\theta})}{(H^2+l^2)(H^2+l^2+d^2-2\,dl\cos\theta)} = L_S$$

be the signal transmission coefficient on the emitter–reflector–detector path.

Then Eq. (1) can be written in the form $E_{\text{rec}} = E_0 L_S$. In the general case

$$L_S = f(E_\gamma, d, \Psi_0, H). \tag{2}$$

Varying the numerical values in the right-hand side of Eq. (2) within broad limits (E_γ = 0.06–1 MeV;

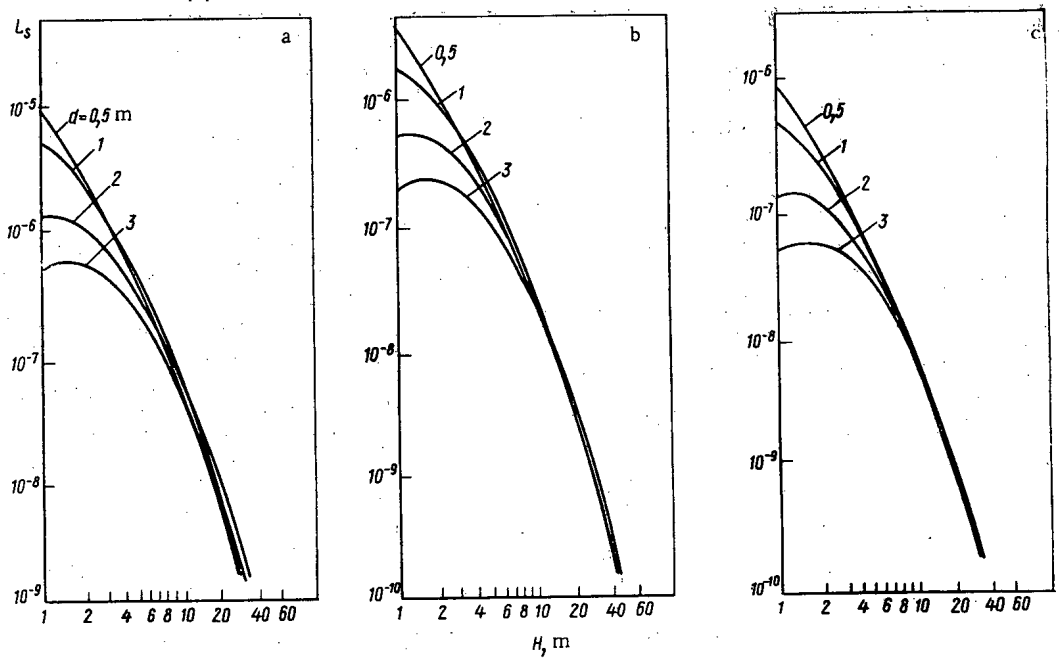

Fig. 3. Change in the signal reflected from water (a), concrete (b), and iron (c) as a function of d.

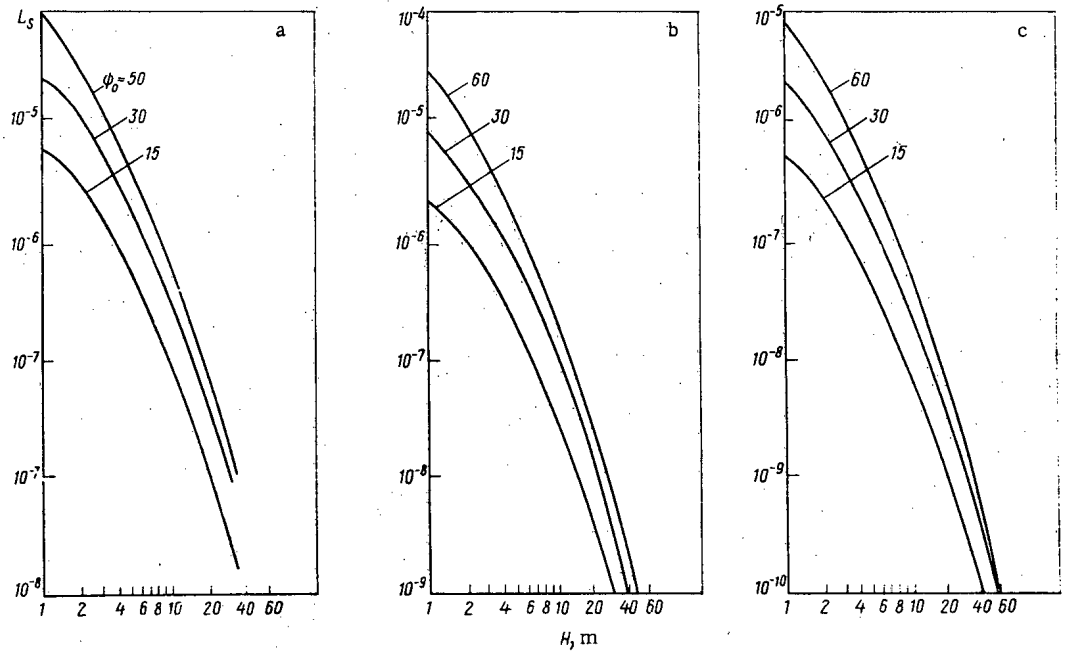

Fig. 4. Change in the signal reflected from water (a), concrete (b), and iron (c) as a function of $2\Psi_0$.

d = 0.5-3 m; $2\Psi_0$ = 30-120°) determined by the possibility of practical realization with acceptable size, weight, and energy characteristics of the designed control system, we obtained corresponding values of L_S by the method of numerical integration on a BÉSM-4 computer.

The results of the calculation are as follows. In the range E_γ = 0.06-0.15 MeV (Fig. 2), the value of the signal reflected from concrete to the detector inlet increases. The transmission coefficient of the useful signal for d = 0.5-3 m and small collimation angles is $L_S = 10^{-7}$-10^{-8} for H ≤ 10 m; with increase in H from 10 to 30 m, $L_S = 10^{-9}$-10^{-10}; and when H is more than 60 m, $L_S < 10^{-11}$. With increase in E_γ from 0.2 to 1 MeV, the absolute value of the signal reflected from concrete to the detector inlet is decreased, since A_E decreases.

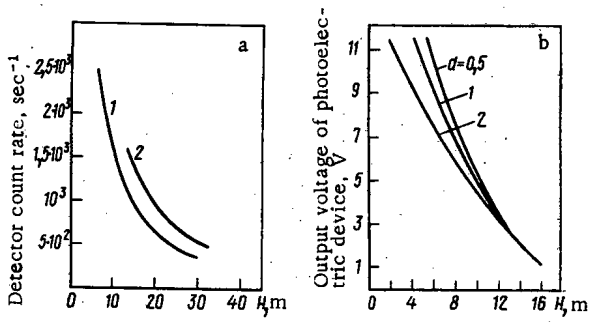

Fig. 5. Experimental values of the backscattered radiation: a) from concrete (1) and water (2) for E_γ = 0.661 MeV [1]; b) from concrete for various values of the base d and E_γ = 0.06 MeV.

Similar calculations for water and iron have allowed the optimal energy from the point of view of the maximum value of the signal at the detector inlet to be determined for water, concrete and iron: 0.1, 0.15, and 0.2 MeV, respectively.

With decrease in the distance between the emitter and the detector, d, the value of the signal at the detector inlet rises. In the range 0.06-0.2 MeV with $2\Psi_0$ = 30-120°, $L_S = 5 \cdot 10^{-8}$-$3 \cdot 10^{-5}$ for d = 0.5-3 m at distances of less than 10 m from a concrete reflector. For H > 10 m, the dependence of the signal on the base d becomes insignificant (Fig. 3). For an energy of 0.06 MeV and H = 1-10 m, with d = 0.5 m and $2\Psi_0$ = 30°, the values of L_S for water, concrete, and iron are 10^{-5}-10^{-7}; $5 \cdot 10^{-6}$-10^{-7}; and 10^{-6}-$2 \cdot 10^{-8}$, respectively.

With increase in the radiation collimation angle, the value of the useful signal increases. For E_γ = 0.06-0.2 MeV, d = 0.5-3 m, and $2\Psi_0$ = 30-120°, $L_S = 10^{-4}$-10^{-6} for a concrete reflector (Fig. 4). With increase in H, the dependence $L_S = f(\Psi_0)$ grows less significant.

For E_γ = 0.06 MeV and d = 1 m, with $2\Psi_0$ = 30° and H = 1-10 m, the values of L_S for water, concrete, and iron are 10^{-7}-$6 \cdot 10^{-6}$; $5 \cdot 10^{-8}$-$2 \cdot 10^{-6}$; and $6 \cdot 10^{-9}$-$9 \cdot 10^{-7}$, respectively.

Experiments on testing units and objects confirm that the theoretical assumptions and calculations are correct (Fig. 5). In particular, the experimental measurements given in [1] show that the calculated signal transmission coefficient L_S for energy quanta E_γ = 0.661 MeV agrees closely with experiment. Both in theory and practice, the maximum intensity of backscattered radiation is observed for reflection from water. The measured values of the backscattered radiation for water and concrete [1], recorded systematically for H = 0-30 m, are in good agreement with the calculated signal transmission coefficient L_S in this range of H. Experimental measurements of backscattered x radiation for different values of the base d are in good agreement with the calculated values. Both in theory and practice, it is clear that the effect of d on the value of the backscattered signal at the detector inlet becomes less pronounced for distances H ≥ 10 m.

Thus, the value of the signal at the detector inlet in x-ray control systems is determined by the energy of the x-ray beam, the geometry of the receiver–transmitter channel, and the collimation angle of the emitter. By varying these parameters for each type of reflector, a maximum value of the signal can be obtained at the detector inlet for minimum size, weight, and energy characteristics of the apparatus.

In conclusion, the author would like to thank N. F. Andryushin and V. N. Barkovskii for critical comments made on reading the manuscript.

LITERATURE CITED

1. B. P. Bulatov and N. F. Andryushin, Backscattered γ Radiation in Radiation Engineering [in Russian], Atomizdat, Moscow (1971).
2. V. I. Glagolev et al., in: Nuclear Instrument Design. Proceedings of the Soviet Scientific-Research Institute of Instrument Design [in Russian], No. 10, Atomizdat, Moscow (1969), p. 85.
3. I. Ya. Serebrennikov et al., in: Radiation Engineering [in Russian], No. 3, Atomizdat, Moscow (1969), p. 114.

LIBERATION OF HELIUM IN THE UNIFORM HEATING OF NEUTRON-IRRADIATED OKh16N15M3B STEEL

N. P. Agapova, I. N. Afrikanov,
A. I. Dashkovskii, A. G. Zaluzhnyi,
V. D. Onufriev, D. M. Skorov,
Yu. N. Sokurshii, and O. M. Storozhuk

UDC 621.039.546:541.183.5:546.291

It is known that, under the action of neutron irradiation, (n, α) and (n, p) nuclear reactions in constructional materials lead to the formation of helium and hydrogen, accumulation of which in the material may cause undesirable changes in its mechanical and physical properties. Therefore, it is important to investigate the accumulation and behavior of gaseous nuclear-reaction products in materials and, in particular, the processes by which they are liberated from the material.

In [1] an account was given of the method used and the results obtained in a study of the kinetics of helium liberation from samples of nickel and OKh16N15M3B steel (in its initial state, a foil of thickness ~ 100 μ with recrystallized grains of size 30-50 μ), in which helium was produced by bombardment with α particles in a cyclotron. In the course of uniform heating of the given samples at a rate of 7 deg C/min, 6 peaks in the rate of helium liberation were observed.

The present paper reports an investigation of the liberation of helium from samples of steel OKh16N15M3B of analogous initial state, irradiated in a reactor at a temperature not exceeding 500°C by a neutron flux of $4.0 \cdot 10^{22}$ neutrons/cm^2 (E > 0.1 Mev). The kinetics of gas liberation in the course of uniform heating at a rate of 7 deg C/min was investigated by the method described in [1]. A typical curve for the liberation of helium in these conditions, obtained for a constant rate of drawing off the helium, is shown in Fig. 1. At temperatures above 500°C on the kinetic curve, five high-temperature peaks of helium-liberation rate can be observed (II'-VI'). Comparing this curve with that for the cyclotron-irradiated samples, we see that they are identical at temperatures above 500°C (the peaks of gas-liberation rate are labelled in accordance with [1]).

At temperatures above 500°C, the liberation of helium from samples of steel in which helium is formed

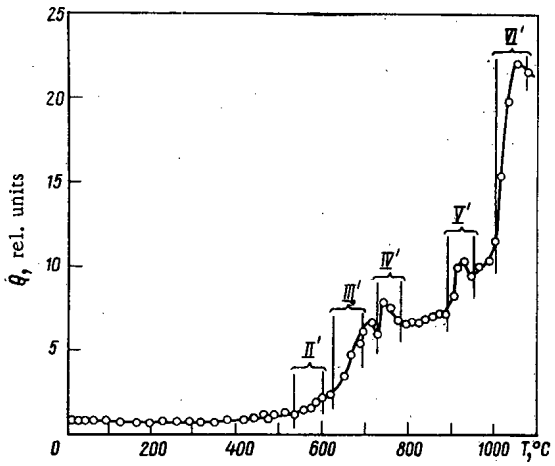

Fig. 1. Kinetics of helium liberation from irradiated samples of OKh16N15M3B steel ($4.0 \cdot 10^{22}$ neutrons/cm^2) in the course of uniform heating at a rate of 7 deg C/min.

Translated from Atomnaya Énergiya, Vol. 40, No. 6, pp. 490-491, June, 1976. Original article submitted May 26, 1975; revision submitted December 15, 1975.

in the (n, α) reaction on irradiation by fast neutrons in a reactor is characrerized by the same stages as the helium liberation from samples subjected to irradiation in a cyclotron. Hence, the liberation of helium from the steel at temperatures of 600-700°C corresponds to the diffusion of gas atoms by a vacancy mechanism, while the liberation of helium at temperatures of 900°C and above corresponds to the migration of gas bubbles to the sample surface [1].

Investigation of the irradiated samples of steel by transmission electron spectroscopy showed the presence of pores with distinct boundaries. The pore size lay in the range 50-250 Å (mean value 150 Å), while the pore concentration was $\sim 2 \cdot 10^{15}$ cm^{-3}. Calculation showed that the creation of an equilibrium pressure of helium in the pores would require a helium content larger by a factor of 35 than that observed experimentally using the apparatus and the procedure described in [2]. This means that the pores have the character of vacancies, i.e., they are not filled with helium atoms. The vacancy pores, naturally, provide a channel for the helium atoms present in the lattice of the material, but evidently they do not absorb all of the helium atoms diffusing by a vacancy mechanism, and some of them appear at the surface, causing the peak in the gas-liberation rate in the range 600-700°C. When the temperature is increased, the helium atoms evidently collect in the pores. At high temperatures, helium liberation from irradiated samples of OKh16N15M3B steel occurs through the migration of pores to the sample surface and the release of their helium content. In the absence of neutron irradiation, the solution in the lattice of helium present in the pores is unlikely [3].

The curve of helium liberation (Fig. 1) lacks the low-temperature peak in the helium-liberation rate (300-400°C) observed on the corresponding curve for samples of the same steel saturated with helium in a cyclotron. The explanation is that, on irradiation in the reactor, the maximum temperature of the samples reaches 500°C, and the process of gas liberation at these temperatures goes to completion in the course of irradiation. Hence, in the subsequent uniform heating of the samples of steel irradiated in the reactor, there is scarcely any further liberation of helium at temperatures below 500°C (Fig. 1).

LITERATURE CITED

1. D. M. Skorov et al., At. Énerg., 40, No. 5, 387 (1976).
2. A. I. Dashkovskii et al., At. Énerg., 40, No. 3, 251 (1976).
3. D. Rimmer and A. Cottrell, Philos. Mag., 2, 1345 (1957).

SEARCH FOR FISSILE ISOMERS IN THE (n, 2n) REACTION*

J. S. Browne and R. E. Houve

UDC 539.172.4

The formation of spontaneously fissioning isomers of various actinide nuclei in the (n, 2n) reaction produced by 14-MeV neutrons has been reported [1, 2]. A ratio between the isomer formation cross section and the prompt fission cross section in the range $(1\text{-}2)\cdot10^{-4}$ was obtained for the reactions ^{240}Pu(n, 2n)^{239m}Pu ($T_{1/2}$ = 8.5 μsec) and ^{242}Pu(n, 2n) ^{241m}Pu ($T_{1/2}$ = 27 μsec).

It was suggested [3] that one should expect to find an as yet unknown isomer ^{243m}Pu with a half-life of the order of 10 μsec according to Metag's systematics [4] for isomeric lifetimes. The only known isomer of ^{243}Pu has a lifetime of 33 nsec, which is not in agreement with the systematics based on calculations of the fission barrier. Since the (n, 2n) reaction appears to be a good mechanism for the formation of fissile isomers, we decided to look for an isomer of ^{243}Pu in the reaction ^{244}(n, 2n)^{243}Pu.

A device at the Lawrence Livermore Laboratory having a high-intensity beam of 14-MeV neutrons was used for this purpose. A beam of 500-keV deuterons created in the device was incident on a rotating titanium – tritium target at a current of 10 mA. With a continuous beam, the neutron yield was of the order of $3\cdot10^{12}$ n/sec. The beam was pulsed at frequencies of 10 and 100 KHz, and 2.5 MHz for isomer searches between pulses in the time intervals 100 and 10 μsec and 400 nsec, respectively. The pulse widths were 1.5 μsec, 130 and 1.5 nsec, respectively.

A diagram of the device is shown in Fig. 1. Samples of ^{238}U, ^{242}Pu, and ^{244}Pu were set up in the ionization chamber. The mass and isotopic composition of the samples are given in Table 1. Fission events were recorded with a fast current-sensitive preamplifier (rise time < 10 nsec) having a time resolution of 2 nsec. Analysis of the time between pulses from neutrons and from fission was made with a fast discriminator and a

TABLE 1. Sample Composition

Sample	Mass, mg	Purity, %	Density, μg/cm^2
^{238}U	1,0	99,9	~ 500
^{242}Pu	1,0	99,9	~ 500
^{244}Pu	0,59	99,1	~ 500

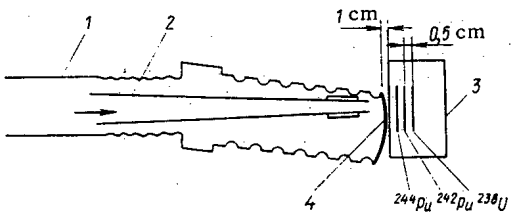

Fig. 1. Diagram of arrangement of ionization chamber and 14-MeV neutron source: 1) deuterons; 2) collimator; 3) ionization chamber (96% Ar and 4% CO_2); 4) rotating tritium target.

* Work supported by the Energy Research and Development Administration (ERDA).

University of California Lawrence Livermore Laboratory. Translated from Atomnaya Énergiya, Vol. 40, No. 6, pp. 491-492, June, 1976. Original article submitted July 7, 1975.

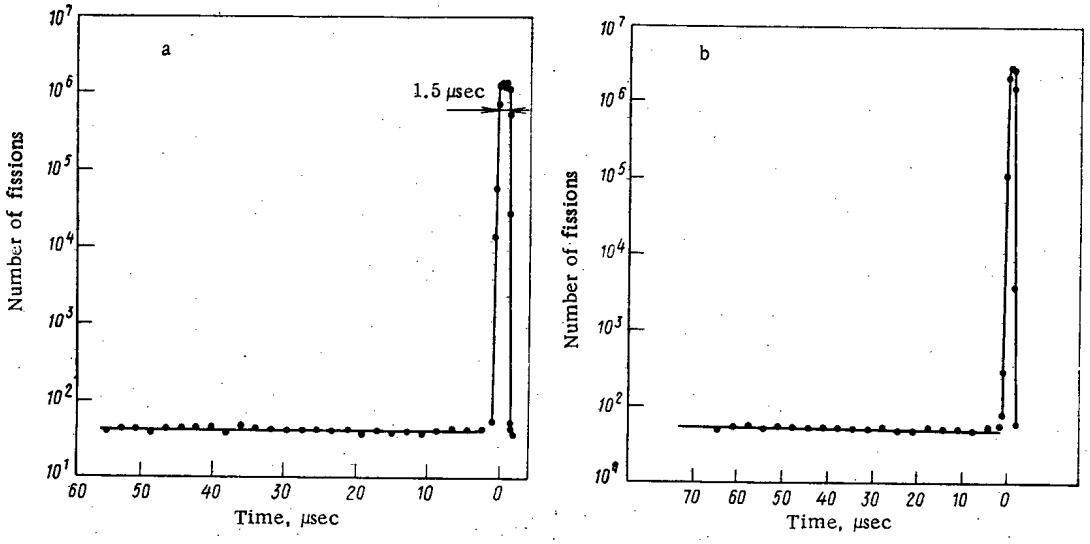

Fig. 2. Time spectra corresponding to fission events in samples of ^{242}Pu and ^{244}Pu: a) ^{242}Pu·(n, 2n)^{241}Pu; b) ^{244}Pu(n, 2n)^{243}Pu (background level given by the solid line outside the bound of the prompt fission peak).

time-to-pulse-height converter (TPC), the output signal of which was fed to a multichannel analyzer. Pulse-height spectra from the TPC for ^{242}Pu and ^{244}Pu at 10 KHz and 1.5 μsec are shown in Fig. 2. None of the spectra showed the presence of a decaying isomer. A 27-μsec activity was reported [2] for ^{242}PU.

The total number of counts in two successive half-lives is compared in order to determine the sensitivity of the measurements. If an isomer with a half-life of 27 μsec is present during an experiment, there should be a difference between the number of counts in the intervals 0-27 μsec (first half-life) and 27-54 μsec (second half-life). Denoting these sums by S_1 and S_2, we find that $S_1 = 5700 \pm 75$ and $S_2 = 5715 \pm 75$; consequently, there is no activity with a half-life of 27 μsec observed within the limits of the statistics. If one takes a deviation of three standard errors from the mean (Poisson distribution) as the minimum observable activity in order to record some kind of activity, one can then determine the ratio of isomeric decay to prompt decay (only 0.13% of the cases were outside the 3σ limit in the Poisson distribution in our measurements; consequently, the probability limit of the present work is better than 99%). For ^{242}Pu, $3\sigma = 3 \cdot 75 = 225$. Since only half the decays fall in the first half-life, the required minimum is 450. The number of prompt counts is $1.0 \cdot 10^7$ and consequently the ratio is $450/10^7 = 4.5 \cdot 10^{-5}$, i.e., four times less than that observed in [2]. If the ratio given in [2] were correct, 700 counts above background would have been observed in first half-life. Note that the background is produced by spontaneous fission in measurements of ^{242}Pu and ^{244}Pu. Our conclusion that the ratio of isomeric decay to prompt decay for the reaction ^{242}Pu(n, 2n)^{241m}Pu ($T_{1/2} = 27$ μsec) must be less than $4.5 \cdot 10^{-5}$ disagrees with the data of [2].

We also failed to observe an activity in the 10-μsec range, the appearance of which was expected in the ^{244}Pu(n, 2n)^{243}Pu reaction according to [3, 4]. The upper limit of the ratio established by the same method is $2 \cdot 10^{-5}$ for the same 3σ criterion.

As should be expected, a fissile isomer was not observed for ^{238}U either since an isomer of ^{237}U has not been observed thus far.

These results for the (n, 2n) reaction can be compared with other results in which the compound nucleus evaporates two neutrons, the (p, 2n) reaction for example. The (p, 2n) reaction was used [5-7] for the production of isomers of various actinides. The maximum ratios of isomeric to prompt fission fall within limits from $5 \cdot 10^{-5}$ to $5 \cdot 10^{-6}$ for $E_p = 13$ MeV. This is in agreement with the limit obtained in our experiment. Therefore, if isomers are formed in the (n, 2n) reaction produced by 14-MeV neutrons, their formation cross sections for ^{241}Pu and ^{243}Pu are at least four times less than previously reported.

The authors thank Dr. G. Otampo for furnishing the ^{244}Pu sample and Dr. M. S. Coops for preparation of high-purity ^{242}Pu and ^{238}U samples.

LITERATURE CITED

1. Yu. P. Gangrskii et al., At. Énerg., 31, No. 2, 156 (1971).
2. A. Belov et al., JINR Preprint E15-6807 (1972).
3. J. Browne and C. Bowman, Phys. Rev., 9, 1177 (1974).
4. V. Metag et al., in: Proc. IAEA, Physics and Chemistry of Fission, Vol. 1, Vienna (1969), p. 325.
5. J. Borggreen et al., Phys. Letters, 25, 402 (1967).
6. N. Lark et al., Nucl. Phys., A139, 481 (1969).
7. S. Bjornholm et al., Nucl. Phys., A95, 513 (1967).

OPTIMAL ARRANGEMENT OF EFFECTIVE ABSORBER IN A REACTOR

A. M. Pavlovichev and A. P. Rudik

UDC 621.039.51

Among the many reactor optimization problems associated with the arrangement of fuel and absorber within the volume of a reactor [1], the problem of optimal arrangement of effective absorber has not yet been considered. Strictly speaking, one should introduce in its formulation two control factors – the concentration of effective absorber and the concentration of fissile material – and one should also take into account the burnup of nuclides during an operating period. To simplify matters, we assume that the distribution of fissile material is constant over the reactor volume and changes only because of displacement during the arrangement of effective absorber. It is required to find an arrangement for which the reactor is critical and for which the amount of neutrons captured by the effective absorber at fixed reactor power is a maximum. Questions associated with the burnup of nuclides are not discussed.

We discuss this problem for a thermal reactor in a two-group diffusion approximation where the initial equations for the one-dimensional problem have the form

$$\left.\begin{aligned} D_1\Delta\phi_1 = D_1\alpha_z^2\phi_1 - (\Sigma_1+\Sigma_{1-2})\,\phi_1 + \\ +\nu\Sigma_{f1}\phi_1+\nu\Sigma_{f2}\phi_2 = 0; \\ D_2\Delta\phi_2 - D_2\alpha_z^2\phi_2 - \Sigma_2\phi_2 + \Sigma_{1-2}\phi_1 = 0 \end{aligned}\right\} \quad (1)$$

with the boundary conditions

$$\nabla\phi_1(0) = \nabla\phi_2(0) = 0; \quad (2)$$

$$\left.\begin{aligned} \phi_1(R) = g_1\nabla\phi_1(R)+g_2\nabla\phi_2(R); \\ \phi_2(R) = g_3\nabla\phi_1(R)+g_4\nabla\phi_2(R). \end{aligned}\right\} \quad (3)$$

Here, ϕ_1 and ϕ_2 are, respectively, the fluxes of fast and thermal neutrons; R is the external radius of the reactor region in which redistribution of absorber is allowed; the other notation is standard. The boundary conditions (3) make it possible to take into account the existance of a region on the periphery of the reactor in which redistribution of absorber is not allowed, e.g., a reflector.

The concentration of useful absorber per unit volume of the reactor was taken as the control factor u(r) which was subject to the limitation $u_{min} \le u(r) \le u_{max}$. The maximizable functional was selected either in the form

$$J_1 = \int_V u(r)\,\phi_1(r)\,dV. \quad (4)$$

Translated from Atomnaya Énergiya, Vol. 40, No. 6, pp. 493-494, June, 1976. Original article submitted June 10, 1975.

if the effective absorber captured only fast neutrons, or in the form

$$J_2 = \int_V u(r)\,\phi_2(r)\,dV. \tag{5}$$

if the effective absorber captured only thermal neutrons. The total reactor power was assumed given:

$$W = \int_V (\Sigma_{f1}\phi_1 + \Sigma_{f2}\phi_2)\,dV. \tag{6}$$

If necessary, a limitation can be placed on the energy density – the power removed from a unit volume of the reactor.

A linear dependence of cross sections on the control factor was considered: $(-\Sigma_1 - \Sigma_{1-2} + \nu\Sigma_{f1})/D_1 = a_1 + b_1u$; $\nu\Sigma_{f2}/D_1 = a_2 + b_2u$; $\Sigma_{1-2}/D_2 = a_3 + b_3u$; $-\Sigma_2/D_2 = a_4 + b_4u$; $\Sigma_{f1} = a_5 + b_5u$; $\Sigma_{f2} = a_6 + b_6u$; $|a_i|, > |b_i|$, $i = 1, 2, \ldots, 6$; $b_4 \geq 0$, the remaining $b_i \leq 0$; $a_1 < 0$, $a_4 < 0$, the remaining $a_i \geq 0$. The diffusion coefficients were assumed independent of the control factor. The numerical values of the coefficients a_i and b_i selected for the calculations were typical of a heavy-water reactor.

Using the methods of the mathematical theory of optimal processes [2, 3], one can obtain some information about the optimal distribution of effective absorber prior to numerical calculations. It is well known that in the absence of limitations on phase variables in linear control problems, the optimal arrangement can consist of three types of regions: $u = u_{min}$, $u = u_{max}$, and a region of special control $u = u_{sp}$ (in [1], the last region is called the region of classical control). An analysis of the switching function in a "bare" reactor ($g_1 = g_2 = g_3 = g_4 = 0$) shows that the region $u = u_{max}$ should be located on the periphery of the reactor. In addition, by using the Kelly condition [3], or the zero value of the switching function in the region of special control, one can determine in certain particular cases whether a special control region is included in the optimal arrangement. For example, when $b_1 = b_3 = b_5 = 0$, the special control factor satisfies the Kelly condition for $J = J_1$ and is included in the optimal arrangement but the special control factor is not included in the optimal arrangement for $J = J_2$.

The complete solution of the optimization problem was carried out by using an optimization program based on the gradient method. An optimal arrangment was sought for various values of α_Z^2, R, and reflector thickness. The quantitative solutions obtained had the following qualitative features. The optimal value of the functional J increases with decrease in α_Z^2, and with increase in R and reflector thickness.

For maximization of the functional (4), the optimal arrangement of the reactor, both with and without a reflector, had the following form (from center to periphery): $u = u_{min}$, $u = u_{sp}$, $u = u_{max}$. For maximization of the functional (5), the optimal arrangement consisted of two regions: $u = u_{min}$ and $u = u_{max}$. For a cylindrical geometry, the maximum gain which is achieved as the result of redistribution of absorber in comparison with its uniform distribution is obtained in a "bare" reactor where R = 85 cm, which is the minimum of the values considered. This gain was ~ 30% and ~40% for J_1 and J_2, respectively. The gain from absorber redistribution was reduced as R and reflector thickness were increased. It was 8% and 12% for J_1 and J_2 when R = 140 cm and the reflector thickness was 25 cm.

It should be noted that with optimum absorber distribution from the viewpoint of maximum J, the maximum energy density is considerably greater than for a uniform absorber distribution. If it is necessary that the maximum energy density in an optimized device not exceed the maximum energy density in a reactor with uniform absorber distribution, the gain in the value of the functional J is decreased by approximately a factor of two. In this case, a region of heat-engineering limitation appears in the center of the reactor.

LITERATURE CITED

1. A. P. Rudik, Optimal Arrangement of Nuclear Fuel in a Reactor [in Russian], Ser., Physics of Nuclear Reactors, No. 2, Atomizdat, Moscow (1974).
2. L. S. Pontryagin et al., Mathematical Theory of Optimal Processes [in Russian], Nauka, Moscow (1969).
3. R. Gabasov and F. M. Kirillova, Special Optimal Control Factors [in Russian], Nauka, Moscow (1973).

EVALUATION OF DOSE RATE FROM RADIATION HEATING OF A SAMPLE DURING IRRADIATION

A. P. Balashov and A. M. Mamontov

UDC 539.12.08

Nonuniformity of energy deposition and of the temperature field can be neglected for a sample of small size irradiated by high-energy particles or quanta. Under conditions of convective heat transfer, heat losses are proportional to the temperature difference between the body and environment to a power close to one [1]. The temperature variation of a body during irradiation can be described by the equation

$$\frac{dT}{d\tau}+\frac{\lambda S}{c\rho V}T^n=\frac{D}{c}, \tag{1}$$

where T is the temperature difference between the body and its environment (T = 0 at τ = 0); τ is the irradiation time; D is the dose rate, which is constant in time; c is the specific heat capacity of the sample; ρ, S, and V are the density, surface area, and volume of the sample; λ is the coefficient of heat transfer.

We introduce the coefficient $k = \lambda S/\rho V$ which takes into account the dimensionality of the factor T^n.

In the initial stage of irradiation, heat loss is negligibly small, and the rise in temperature is linear,

$$\frac{dT}{d\tau}=\frac{D}{c}, \tag{2}$$

which makes it possible to evaluate the absorbed radiation dose rate from an experimentally determined rate of temperature rise [2].

With further irradiation, the heat losses gradually increase, the rate of temperature rise tends to zero, and its maximum value is found from Eq. (1) when $dT/d\tau = D$. The dose rate can be determined from the stable temperature difference T_{max},

$$D=kT_{\max}^n. \tag{3}$$

For an arbitrary value of the parameter n, we write the solution of Eq. (1) in the implicit form

$$c\int_0^T\frac{dT}{D-kT^n}=\tau, \tag{4}$$

which defines the inverse relation $\tau = \tau(T)$; the value of the dose rate can be found from a comparison of calculated and experimental relations $\tau(T)$. In practice, the problem reduces to minimization of a function of the form

$$\Phi=\frac{1}{\sum_{i=1}^{m}f_i}\sum_{i=1}^{m}\left(\frac{\tau_i-R_i}{\tau_i}\right)^2 f_i, \tag{5}$$

where τ_i and R_i are experimental and calculated values of the time in which the temperature difference T_i is attained; m is the number of experimental points; the f_i are weighting factors which take into account the "density" of the points on the experimental curve.

Translated from Atomnaya Énergiya, Vol. 40, No. 6, pp. 494-495, June, 1976. Original article submitted July 18, 1975.

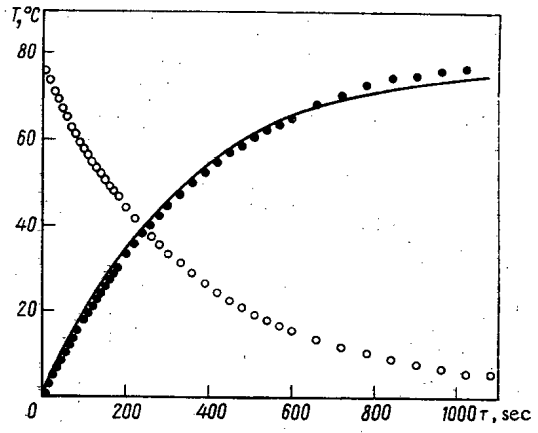

Fig. 1. Time variation of sample temperature: ●) during irradiation; ○) after end of irradiation.

TABLE 1. Results of Analysis of Radiation Heating of Sample for Irradiation by 8.5-MeV Electrons

j, μA/cm²	$k \times 10^4$, erg/sec·deg	$D_1 \times 10^4$, rad/sec	$D_2 \times 10^4$, rad/sec
0,033	1,92	0,64	0,68
0,067	1,75	1,42	1,43
0,083	1,99	1,67	1,90
0,100	1,72	1,68	1,96
0,117	1,51	2,52	2,42
0,130	1,91	2,23	2,57
0,133	1,30	2,75	2,65

The values of $R_i(T_i)$ are found from Eq. (4) by numerical integration for known parameters n and k. An a priori estimate of the latter is difficult because of the dependence of the coefficient of heat transfer on many factors [1]. It is simple to determine n and k by analyzing the curve for the drop in sample temperature after the end of irradiation. The cooling process is described by Eq. (1) with D = 0 and the initial conditions $T = T_0$ when $\tau = 0$. The solution has the form

$$T = T_0 \exp\left(-\frac{k}{c}\tau\right), \quad n = 1;$$
$$T = \left[T_0^{1-n} - \frac{(1-n)\,k}{c}\tau\right]^{1/1-n}, \quad n \neq 1. \tag{6}$$

The value of n can be found by fitting a function similar to (5) by means of well-known methods of minimization [3]. Furthermore, the value of k is determined by the least-squares method through linearization of the experimental relation $T(\tau)$ in appropriate coordinates.

In order to evaluate the effect of experimental error on the parameters found, test problems were solved in which cooling curves $T(\tau)$ (20-30 points) with an introduced random error of 1-5% normally distributed were constructed for given values of n, k, and T_0. The relations obtained were subject to the analysis described above in order to determine the parameters n and k. The results of the calculations indicate a noticeable effect of the introduced errors on the magnitude of the heat-transfer parameters, which were calculated from a small number of "experimental" points. However, it was established that this error has a very slight effect on the value of the dose rate determined by means of Eq. (3), or by means of the minimization procedure (5), which is explained by the dependence of the dose rate on both parameters.

The proposed method for evaluation of the dose rate was tested in a series of experiments. Aluminum samples 10 × 15 × 30 mm in size were irradiated with 8.5-MeV electrons incident on the broad face under conditions of natural convective heat transfer. A platinum resistance thermometer glued to one of the faces of the sample and a digital voltmeter were used for temperature measurement during irradiation. The error in the determination of temperature was no more than 0.3°C. The electron current density j was determined with a Faraday cup and had a relative error of 3-7%. The stability of the beam current was monitored with an

induction sensor.

Figure 1 shows typical heating and cooling curves for a test sample corresponding to a current density of 0.1 $\mu A/cm^2$. The calculated heating curve (solid line) agrees with experimental temperature values with an error of < 4%; for cooling, the calculated values practically coincide with the experimental values (calculated values omitted in the figure).

Some results of analysis of temperature curves for different current densities are given in Table 1. It was found experimentally that for a choice of the exponent n = 1.085, the calculated cooling curves matched the measured curves with an error of no more than 4%.

The selection of a fixed value of n ensures a relatively slight spread in the parameter k, which depends on the coefficient of heat transfer. The dose rates D_1 were obtained from the initial portion of the heating curves in accordance with Eq. (2); the dose rates D_2 were obtained from analysis of the entire set of experimental points by the proposed method. The dependence of D_2 on electron current density is characterized by a small deviation from linearity (maximum deviation, < 12%) while the analogous relation $D_1(j)$ is characterized by a relatively large spread in values, particularly at high current densities.

The proposed dosimetry technique, which is based on analysis of radiation heating of a body during irradiation, makes it possible to obtain an independent evaluation of the dose rate from radiation directly absorbed in the irradiated object. It can be used for studies in the fields of radiation physics and materials testing. For a known dose rate, the results obtained make it possible to predict the kinetics of the temperature variation of an object during irradiation. The required heat-transfer parameters can be determined in advance from heat experiments. It should be noted that the possibility of using the proposed method is limited to conditions of small radiative heat loss. If radiative heat transfer predominates, one can use the results in [4], in which the characteristics of radiative heating of solids in a vacuum were studied.

LITERATURE CITED

1. H. Carslaw and J. Jaeger, Conduction of Heat in Solids, Clarendon (1959).
2. V. D. Anan'ev and I. M. Matora, At. Énerg., 29, No. 4, 285 (1970).
3. D. J. Wilde, Optimum Seeking Methods, Prentice-Hall (1964).
4. Sh. Sh. Ibragimov, V. F. Reutov, and I. Yu. Abrashitov, Izv. Kazakh SSR, Ser. Fiz. Mat., No. 6, 84 (1974).

THE CRYSTAL STRUCTURE OF THE COMPOUNDS Pu_5Rh_4 and Pu_5Ir_4

A. V. Beznosikova, N. T. Chebotarev,
A. S. Luk'yanov, M. P. Shapovalov,
and L. F. Timofeeva

UDC 548.73

Monocrystals of the componds Pu_5Rh_4 and Pu_5Ir_4 were studied by Laue's method, vibrations and photography of the reciprocal lattice (molybdenum emission). The intensities of the reflections were estimated visually by the quality of blackening, taking account of the Lorentz and polarization factors. For the compounds Pu_5Rh_4 and Pu_5Ir_4, the 354 and 173 reflections respectively, were used. The dimensions of the elementary lattice were determined by oscillating crystal x-ray photography and they were refined by powder x-radiography. Calculations to determine the structure were carried out on a Minsk-32 computer according to a program devised by the authors.

It was established that the compounds Pu_5Rh_4 and Pu_5Ir_4 are isostructural, related to a rhombic system of the Pnma space group, Z = 4.

In the first stage of determining the structure, the coordinates of the atoms were found by the minimization of the R factor as a function of the coordinates. In order to find the extremum, the complex-method of Box was used. By achieving a value of R of the order 0.25-0.30, the distribution of the electron density in the cell was found. The maxima of the electron densities were compared with the provisional values of the atom coordinates. After quite good agreement, the final values of the coordinates were found by the least-squares method, using a linearization procedure, which permitted the dispersion of the coordinates to be estimated.

In order to reduce the effect of factors which are dependent on the ratio of the sine of the angle of reflection and wavelength of the emission, the theoretical and experimental values of the intensity were reduced to a single scale according to groups, with near values of this ratio. There were 12-22 reflections in each group. The final values of the R factors for the compounds Pu_5Rh_4 and Pu_5Ir_4 amounted to 0.17 and 0.18, respectively.

TABLE 1. Structure of Pu_5Rh_4 and Pu_5Ir_4 Compounds

Compound lattice period	Positions of atoms		Atomic parameter	
			Pu_5Rh_4	Pu_5Ir_4
Pu_5Rh_4	$Pu_I-8(d)$	x	0,158±1	0,155±1
$a=7,263$		y	0,122±1	0,123±1
$b=14,48$		z	0,338±1	0,338±1
$c=7,464$	$Pu_{II}-8(d)$	x	0,001±1	—0,002±1
		y	0,090±1	0,091±1
		z	—0,180±1	—0,183±1
Pu_5Ir_4	$Pu_{III}-4(c)$	x	0,322±1	0,319±2
$a=7,245$		z	—0,011±1	—0,007±1
$b=14,60$	$X_I-4(c)$	x	—0,041±2	—0,047±2
$c=7,455$		z	0,107±2	0,114±2
	$X_{II}-4(c)$	x	0,190±2	0,193±2
		z	—0,356±2	—0,368±1
	$X_{III}-8(d)$	x	0,194±2	0,183±1
		y	—0,034±1	—0,035±2
		z	—0,451±1	—0,460±1

*Density 13.59 and 16.54 g/cm^3, respectively.

Translated from Atomnaya Énergiya, Vol. 40, No. 6, pp. 495-498, June, 1976. Original article submitted September 23, 1975.

Interatomic Distances and Coordination of Atoms in Pu_5Rh_4 and Pu_5Ir_4 Compounds

Distance	Pu_5Rh_4 X=Rh	Pu_5Ir_4 X=Ir	Distance	Pu_5Rh_4 X=Rh	Pu_5Ir_4 X=Ir
Pu_I—Pu_I	3,70 Å	3,71 Å	Pu_{II}—X_{II}	3,24 Å	3,22 Å
—2Pu_I	3,85	3,86	—X_{III}	2,91	2,97
—Pu_{II}	3,49	3,51	—X_{III}	3,03	3,12
—Pu_{II}	3,59	3,60	—X_{III}	3,06	3,08
—Pu_{II}	3,80	3,78	—X_{III}	3,20	3,05
—Pu_{III}	3,32	3,31	Pu_{III}—2Pu_I	3,32	3,31
—Pu_{III}	3,41	3,39	—2Pu_I	3,41	3,39
—X_I	2,89	2,87	—2Pu_{II}	3,51	3,52
—X_I	2,92	2,89	—2Pu_{II}	3,52	3,54
—X_{II}	2,95	2,88	—X_I	2,78	2,80
—X_{III}	2,73	2,82	—X_I	3,18	3,08
—X_{III}	2,77	2,75	—X_{II}	2,75	2,84
—X_{III}	2,98	2,90	—X_{II}	2,85	2,87
Pu_{II}—Pu_I	3,49	3,51	—2X_{II}	3,15	3,15
—Pu_I	3,59	3,60	X_I—2Pu_I	2,89	2,87
—Pu_I	3,80	3,78	—2Pu_I	2,92	2,89
—Pu_{II}	3,75	3,81	—2Pu_{II}	3,16	3,22
—2Pu_{II}	3,78	3,76	—Pu_{III}	2,78	2,80
—Pu_{III}	3,51	3,52	—Pu_{III}	3,18	3,08
—Pu_{III}	3,52	3,54	—X_{II}	2,71	2,63
—X_I	3,16	3,22	X_{II}—2Pu_I	2,95	2,88
X_{II}	2,99	3,05	—2Pu_{II}	2,99	3,05
X_{II}—2Pu_{III}	3,24	3,22	X_{III}—Pu_I	2,98	2,90
—Pu_{III}	2,75	2,84	—Pu_{II}	2,91	2,97
—Pu_{III}	2,85	2,87	—Pu_{II}	3,03	3,12
—X_I	2,71	2,63	—Pu_{II}	3,06	3,08
X_{III}—Pu_I	2,73	2,82	—Pu_{II}	3,20	3,05
Pu_I	2,77	2,75	—Pu_{III}	3,15	3,15

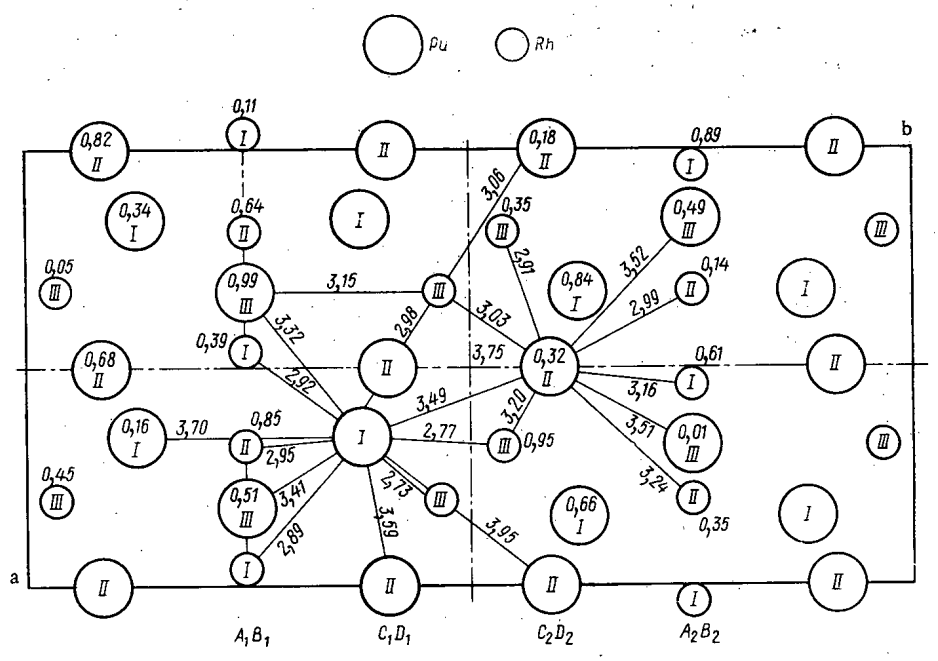

Fig. 1. Projection of the structure of the compounds Pu_5Rh_4 on the plane (001).

Table 1 shows the dimensions of the elementary cell, position of the atoms, atomic parameters, and the theoretical density of the compounds.

Table 2 shows the interatomic distances and coordinations of the atoms. The maximum error in determining the interatomic distances is ± 0.03 Å.

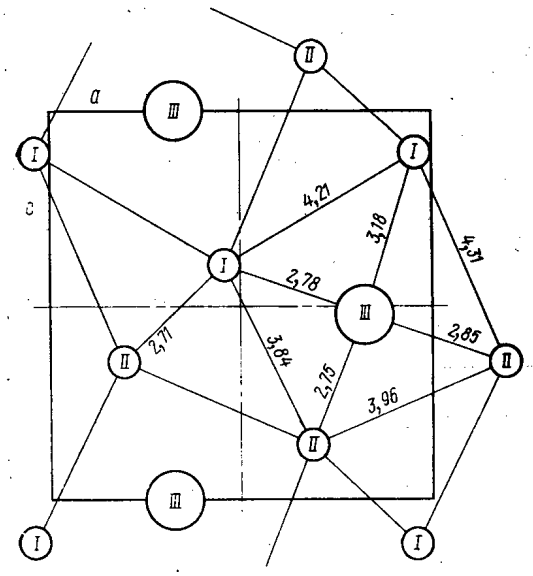

Fig. 2. Type AB layers in the structure of the compound Pu_5Rh_4.

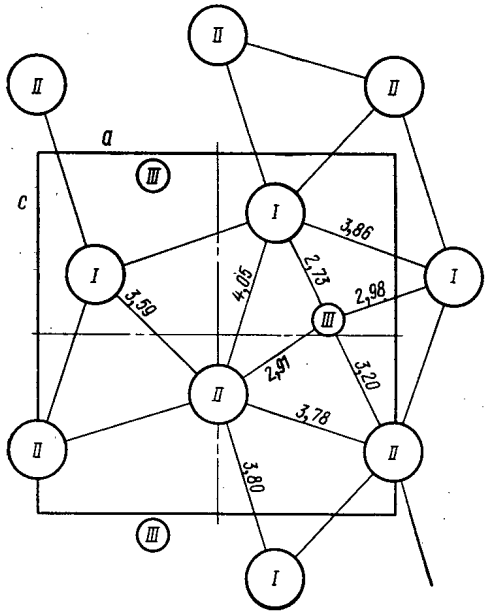

Fig. 3. Type CD layers in the structure of the compound Pu_5Rh_4.

Figure 1 shows the projection of the structure of the compound Pu_5Rh_4 on the density (001). The structure consists of an alternation of plane layers of the type A_1B_1 and A_2B_2, passing through the axis b perpendicularly at a distance of V/2 from each other. Between these layers, two zigzag layers of type C_1D_1 and C_2D_2 are disposed. Figure 2 shows the position of the atoms in the layers of type AB. Each atom of plutonium is surrounded by a tetragon of rhodium atoms. The distances Pu–Rh are 2.75, 2.78, 2.85, and 3.18 Å. The tetragons are linked between themselves by means of a common atom of rhodium and a short bond Rh–Rh = 2.71 Å. Figure 3 shows the arrangement of the atoms in the zigzag layer of type CD. Here, on the contrary, each rhodium atom is surrounded by a tetragon of plutonium atoms. The distances Pu–Rh are 2.73, 2.91, 2.98, and 3.20 Å. The tegragons are linked by means of a common atom of plutonium and the Pu–Pu bond is equal to 3.59 Å. Bonds are achieved between adjacent layers of type CD because of the short distances, Pu–Rh = 2.77 Å. There are short bonds Pu–Rh = 2.89, 2.92, and 2.95 Å between layers of types AB and CD. Thus, bonds within the layers of types AB and CD, and also between the layers, are formed mainly because of the short distances between atoms of plutonium and rhodium. The structure of the compounds Pu_5Rh_4 and Pu_5Ir_4 is close to the structure of the compounds Sm_5Ge_4 [1] and Gd_5Si_4 [2], which have very much in common, although they belong to different structural types [2].

One of the differences of these structures consists in that in the compound Gd_5Si_4, there is an additional bond between atoms of Gd_I and Gd_{II}, which there is not in the compound Sm_5Ge_4. This bond, however, is not strong as the distance $Gd_I - Gd_{II}$ is greater by 8% than twice the radius of gadolinium. In the structure of the compounds Pu_5Rh_4 and Pu_5Ir_4 this distance $Pu_I - Pu_{II}$ amounts to 3.95 and 4.02 Å respectively, which is approximately 25% greater than twice the plutonium radius. Another difference between the structures of Sm_5Ge_4 and Gd_5Si_4 consists in the presence near the atom of silicon (in Gd_5Si_4), and located in the type CD layer, of a short bond with another atom of silicon from the adjacent layer. This distance is equal to 2.47 Å. There is no similar bond in the Sm_5Ge_4 structure. This bond is absent also in the plutonium compounds. However, in the plutonium compounds near the atoms of rhodium and iridium, and located in the type CD layer, there is a bond with atoms of plutonium (Pu_{II}) from the adjacent layer, which is not present in the compounds with the rare-earth elements. These distances $Pu_{II} - Rh_{III}$ = 3.03 Å.and $Pu_{II} - Ir_{III}$ = 3.12 Å.

LITERATURE CITED

1. G. Smith, Q. Johnson, and A. Jharp, Acta Crystallogr., 22, 269 (1967).
2. J. Iglesias and H. Steinfink, J. Less-Common Met., 26, 45 (1972).

NEWS ITEMS FROM THE COUNCIL FOR MUTUAL ECONOMIC AID (CEMA)

DIARY OF COLLABORATION

Conference of Specialists on Problems of the Transportation of Spent Fuel Elements and the determination in them of the fissile material content by a nondestructive method took place on December 1-4, 1975 in Moscow. Reports were heard from specialists from the German Democratic Republic, Poland, Romania, the Soviet Union, and Czechoslovakia on thermal and stability calculations of the maximum constitution of gas mixtures and an estimate of their explosion hazard, model studies of the service life of containers, the transportation of spent fast-reactor fuel, experience in the transportation of spent fuel from the VVÉR-440 and KS-150 reactors, and the determination of the extent of burnup and the content of fissile materials in them. Also reported was the development of documentation for the transportation of spent fuel and the taking of special measures for the prevention and elimination of possible consequential hazards. The timeliness, and high technical and scientific level of these papers is noteworthy.

The specialists drew attention to the advisability of:

1. Further development and unification of transportation methods for the conveyance of spent fuel assemblies from the unified reactors of the member countries of the CEMA.

2. The development of recommendations for the conditions of transportation of spent fuel elements as a function of the extent of burnup, time of cooling, and leak tighteness.

3. The improvement of procedures for thermophysical and stability calculations of transport containers with their verification under test bench conditions.

4. The investigation of new structural materials for transportation containers.

5. The improvement of the method of γ-scanning and methods based on the recording of natural and induced neutron radiation for determining the depth of burnup and the content of uranium and transuranic elements in spent fuel.

The conference of specialists considered and approved plans for technical assignments on the stages of a working plan on the theme "The transportation of spent fuel elements and nondestructive methods of determining in them the content of fissile meterials" by 1976 to 1980, presented by the delegation from the German Democratic Republic, the USSR, and CzSSR in the Council for Scientific and Technical Collaboration on the processing of irradiated fuel from nuclear power stations.

The Conference of Secretaries of Delegations of the Member Countries of CEMA in the Permanent Commission of CEMA on the utilization of nuclear energy for peaceful purposes took place on February 17-19, 1976 in Moscow.

The conference considered and provisionally ratified the report of the Permanent Commission on the work carried out in 1975 and its future activity, and a plan of resolution of the Commission on the report. These documents were referred by the delegations of the countries in the Commission for their agreement in the working agenda.

The participants of the conference heard and discussed information from the division on the utilization of atomic energy for peaceful purposes of the Secretariat of CEMA, concerning the path for accomplishing the work plan of the Commission in 1976-1977.

An exchange of opinions also took place at the conference, concerning the problem of the manufacture of materials and proposals in the departments of nuclear power generation toward a plan for a long-term purposeful program of cooperation for guaranteeing the economics of the basic requirements of the member countries of CEMA on the principal forms of energy, fuel and raw materials in the period up to 1990.

Translated from Atomnaya Énergiya, Vol. 40, No. 6, p. 499, June, 1976.

INFORMATION

THE I. V. KURCHATOV GOLD MEDAL COMPETITION

The Division of Nuclear Physics of the Academy of Sciences of the USSR reports on conducting the competition for the I. V. Kurchatov gold medal of 1977 with financial prize. The gold medal is conferred for outstanding work in the field of nuclear physics.

In the competition for the I. V. Kurchatov medal, papers or series of papers may be presented, on a single thematic, as a rule, of individual authors. In presenting the collective papers, only the leading authors, but not more than three, are to be mentioned. Papers, honored by the Lenin and State Prizes of the Soviet Union, and also prizes of the Academies of Science of the Union Republics and Branch Academies, are not accepted in the medal competition.

The right to put forward candidates for the gold medal competition is vested in the academicians and corresponding members of the Academy of Sciences of the USSR and the Academies of Science of the Union Republics; the scientific institutions; universities; scientific and engineering-technological societies; scientific-technical councils of the state committees, ministries and departments; the technical councils of industrial concerns; the constructional bureau; the Scientific Councils of the Academy of Sciences of the USSR, and other departments concerned with the most important problems of science.

Organizations and individuals putting forward a candidate for the medal competition must present to the Presidium of the Academy of Sciences of the USSR (Moscow, V-71, Lenin Prospekt, 14) with the inscription "The I. V. Kurchatov Gold Medal Competion," the following information (each in triplicate):

1. Motivating presentation, including the scientific feature of the paper, its value for the development of science and the national economy.

2. The published scientific paper (or series of papers), and data of scientific discovery or invention.

3. Information about the author (surname, Christian name, patronym, year of birth, academic degree and title; list of principal scientific papers, discoveries and inventions; place of work and occupational function, official and domestic address and telephone number).

Date of presentation of papers to the competition, up to October 12, 1976.

Division of Nuclear Physics, Academy of Sciences of the USSR. Translated from Atomnaya Énergiya, Vol. 40, No. 6, p. 500, June, 1976.

STILL NO "COSMION"

N. A. Vlasov

Recent investigations of the annihilation of antiprotons with a neutron have detected a certain unexpected excess of γ quanta [1]. In order to explain it, the authors have suggested that before annihilation a bound state of the antiproton with one of the nucleons is formed, which they have also designated a "cosmion." The surplus γ quanta, according to the author's supposition, were emitted by the cosmion during transition from one state to another.

The resounding title attracted attention to the paper, and reports on it were published in many journals (e.g., [2]). Meanwhile, for conclusiveness, data were lacking about the spectrum of the surplus γ quanta [3]. Recently, special investigations of the spectrum have been published [4]. Spectral lines were sought, which should correspond to transitions between states with a quite long lifetime and, consequently, with a small energy width. The result was negative – the expected spectral lines were not detected. The discovery of the cosmion was found to be premature. The existence of bound states of an antinucleon with a nucleon is not surprising, as their interaction is stronger than pairs of nucleons. Even from the time of É. Fermi, attempts have been well known to interpret pions and other mesons as bound states of a nucleon with an antinucleon. The supposedly detected radiative transition proved to be surprising. It is well known in nuclear physics, that in those cases when the excited nucleus can emit a nucleon (not very slow), radiative transition is of low probability. A nucleon pair plus an antinucleon in any state, has many channels of decay (annihilation) into adrons by the action of a strong interaction. Therefore, the detection of a radiative transition should be very interesting, if it should occur. So far this has not happened.

LITERATURE CITED

1. T. Kalogeroponlos et al., Phys. Rev. Lett., 33, 1635 (1974).
2. I. S. Shapiro, Priroda, No. 12, 68 (1975).
3. N. A. Vlasov, At. Énerg., 39, No. 1, 73 (1975).
4. T. Kalogeroponlos, Phys. Rev. Lett., 35, 824 (1975).

Translated from Atomnaya Énergiya, Vol. 40, No. 6, p. 500, June, 1976.

CONFERENCE OF THE FOURTH COMMITTEE OF THE INTERNATIONAL COMMISSION ON RADIOLOGICAL PROTECTION (ICRP)

A. A. Moiseev

The regular session of the Fourth Committee of the International Commission on Radiological Protection (ICRP) took place from December 1-6, 1975 in Moscow, in the work of which nine of the 13 members participated. The only problem discussed at this conference was the project, Publication No. 29. It provides an account of the approach of the Commission to the normalization of the level of irradiation of professional workers and the population. It is proposed that the new ICRP publication will be approved by the Principal Commission in 1976 and issued in 1977 by Pergamon Press in English.

The Joint Session of the National Commission on Radiological Protection with Minzdrave USSR and the Fourth Committee of the ICRP, held on December 6, 1975, took place in a businesslike and friendly environment.

In Moscow the foreign participants of the conference visited the Radiological Center of the Central Institute for the Advancement of Medicine. A large group of scientists departed for Leningrad, where the group acquainted themselves with the principal trends of the work on radiation safety at the Leningrad Scientific-Research Institute of Radiation Hygiene.

During the stay of the foreign scientists in the Soviet Union, meetings and discussions were held with leading Soviet scientists, with the Chairman of the Fourth Committee of the ICRP, A. Jammet, the Scientific Secretary of the Scientific Committee of the United Nations on the effects of nuclear radiation, D. Benninson, and the chief of the division of radiation medicine of the World Health Protection Organization, V. Seelentag. During these meetings and talks, plans were discussed for the further development of scientific research in the fields of radiological protection, the participation of Soviet specialists in the work of the International Association on Radiological Protection and the Fourth International Congress on Radiological Protection, which will be conducted by the International Association in April 1977 in France (Paris).

Translated from Atomnaya Énergiya, Vol. 40, No. 6, p. 501, June, 1976.

THE BETA-MIKROMETR-3 DOUBLE-LAYER COATING RADIOISOTOPE THICKNESS GAUGE

I. I. Kreindlin, V. S. Novikov,
A. A. Pravikov, and I. R. Rubashevskii

In the All-Union Scientific-Research Institute of Radiation Technology (VNIIRTe) production models of the Beta-micrometr-3 radioisotope instrument have been manufactured (see Fig. 1), which enables noncontact, nondestructive measurements of the thickness of double-layer metallic and nonmetallic coatings of complex configuration to be carried out (as in Fig. 1) on small-scale fragile metallic and nonmetallic manufactured articles, with a minimum monitoring area of 0.25 mm^2. Beta-mikrometr-3 is designed on the basis of previously developed instruments, Beta-mikrometr and Beta-mikrometr-2 [1, 2]. In contrast from the first two modifications, the instrument is provided with three interchangeable β-emitting sources with a wide range of boundary energies. In order to select the optimum source for monitoring a specified combination of materials of coatings and backings, a procedure was developed for calculating the effect of variation of the layer thickness, located above or below the layer being monitored.

The circuit of the DOT-3 primary transducer is achieved by integrated microcircuits, which increases significantly the reliability of the instrument. The measurement time is recorded by small-scale duplexers and can be set up from 1-1000 sec depending on the required monitoring accuracy. The Beta-mikrometr-3 instrument has an output at the BZ-15 pen recorder. In combined operation with the BZ-15, the measurement result is printed out on a paper strip: in the first column – the serial number of the measurement and in the second column – the readings of the instrument signal panel. The instrument is powered from 220-V, 50-Hz mains; power requirement is not more than 100 VA. Working range 10-35°C.

LITERATURE CITED

1. I. I. Kreindlin, V. S. Novikov, and A. A. Pravikov, At. Énerg., 30, No. 5, 47 (1971).
2. T. G. Zvereva et al., At. Énerg., 36, No. 5, 413 (1974).

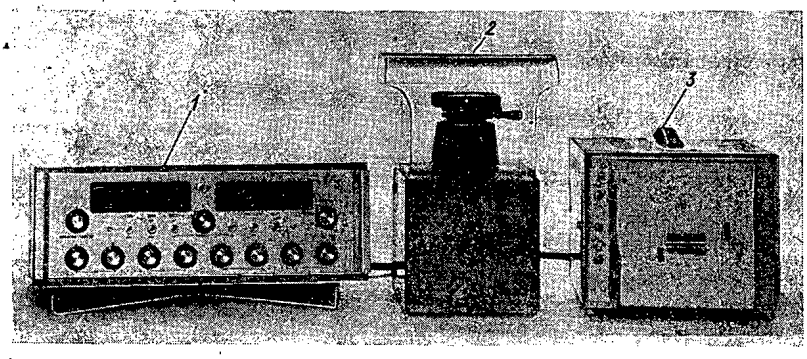

Fig. 1. Beta-mikrometr-3 double-layer coating thickness gauge: 1) PU-2 scaler; 2) DOT-3 primary transducer; 3) BZ-15 pen recorder.

Translated from Atomnaya Énergiya, Vol. 40, No. 6, p. 501, June, 1976.

A. M. Petros'yants

NUCLEAR POWER GENERATION*

Reviewed by Yu. I. Koryakin

To write books about nuclear power generation aimed at analyzing and reviewing the power-economic and nuclear power generating situation in the countries of the world at present has become incomparably more difficult than a few years ago. A nuclear power station was small then, the specific features and structural characteristics were not so diverse as at present, and the problems solved by means of them appeared to be easily examinable for the future. The quantitative and qualitative factors responsible for the connection between nuclear power generation and the surrounding medium simply did not enter into the order of the day, in view of the negligibly small role of nuclear power stations in the energy supplies and power-economy of industrially developed countries.

The position now has changed, but not so much in the qualitative aspect as in the quantitative aspect which, on the whole, is characterized by nuclear power generation acquiring the qualities of a complex system and strict complexity. Therefore, an attempt is hopeless at present and the method is unacceptable of the simple listing and descriptive account of the engineering-design decisions of nuclear power stations which was possible a few years ago.

The author of the book being reviwed, clearly understanding these difficulties, has undertaken the solution of the difficult problem of interpreting the complex picture of the state of nuclear power generation in the world and, it would appear, has dealt with it successfully, and although the description of nuclear power stations and their structural features predominates in the book, the main consideration even within these limitations is given to the typical properties of nuclear power stations, the development of tendencies in structural and circuit decisions, constraints and origins of these decisions arising from the systematic aspects and specific characteristics of the development of nuclear power generation in every country.

It is important that the author has not confined himself to consideration of nuclear power stations as electric power generating facilities. The conditions, which shape the national demand on them and the necessary scientific and production basis of nuclear power generation (nuclear research centers, nuclear mechanical engineering factories, etc.) in the book have been an important element to demonstrate the systemic qualities and complexity of the nuclear engineering industry. A description is referred here of the expected role and position of nuclear power generation in solving the problem of the power demands of countries in the long-term and also the participation of nuclear power stations and their special operating features in national power systems.

Certainly, the systemic aspects of nuclear power generation recounted by the author are the results of an analytical approach to the numerous publications in Soviet and foreign nuclear power literature. An analysis of this literature, even in itself, is not a simple task and a discussion of the results of this analysis and generalization of the data in the thematic plan of the book at the level, and in the key, which corresponds to the purposeful task of the author is no less difficult.

On the whole, this book broadly and systematically informs the Soviet reader about the outside situation and the state of nuclear power generation in the Soviet Union and abroad. Naturally, Soviet nuclear power generation is afforded special consideration and among the types of nuclear power stations are nuclear power stations with channel-type reactors. The latter, as is well-known, made an overwhelming contribution to the introduction of the nuclear power capacities of the Soviet Union in the Ninth Five-Year Plan, and this situation in the 10th Five-Year Plan will be maintained. Moreover, nuclear power stations with these reactors have the

*Nauka, Moscow (1976).

Translated from Atomnaya Énergiya, Vol. 40, No.6, p. 503, June, 1976.

greatest capabilities for the enlargement and concentration of individual outputs, which is particularly important for the Soviet Union, whose power system is capable of accepting the extremely large outputs of the nuclear power-generating units. Obviously, the large unified electric power of the units is an important factor for accelerating the growth of the nuclear power station outputs, economy of financial means and labor resources in the field of power reactor construction and nuclear engineering. These qualities of channel-type reactors are emphasized by the author. It is only a pity that the author did not succeed in introducing into the book a description of the intermediate modification of the RBMK-1500 channel-type reactor, recently defined and brought on stream (intermediate between the RBMK-1000 and the RBMK-2000), achieved by the first nuclear power station to be built with these reactors in accordance with the current five-year plan – the Ignalinsk nuclear power station (Lithuanian SSR).

The scope of the review does not permit the information in the book concerning foreign nuclear power generation to be dealt with extensively. Nevertheless, it should be noted that it leaves at the disposal of the reader, rich factual and substantial reference data. The numerous photographs of nuclear power stations and other nuclear facilities, both Soviet and foreign, are immensely valuable for illustrating and brightening up the book.

Unfortunately, it has not been managed without individual slight errors, inaccuracies, or even obsolete data. The reason for the majority of these, is that the rate of scientific-technological progress in nuclear power generation has outstripped the period of writing of the manuscript of the book and its editing–publishing progress.

On the whole, the issue of the book "Nuclear Power Generation" can be evaluated as an undoubtedly positive event in nuclear scientific-technological literature.

engineering science

continued from back cover

Title	# of Issues	Subscription Price
Metallurgist *Metallurg*	12	$225.00
Metal Science and Heat Treatment *Metallovedenie i termicheskaya obrabotka metallov*	12	$215.00
Polymer Mechanics *Mekhanika polimerov*	6	$195.00
Problems of Information Transmission *Problemy peredachi informatsii*	4	$175.00
Programming and Computer Softwave *Programmirovanie*	6	$95.00
Protection of Metals *Zashchita metallov*	6	$195.00
Radiophysics and Quantum Electronics (Formerly Soviet Radiophysics) *Izvestiya VUZ. radiofizika*	12	$225.00
Refractories *Ogneupory*	12	$195.00
Soil Mechanics and Foundation Engineering *Osnovaniya, fundamenty i mekhanika gruntov*	6	$195.00
Soviet Applied Mechanics *Prikladnaya mekhanika*	12	$225.00
Soviet Atomic Energy *Atomnaya energiya*	12 (2 vols./yr. 6 issues ea.)	$235.00
Soviet Journal of Glass Physics and Chemistry *Fizika i khimiya stekla*	6	$ 95.00
Soviet Journal of Nondestructive Testing (Formerly Defectoscopy) *Defektoskopiya*	6	$225.00
Soviet Materials Science *Fiziko-khimicheskaya mekhanika materialov*	6	$195.00
Soviet Microelectronics *Mikroélektronika*	6	$135.00
Soviet Mining Science *Fiziko-tekhnicheskie problemy razrabotki poleznykh iskopaemykh*	6	$225.00
Soviet Powder Metallurgy and Metal Ceramics *Poroshkovaya metallurgiya*	12	$245.00
Strength of Materials *Problemy prochnosti*	12	$295.00
Theoretical Foundations of Chemical Engineering *Teoreticheskie osnovy khimicheskoi tekhnologii*	6	$195.00
Water Resources *Vodnye Resursy*	6	$190.00

Back volumes are available. For further information, please contact the Publishers.

SEND FOR YOUR FREE EXAMINATION COPIES

Plenum Publishing Corporation
Plenum Press • Consultants Bureau
• IFI/Plenum Data Corporation
227 WEST 17th STREET
NEW YORK, N. Y. 10011

United Kingdom: Black Arrow House
2 Chandos Road, London NW10 6NR England

Declassified and Approved For Release 2013/04/10 : CIA-RDP10-02196R000700070006-5

breaking the language barrier

WITH COVER-TO-COVER
ENGLISH TRANSLATIONS
OF SOVIET JOURNALS

in engineering science

Title	# of Issues	Subscription Price
Automation and Remote Control *Avtomatika i telemekhanika*	24	$260.00
Biomedical Engineering *Meditsinskaya tekhnika*	6	$195.00
Chemical and Petroleum Engineering *Khimicheskoe i neftyanoe mashinostroenie*	12	$275.00
Chemistry and Technology of Fuels and Oils *Khimiya i tekhnologiya topliv i masel*	12	$275.00
Combustion, Explosion, and Shock Waves *Fizika goreniya i vzryva*	6	$195.00
Cosmic Research (Formerly Artificial Earth Satellites) *Kosmicheskie issledovaniya*	6	$215.00
Cybernetics *Kibernetika*	6	$195.00
Doklady Chemical Technology *Doklady Akademii Nauk SSSR*	2	$65.00
Fibre Chemistry *Khimicheskie volokna*	6	$175.00
Fluid Dynamics *Izvestiya Akademii Nauk SSSR mekhanika zhidkosti i gaza*	6	$225.00
Functional Analysis and Its Applications *Funktsional'nyi analiz i ego prilozheniya*	4	$150.00
Glass and Ceramics *Steklo i keramika*	12	$245.00
High Temperature *Teplofizika vysokikh temperatur*	6	$195.00
Industrial Laboratory *Zavodskaya laboratoriya*	12	$215.00
Inorganic Materials *Izvestiya Akademii Nauk SSSR, Seriya neorganicheskie materialy*	12	$275.00
Instruments and Experimental Techniques *Pribory i tekhnika éksperimenta*	12	$265.00
Journal of Applied Mechanics and Technical Physics *Zhurnal prikladnoi mekhaniki i tekhnicheskoi fiziki*	6	$225.00
Journal of Engineering Physics *Inzhenerno-fizicheskii zhurnal*	12 (2 vols./yr. 6 issues ea.)	$225.00
Magnetohydrodynamics *Magnitnaya gidrodinamika*	4	$175.00
Measurement Techniques *Izmeritel'naya tekhnika*	12	$195.00

SEND FOR YOUR FREE EXAMINATION COPIES

Back volumes are available.
For further information,
please contact the Publishers.

continued on inside back cover